DETERMINATION OF THERMODYNAMIC PROPERTIES OF GOLD FROM ITAGUNMODI, SOUTHWEST NIGERIA

By

BELLO, ADEKUNLE KAZEEM

Matric. No.: 109502

B.Sc. (Hons) Physics (Ago Iwoye), M.Sc. Physics (Ibadan)

A THESIS IN THE DEPARTMENT OF PHYSICS SUBMITTED TO THE FACULTY OF SCIENCE

IN PARTIAL FULFILLMENT OF THE REQUIREMENTS FOR THE DEGREE OF

DOCTOR OF PHILOSOPHY

OF THE

UNIVERSITY OF IBADAN

MAY, 2020

CERTIFICATION

This is to certify that this work has not been carried out for a higher degree of any other University elsewhere; it was carried out by BELLO Adekunle Kazeem under my supervision. All citations and sources of information are clearly acknowledged by means of references.

_____ _____

Dr. A. A. ADETOYINBO Date

Supervisor

DEDICATION

This work is dedicated to my spouse Hajia Bilqis Omosalewa and our children Abdullahi, Muhammed and Ibrahim for their patience and love throughout the period of the program.

ACKNOWLEDGEMENTS

First and foremost, my profound gratitude goes to my Supervisor Dr. Adegoke Adedeji Adetoyinbo, for his fatherly advice and guild throughout the trying and hard period of the program for never turning me back or discouraged me instead, he gave me his full support and backings. There is no way I could appreciate your kind love than pray to Almighty God to continue to protect, guide you, always open ways even whenpeople think there is no way and give you long live with satisfaction and peace of mind.

Also, I appreciate the Head of my Department Prof. J. A. Ademola and the entire staff of the Department of Physics for the success of the work.

I also appreciate the contributions made by Dr. T. T. Ogunseye, Dr. A. I. Ojoawo, Dr. F. L. Aderemi, Prof. J. A. Adegoke, Dr. E. O. Joshua and Dr. I. O. Popoola all of the Geophysics group, Department of Physics University of Ibadan. I also appreciate the suggestion made by Prof. F. Ogundare of Physics Department University of Ibadan.

Also, I appreciate the contributions of Prof. A. A. Okunade and Dr. M. O. Awoyemi both of Obafemi Awolowo University Ile-Ife for their suggestions. Also, I said thanks to Mr. Niyi of Itagunmodi for his support for accessing gold mining sites in his town.

I appreciate the supports of Dr. A. K. Ademola and other members of staff of the Department of Physical Sciences Bells University of Technology, Ota and Prof. G J. Oseomebo, the Dean of College of Natural and Applied Sciences for his fatherly advice.

I also appreciate the love and encouragement from my family member my mother, Mama MisturaTayelolu Bello and my late father, Imam Alhaji Y. A.S. Olayiwola Bello of Blessed memory and all my family members.

ABSTRACT

The Thermodynamic Properties (TP) of gold usually gives an insight into the nature of gold occurrences. However, only geophysical characterization of gold deposits are often undertaken to confirm mineralisation with little attention paid to the TP of gold. Therefore, this work was designed to determine the TP of gold around Itagunmodi and their consequences on and or correlation with temperature profile in the lithosphere.

Thirty samples of gold were purposively collected from selected locations in Itagunmodi Southwestern Nigeria. One gramme of each unrefined gold sample was analysed for variations in volume when subjected to high pressure ($600\ MPa$) and temperature (3000 ℃) using highly improved-pressure vessel. The TP (bulk modulus, thermal pressure, compressed volume and volume strain) were determined using standard methods. The parameters served as input to the Mie-Grüneisen equation of state for lithological classification. The temperature profile from the crust based on average values of volume and temperature to the lithosphere was determined using: $\dot{Q} = \dot{Q}_{MC} + \dot{q}_0 z_0 - \int_0^z \dot{q} dz$, where $\dot{Q}, \dot{Q}_{MC}, \dot{q}, \dot{q}_0, z_0, z$, are mean continental, mantle crustal heat flux, exponential variation of radiogenic heat with depth, mean radiogenic heat flux, fixed reference depth for crustal part of the lithosphere and varying reference depths for crustal part of the lithosphere, respectively. Lithospheric stress was determined using standard procedure, while the variation of melting point with pressure was determined using the plot of temperature against pressure. Data were analysed using descriptive statistics.

The bulk modulus of gold was obtained within $0.68 - 9.85\ GPa$and it decreased with temperature rise. The compression in volume of the unrefined gold samples increased with increase in both temperature and pressure because the increase in temperature will not cause any increase in volume as a result of the application of pressure. The initial average values of pressure, thermal pressure, temperature and compressed volume ranged from $436.40 - 549.00\ MPa$,$0.150 - 0{,}831\ GPa$, $2327.30 - 2871.70$ ℃and$0.041 - 0.69 \times 10^{-3} m^3$, respectively. The strain rate was $10^{-5} s^{-1}$, which conformed to literature laboratory values for materials ($10^{-5} - 10^{-9} s^{-1}$) such as copper, aluminium and polycrystalline tantalum. The calculated temperature profile ranged from $27 - 1483$ ℃and the depth from $0 - 150\ Km$. The calculated base value of 1483 ℃, agreed with literature values (1280 ℃and 1600 ℃). The stress in the lithosphere increased at $33\ MPa/Km$, while bulk modulus increased at $1.136\ GPa/Km$. The temperature of the melting curve value from 1064 ℃and 1394.3 ℃in the pressure ranged between $0\ and\ 6500\ MPa$. This corresponds to temperature range of $1045\ and\ 1483$ ℃and pressure range of $0\ and\ 4900\ MPa$in the lithosphere.

The determined thermodynamic properties to the depth of the lithosphere of gold deposit at Itagunmodi showed that the nature of the gold existed as solid mass at the source.

Keywords: Gold, Compressed volume, Temperature profile,Mie-Grüneisen equation, Bulk Modulus

Word count: 480

LIST OF FIGURES

LIST OF TABLES

Table of Contents page

CHAPTER ONE

INTRODUCTION

1.1 Background to the Research

The lithosphere is the outer part of the Earth's interior, it can be found above the asthenosphere, this region is hard or brittle portion(Kenneth and Bunge, 2008), it is the region where various activities are taken place, and this part of the Earth's interior which is the concrete basement is in form of plates that carries all loads. There are mountains that are also located at various places in different sizes in the lithosphere and these acts as support for Earth's stability.The lithosphere has two layers which extends from the crust and enters part of the upper mantle down to a depth of about 70 – 100 km under deep ocean basins and 100 – 150km under continents. Beneath the lithosphere lies the asthenosphere, a layer in which the seismic velocities decrease which suggests lower rigidity. It has thickness of about 150 km; the upper and lower boundaries are not sharply defined. This weaker layer is believed to be partially molten, William (2007). It may be able to flow over long periods of time like a viscous liquid or plastic solid in a way that depends on temperature and composition. The asthenosphere plays an important role in plate tectonic because it allows the relative motions of the overlying lithospheric plates to be possible, William (2007).

The brittle condition of the lithosphere causes it to fracture when strongly stressed. The rupture produces an earthquake, which is the violet release of elastic energy due to sudden displacement of a fault plane. Seismic Earthquakes are not distributed evenly over the surface of the globebut occur predominantly in a well-defined narrow seismic zones that are associated with volcanic activity.

If the lithosphere is strongly stressed either by any natural process or anti-Earth activities, the pressure within it will look for weak areas such as fault zones to escape and when this happen, it can lead to Earthquake or Tsunami. The study of stress field of the Earth is very useful, it can be

used for proper planning by engineers, miners and other people that study the Earth. The knowledge will be useful both locally and globally. When there is relative motion mantle flow and the motion of the lithospheric plate, stress is formed. In this work, the findings involved why some deposits of gold exists in the form grain and not mined as solid minerals and its source using temperature profile in the lithosphere.

Gold is a metallic element with chemical symbol, Au and atomic number, 79. It has atomic weight of 196.966with melting point, about 1064 ºC and the boiling point is 2,966.0ºC, it has specific gravity of 19.32;its valences are +1 or +3. Gold occur as dense, yellow, malleable and indestructiblemetal that can be found in uncombined state. Although gold is widely distributed on the Earth, larger amounts can be found in seawater. Gold occur in metallic state and could be in the form of dust, grains, flakes(Harold, *et al.,* 1997).Some of the deposits occur together with silver or other metals.

1.2 Research Problem and Hypothesis

Most metallic ores occur as solid minerals in rock, it was observed that the samples for the study were in form of grain that made the mining process to be stressful than the solid rock mineral type. The mining process involves panning; these are used to separate gold from other mixtures such as Au-Ag. Cu-Au deposits. Hence, a hypothesis was proposed having seen the nature of the gold deposits in that area, the question that came up was “what could be responsible for the nature of gold in this area to be in the form grain? “From the nature of gold found in the area, analyses such as high pressure and high temperature on the volume of gold were proposed. Also, the stress and strain rates of the samples were determined and these were compared to the stress in the lithosphere.

1.3 Justification for the Research

The geophysical characterization such as melting, boiling, critical points of gold deposits have been undertaken with little attention paid to the thermodynamic properties of gold and the stress in the lithosphere have been studied by various researchers. However, there is scanty information

about temperature profile within the Lithosphere for the area. With Fourier law, the temperature profile in the Lithosphere was determined as well as depth of formation of gold in this area.

1.3.1 Statement of the Research Problem

Previous researches have been done on the determination of the melting point of gold, the critical point of gold and the stress in the crust. However, there is scanty information on the determination of the following:

(i) The strain effect on bulk modulus of unrefined gold

(ii) Bulk modulus of unrefined gold

(iii) The stress and temperature profile of the lithosphere

1.4 Aim and Objectives

The aim of the work is to determine the form and thermodynamic bulk properties of unrefined gold deposits at Itagunmodi at the source using temperature profile in the lithosphere. The objectives were to:

(i) determine the impact of high temperature and pressure on volume of unrefined gold;

(ii) investigate the strain effect on unrefined gold;

(iii) estimate the bulk modulus of unrefined gold deposits;

(iv) determine the temperature profile in the lithosphere to predict the depth of unrefined gold deposit and

(v) carried out the stress and bulk modulus in the lithosphere.

The aim and objectives were achieved using the method stated below:

i. Using Mie-Grüneisen equation of state- the strain, stress and bulk modulus of unrefined gold were determined.

ii. Temperature profile for the lithosphere was determined using the Fourier Law.

iii. The stress and bulk modulus in the lithosphere were also estimate using Heim's rule.

1.5 Outline of the Thesis

The thesis is divided into five chapters. Chapter one is the introduction. Chapter two contains relevant literature review. Chapter three contains materials and methodology of the work. The result obtained, analyses and discussions are contained in chapter four and the last chapter contains conclusion and recommendation based on the findings obtained in this work.

CHAPTER TWO

LITERATURE REVIEW

2.1 Theoretical Background

2.1 Lithosphere

Lithosphere is the solid, brittle rock that occurs just above the asthenosphere as stated byKenneth and Bunge, (2008). This layer is the strong layer of the earth that comprises mobile tectonic plates and heat is transferred conductively as reported by Roland and George, (2008).This layer includes the crust, the Moho, and the upper part of the mantle. The lithosphere is characterized by instantaneous elasticity, but is also capable of long-term deformation, such as the deformation around oceanic islands and post-glacial rebound following ice-load. The oceanic lithosphere thickens away from mid-ocean regions where new oceanic crust is generated according to Kenneth and Bunge, (2008).

The base of the lithosphere may be quite sharp in the oceanic environment, with distinct changes in seismic wave speed and electrical conductivity. Kenneth and Bunge, (2008) stated that the mantle component of the oceanic lithosphere appears to be relatively strong since it survives the transition into subduction relatively intact to form the distinct subduction zones well-imaged by seismic tomography according to The lithosphere is bent as it descends into the subduction zone and this produces shallow earthquakes near the trench. Earthquakes are generally concentrated near the top of the subducting plate close to the division between the former oceanic crust and mantle component. The base of the lithosphere is only locally sharp. In the near surface the materials are relatively brittle, but plastic deformation becomes more significant with depth. As a result, earthquakes occur predominantly in the top 15 km above the brittle–ductile transition according to Kenneth and Bunge, (2008).

The lithosphere is broken into plates that move on the upper mantle just as massive flat ice sheets floating on water. The arrangement of the plates is the foundation for plate tectonics, it describes changes such as earthquakes, volcanoes, and mountain building that occurs on the earth's surface. The lithospheric plates are about 150 km thick and have variable properties. The most accessible portion of the lithosphere is the crustal part which exhibits a range of character (Kenneth and Bunge, 2008). The materials in the near surface are brittle, but plastic deformation

becomes more significant with depth. According to Turcotte and Oxburgh, (1976), the sources of stress in the lithosphere were reviewed earlier, in their work, it was stated that stress can accumulate in the lithosphere for $10^8 - 10^9$ years and also there are a number of mechanisms leading to the accumulation of stress in the lithosphere such as changes in temperature cause thermal stresses, addition or removal of overburden generates stress. Also, the driving mechanism for plate tectonics results in stress and stresses are generated by changes in crustal thickness(Turcotte and Oxburgh, 1976). It is concluded that tensional fracturing of the lithosphere is a more likely explanation for intraplate volcanism than deep mantle plumes.Also, there are further advances that have been made towards understanding the lithospheric stress since the review, one of the improvements include understanding the nature of boundary forces of the plate and the way stress are being concentration in the uppermost elastic part of the lithosphere. According toBott and Kusznir, (1984), which stated that the stress affecting the lithosphere are classified into two main categories namely renewable and non-renewable types, they explained further that renewable stress persists regardless of continuing stress relaxation and non-renewable stress can be dissipated by relief of the initial strain. An important phenomenon generating large stresses at shallow depth is stress amplification caused by lower lithospheric creep. This applies to renewable stresses but not to the non-renewable type.Bott and Kusznir, (1984)suggested that only renewable stresses contribute significantly to tectonic activity. However, bending and thermal stresses are locally important in subducting lithosphere.The renewable type is a form of stress which persists as a result of the re-application of the causative boundary or body forces whose strain energy is progressively dissipated. It has two main examples; one is the stress systems arising from plate boundary forces and the other is the one from isostatically compensated surface loads. The non-renewable type of stress can be degenerated by release of strain energy which initially exists. Examples include the bending stress, membrane stress and thermal stress. The combination of superimposed stresses which may be affected by lateral variation of mechanical properties gives rise to the actual stress at any point in the lithosphere. The stress field determines stability or instability of underground openings and it plays key role of every rock engineering project (Torbica and Lapcevic, 2016).

The temperature profile in the earth interioras revealed in previous work carried out by some researchers in the past covered the inner core and was extended to some part of the upper mantle while the value for the lithosphere was done through extrapolation of values. Stacey (1977)

estimated temperatureat crust-mantle boundary using Lindemann's Laws of fusion was 277^{o}C (550K). The temperature, according to Anderson(1979), at depth between 100 – 140 Km in the earth interior ranged from 1100 –1400 ^{o}C. The temperature for the same depth between 100 – 140 Km as given by Anderson(1980), rangedfrom 1200 – 1440^{o}C respectively. Also, at the base of the lithosphere, Watts (2007) gave a value of 1330^{o}C while William (2007), gave a value of 1280^{o}C for the base and Chloe and Claude, (2007) gave a value of 1600^{o}C.

2.2 Crust

The earth crust is the thinnest layer which makes up 1% of the Earth's volume as reported by Robertson (1996). Volgyesi and Moser, (1982)stated that it is the uppermost top component of the lithosphere and floats on top of the upper mantle. The crust plus the upper mantle is separated by the Mohorovicic discontinuity- a seismic and compositional boundary (Volgyesi and Moser, 1982). The crust varies in thickness as controlled by the law of isostasy according to Airy's model- the crust responds to topographical changes (loads or unloads) by changing its thickness as compensation, thus tending towards isostatic equilibrium according to Watts (2001). The crust is thickest under mountain ranges and thinnest under mid-ocean ridges (Volgyesi and Moser,1982). There are two main types of crust called the oceanic crust and the continental crust, and they are different from each other. The differences are due to plate tectonics which then refers to plates and the movement of the plates above the asthenosphere, driving lithospheric processes that result in the formation and production of natural phenomena such as earthquakes and ridges. Approximately 35% of the Earth's crust is continental, while the other 65% is oceanicCogley (1984). The different locations of heat sources and thermal conductivity of the crust give rise to temperature variations in the different crust types.

2.2.1 Types of Crust

There are some differences in the crust depending on where on the surface we are. The crust under the ocean is much thinner than the crust under the continents. There are two types of crust namely, the continental crust and the oceanic crust.

2.2.1.1 Continental Crust

Based on seismic investigations, the structure of continental crust is defined to consist of the upper crust, middle crust and lower crustal layers as reported byRudnick and Fountain, (1995), Holbrook *et al.,* (1992). Each layer varies slightly in its composition. The bulk composition is made mostly of rocks with a composition similar to granite rocks, full of substances such as oxygen, aluminium and silicon.The continental crust underlies the continents with average rock density of about 2.7 g/cm^3 and average thickness lies between 38 and 40 km. The material that makes up the continental crust is mostly made up of rocks containing silicon and aluminum. Crustal density controls surface position. The continental crust is less dense and "floats higher."

2.2.1.2 Oceanic Crust

Similarly, oceanic crust is also layered, and each layer varies slightly in its composition (White and Klein, 2014). In general, oceanic crust is basaltic and is rich in minerals and substances like silicon, oxygen and magnesium.The oceanic crust underlies the ocean basins; the density is about 3.0 g/cm^3 and the average thickness lies between 6 and 8 km. The materials that make up the oceanic crust are made up mostly of rocks containing silicon and magnesium. The oceanic crust is denser and "floats lower." Both types of crust behave as if they were floating on the mantle which is denser than either type of crust.

2.3 Asthenosphere

Asthenosphere is a thin zone in the mantle where seismic waves undergo a sharp decrease in velocity, Kenneth and Bunge, (2008). It is a layer of hot, elastic semi-fluid material that extends around the entire Earth. The asthenosphere generally has lowered shear wave speed, enhanced attenuation (i.e. the asthenosphereimproved the reduction of seismic wave speeds) of seismic wave speeds and lowered apparent viscosity,Kenneth and Bunge, (2008). These properties were originally ascribed to the presence of partial melt, but recent studies suggest that enhanced water content could produce the requisite change in physical properties. The rate of change of elastic moduli and attenuation increase significantly with temperatureand for temperatures above 1200 K the effects are noticeable even though there is no actual melt, Kenneth and Bunge, (2008). The knowledge of stress is also useful in the following applications such as when petroleum

engineers are planning and extracting oil and gas from a petroleum field (reservoir), also when tectonic deformations near faults and related earthquake hazard needs to be measured. According to some reviews of stress measurements in the Earth's crust, notable among them are those of Hast (1969) and Zoback (1992) and Richardson (1992), (These are some of the researchers that have reviewed stress measurement in the Earth's crust). Torbica and Lapcevic, (2016), stated that these researchers have noticed that maximum horizontal stress orientation is subparallel with the movement direction of the tectonic plates. They concluded that stress field and tectonic plate's movement have the same cause.

2.4 Gold deposits

Gold has been mined throughout the world from different deposit types and of all geologic ages Boyle (1979). It has been produced from the Precambrian shield areas of Africa, North and South America, Australia mainly from quartz veins. Another deposit is the Paleozoic-age deposits which occur widely andconcentrated in the Ural Mountains, Kazakhstan in southeastern Asia, in eastern Australia, in the Appalachian region of the United States, and in Europe. These deposits are mostly quartz veins and stockworks. There is also Muruntau gold deposit in Kazakhstan which is complex of quartz veins and associated stockworks of quartz veinlets in Paleozoic calcareous siltstones, shales, and schists near Paleozoic granodioritic plutons. Mesozoic deposits of gold occur mostly in the cordilleran belts at the western margins of North and South America, and in eastern Siberia and China. Quartz veins again are the dominant type in some districts forming great regional systems such as the productive Mother Lode of California. Titley (1978) and Sillitoe (1979, 1980 and 1981) stated that some gold occurs in anomalous quantities in many porphyry coppers deposits around the world. Most geochemical studies suggest that the solutions responsible for primary hydrothermal mineralization in these deposits were derived from magmatic water Taylor(1979).

2.4.1 Types of Gold Deposits

There various types of gold deposits based on its formations and the environmental factors regarding where it was found. One of the major types of gold occurrence is the lode deposits, this

type of gold deposits can be within the original solid rock; this type normally appears in rock form. Today in the history of gold deposits in the world, the lode deposits were regarded as the source of the majority of gold that are mined.Harold, *et al*., (1997), stated that there are a lot of hypotheses that have been proposed by many researchers towards the explanation of the solutions from which mineral constituents are precipitated in lode deposits.One of the major areas where gold can be deposited is the fracture zones that occur along faults and one characteristic of such areas is, they are open to circulation of liquids. This is the reasonwhy veins of gold are been associated to fault activity. The percentage of gold that can be found in the deposit is only small fraction and the type minerals associated with the deposit includes products such as quartz, calcite, pyrite among others, Harold, *et al.,* (1997).

The common gold deposits of the world can be found in quartz rock, these gold deposits are believed to originate from circulation of ground water that are driven by heat that comes from magma bodies and interfere into the Earth's crust from depth of about two miles of the earth's subsurface,Harold, *et al.,* (1997).Information also revealed that gold bearing solutions can be expelled from magma as it cools while ore materials are been precipitating as they move into cooler surrounding rocks. Another theory of gold origin is applied mainly to gold-bearing veins in metamorphic rocks that occur in mountain belts at continental margins. The theory suggests that as the minerals changed, water is expelled fromthem, and the water then migrates upward, resulting in precipitation of ore materials as pressures and temperatures decrease. Harold, *et al.,* (1997), also stated that the ore metals are thought to originate from the rocks undergoing active metamorphism deep within the earth. The prospector or miner interested in lode deposit of gold are primarily concerns in determining the average gold content per ton of mineralized rock and the extent of the deposit,Harold, *et al.,* (1997). From the available data, the approximations can be made from the deposit's value. Fire test is one of the most commonly used methods for determining the gold and silver content of mineralized rocks, Harold, *et al.,* (1997).

Apart from lode deposit, there is other form of gold deposit called placer deposits. These types of gold deposits are those that are free from the enclosing lode deposits, they are in the form of loose particles of gold. They are formed by the decomposition of the enclosing rock. The miners of these form deposits are always in search of where there are accumulation of coarse sand and gravel and where black sand settled in the stream. The deposits of this type are mined principally

for the predominant metals; the gold is recovered as a byproduct during processing of the ore because of its value.

There is another type of gold deposit called sediment-hosted disseminated gold SHDG deposit that occur in sediment form and in association with variable amounts of other metals such silver, mercury, arsenide and barium. These deposits are characterized by extremely fine-grained disseminated gold hosted primarily by arsenian pyrite. There are anomalous concentrations of elements such as stibnite, mercury, tantalum and barium that are utilized as exploration tools. According to Guilbert and Park, (1986), SHDG deposits contain very fine gold grains and sulphides disseminated in altered impure carbonates rocks. There is other gold mineralization mined from subsurface in the lithosphere which is in various form such as epithermal gold according to Poulsen *et al*., (2000). The form of deposits is regarded to be primarily associated with continental volcanism or magmatism according to Dube *et al*., (2007). These other deposits, especially those with similar characteristics from marine environments, may also be considered as epithermal deposits. Epithermal gold deposits are distinguished on the basis of the sulphidation state of the sulphide mineralogy as belonging to one of three subtypes: the first type is referred to as high sulphidation-alunite, alunite-kaolinite, high sulfur according to Ashley(1982) and); the second type is called intermediate sulphidation as mentioned by Hedenquist *et al*., (2000), while the third category is called the low sulphidation.

2.4.2 Source of Gold Deposits

There are several hypotheses proposed by researchers which had been used to describe the source of the mineral elements that form lode deposits as stated by Harold *et al*., (1997). Some of the researchers proposed that the gold, heat and fluid (formation water) originate from the host rocks according to He *et al*., (1993) and He(1996). Also, few researchers proposed that the gold of sedimenthosted disseminated gold mineralization was derived from the Mantle was reported by Ni *et al*., (1997), another researcher proposed a mixture of both the mantle and the crust as mentioned by Zhu *et al*., (1998a).

2.4.3 Background to Gold Appearance

Gold can be identifying by its yellowish cast, and is one of the oldest metals used by humans, as far back as the Neolithic period, humans have collected gold from the stream beds, and the actual mining of gold can be traced as far back as 3500 B C, when early Egyptians (the Sumerian Culture of Mesopotamia) used mined gold to craft elaborate jewelry, artifacts, and utensils such as goblets, Harold, *et al.,* (1997). The aesthetic properties of gold combined with its physical properties have long ago made it a valuable metal. Gold has often been the cause of both conflict and adventure throughout history such as the destructive of both the Aztec and Inca civilizations, the Conquest stole the treasuries of these civilizations during their explorations of the New World, and many gold and silver objects were melted and cast into coins and bars, for instance, and the early American gold rushes to Georgia, California and Alaska,Harold, *et al.,* (1997).

2.4.4 Occurrence of Gold

Although gold occurs widely throughout the world, its occurrence is usually very sparsely, so that it is quite a rare element. Low concentration of gold is contained in sea water, on the order of 10 μg per ton (10 parts of gold per trillion parts of water). On Earth, gold is found in ores in rock formed from the Precambrian time onward. Susan (2009) stated that gold often occurs as a native metal, naturally in a metal solid solution with silver. The metal in a native state is also found in the form of free flakes, grains or larger nuggetsthat have been eroded from rocks and end up in alluvial deposits called placer deposits Susan (2009).

2.4.5 Physical Characteristics

Gold is malleable, ductile, and sectile, which have high thermal and electrical conductivity as well as its resistance to oxidation which make its uses innumerable (Harold, *et al.,* 1997).Gold can be hammed with other metals into thin sheets, 10 times as thin as a sheet of paper and these sheets can be evaporated onto glass for infrared reflectivity, molded as fillings for teeth or used as a coating or plating for parts. The ability of gold to be drawn into thin wire enables it to be deposited onto circuits such as transistors and to be used as an industrial solder and brazing alloy. An example is the use of gold wire in integrated circuit electrical connections, prosthetic appliances, and in jet engine fabrication.

2.4.6 Mining

The gold form from lode deposit is obtained by drilling, or shoveling surrounding rock. Small explosives and picks are used to remove the gold ore from the surrounding rock. The gold from placer deposits contain large pieces of gold ore (nuggets) and grains of gold that have been washed downstream from a lode deposit and that are usually mixed with sand and gravel. The three main methods used to mine placer deposits which include hydraulic mining, dredging, and power shoveling. All the methods involve the use of gravity as the basic sorting force. In the first method, a machine called a "hydraulic giant" uses a high-pressure stream of water to knock the gold ore off the banks containing the ore. The gold ore is then washed down into sluices or troughs that have grooves to catch the gold. Dredging and power shoveling involve the same techniques but work with different size of buckets or shovels. In dredging, buckets on a conveyor line scoop sand, gravel, and gold ore from the bottom of streams. In power shoveling, huge machines act like shovels and scoop up large quantities of gold bearing sand and gravel from stream beds. Hydraulic mining and dredging are outlawed in many countries because they are environmentally destructive to both land and streams.

2.4.7 Extraction and Refining

Gold metal is usually found in pure state; however, it can also be extracted from silver, copper, lead and zinc, Seawater can also contain gold, but in insufficient quantities to be profitably extracted- up to one fortieth (1/40) of a grain of gold per ton of water. The mining technique used to extract the gold depends upon the types of deposit Harold*et al*., (1997). The Miller process is used to refine gold to a high degree of purity99.95%. The chemical process involves blowing a stream of pure chlorine gas over and through a crucible filled with molten, but impure gold. Noyes (1993); Pletcher and Walsh, (1990) stated that the process purifies the gold and almost all other elements will form chlorides before gold does and they can be removed as salts that are insoluble in the molten metal. Noyes (1993); Pletcher and Walsh, (1990), stated another method called Wohlwill process which is commonly used for producing high-purity gold. The process produces 99.999% purity. When highest purity gold is not required, refiners often utilize

the Miller process due to its relative ease, quicker turnaround times, and because it does not tie up the large amount of gold in the form of chloroauric acid which the Wohlwill process permanently requires for the electrolyte Noyes(1993); Pletcher and Walsh, (1990).

2.4.8 Gold Pan

The sole piece of equipment that all prospectors need is gold pan. No matter if you run your material through a sluice, high banker or dredging, it all ends up in a gold pan. Gold panning can be exciting as well as rewarding. The panning method is an activity that can be enjoyed by all ages. The most common sizes of gold pans are 8 to 12-inch pan, used primarily for sampling, or clean up. The 14-inch pan is a good multi use pan and seems to be the most popular size. This size of gold pan is useful when working on moderate volume of gravels. Ajeigbe *et al*., (2014), stated that when prospecting for vein gold, a prospector typically washed the gravels in stream beds in a gold pan that is used for separating heavy mineral particles from the lighter stream gravels and silt. Where evidences of gold collected in the pan continued, he would work his way up the stream bed, progressively planning along the way, in the hope of finding it source (the mother Lode) whose outcrop was concealed by the weathering products of the hillside rocks. Ajeigbe *et al*., (2014).

2.5 Effects of Gold Exposure

Dirty gold mining has ravaged landscapes, contaminated water supplies, and contributed to the destruction of vital ecosystems. Cyanide, mercury, and other toxic substances are regularly released into the environment due to dirty gold mining.

2.5.1 Health effects of gold

*When*inhale, it may cause irritation if exposure is prolonged or excessive. Ingestion: No adverse effects expected. Skin: May cause irritation and allergic reaction. Eye: May cause irritation. Gold is used to cure rheumatoid arthritis, under a treatment called *Chrysoteraphy.* It is prescribed when treatment with non-steroid anti-inflammatory drugs is failing to give relief.

2.5.2 Environmental Effects of gold

Gold has not been evaluated for its ecotoxicity. Gold is insoluble; it is believed to have minimal bioaccumulation and bioavailability characteristics. However, the biodegradation of gold under aerobic conditions is expected to be very poor and there is no evidence to suggest it creates ecological problems when released into the environment.

2.6 Heat in the Earth

The heat flux coming from inside the Earth can be measured at the surface. One must also have some idea of the sources of the heat that is transported through the mantle and finally radiated out at the surface.

2.6.1 Sources of heat in the earth

These include the original and those currently produced in the Earth (Porier, 2000). The major heat source is from radioactivity and heat from other sourcessuch as heat from the liquid core and the materials that are present at different regions of the earth interior. The original heat is the heat content of the Earth in the early stages of its history (Porier, 2000). It is essentially heat, due to the dissipation of the gravitational energy when planetesimals bombarded the surface of the growing Earth, which eventually partly melted (Porier, 2000). There was also contribution of short-lived, now extinct, radioactive elements such as ^{26}Al. It is believed that the original heat contributes little to the thermal budget, with the exception of the heat stored in the liquid core.

The decay of the radioactive elements present in the mantle is the main source of heat in the Earth. The principal radioactive elements are: ^{235}U, ^{238}U, ^{232}Th whose decay eventually gives ^{207}Pb, ^{206}Pb, ^{208}Pb respectively, and ^{40}K whose decay gives ^{40}Ca and ^{40}Ar. The heat production per mass unit of each element is well known but their concentration in the Earth is much less certain (Porier, 2000). One estimate (Verhoogen, 1980) leads to the approximate lower bound of 2.4×10^{13} W for the total radiogenic production of heat in the mantle. Radiogenic heat production

is concentrated in continental material, implying that continental roots may cool more rapidly than the underlying mantle because of radiogenic decay (Chloe and Claude; 2007).

Other sources of heat include tidal dissipation in the solid Earth and latent heat released in exothermal phase transitions (e.g. olivine-spinel). However, in addition to the secular cooling of the core, a non-negligible contribution to the heat output of the core is made by the latent heat released during crystallization of the inner core and by the gravitational energy released as the fluid enriched in light elements by crystallization of the inner core rises.

2.7 Review of Existing Knowledge

A lot of works has been carried out on gold which includes: Melting of gold using piston cylinder apparatus with a high-pressure cavity by Jagannaddham and George,(1971).They determined the melting temperature of gold, silver and copper as a function of pressure to 65 kb using piston cylinder apparatus, after the appropriate corrections for the effect of pressure on the emf of thermocouple, the melting curves are linear with the isothermal volume of the melting solid to within the precision of the measurements.Temperature effects on the universal equation of state of solids according to Pascal *et al.*, (1987), they reported that for many solids, the input data needed to predict high temperature thermodynamic properties can be reduced dramatically such that only four numbers areneeded, when tested the predictionsusing experimentaldata for three representative solids: gold, sodium chloride and xenon, there was good agreement between theory and experiment. The determination of the Critical point of gold, using pressure vessel as studied by Boboridis *et al*., (1999), the authors used wire-shaped gold specimens which was placed in a new improved high-pressure vessel and determined the phase transition (critical point) of gold. Their results for temperature, pressure and specific volume at the critical point are as follows: $T_C = 7400 \pm 1100\ K$, $P_C = 530 \pm 20\ MPa$ and $V_C = 0.13 \pm 0.03\ \times 10^{-3}\ m^3.kg^{-1}$.Geochemistry of gold in which the role of organic matter and the source of Au in Sediment Hosted Disseminated Gold (SHDG) mineralization was studied using Rock-eva analysis as studied by Zhiwei, (2001). The author reported that gold in the deposits is most likely derived from a mixed source that includes the host rocks. This study confirmed that there is no correlation between the organic contents and Au concentrations in the

ores. The use of electrical resistivity to delineate gold deposit was carried out by Bello (2012). He carried out electrical resistivity survey on area suspected to have gold deposit. The apparent resistivities obtained from the profiling were used to draw contour lines from eighteen vertical electrical sounding (VES) points located out of which ten were sounded. The author reported that the results obtained from the VES indicated several points having apparent resistivity similar to mineral ores that bear gold.Abdullah *et al*., (2008) carried work on the effect of strain rate on ultra-fine gold wire by considered properties such as strength, yield point and strain, their results showed that the mechanical properties of ultra-fine gold wire are proportional with increasing strain rate. Colins(2014); construct stress-strain curves of gold thin films using force and displacement data and reported that the strain rates ranged from 10^{-6} s^{-1} to 10^{-3} s^{-1}, in which all the specimens exhibited elastic perfectly plastic behavior at all strain rates with the exception of the slowest strain rate $10^{-6}s^{-1}$ in which local stress peaks were observed. The stress-strain response of gold thin film was studied by Gudlavalletti *et al*., (2002) in which the values for ductility yield and maximum stress was reported. The authors reported that the thin-film was tested in simple tension using a novel testing machine which enables measurement of the elastic-plastic stress-strain response of the films with high resolution. Their results showed that there was low ductility resulted from lack of dislocation activity in the smaller grains, whose boundaries then serve as easier sites for alternative inelastic mechanisms such as grain boundary sliding and the cohesion leading to low macroscopic strains to failure.Espinosa and Prorok, (2003); also carried out the studies on gold thin films, it was reported that the size effects on mechanical behavior of gold using a Membrane Deflection Experiment (MDE) was investigated and was observed that a width of $2.5\,\mu m$ and a thickness of $0.5\,\mu m$ correspond to major transitions in the material deformation behavior. Also, Li, (2003), reported the values for bulk modulus and yield strength on thin films gold. The measurement of strain rates for polycrystalline tantalum ranged from $10^{-4}\ to\ 10^{+4}s^{-1}$ was reported by Hoge and Mukherjee, (1977). The strain rate for copper and aluminium crystals usingmultiscale model was investigated by Shehadeh *et al.,* (2005). Computer simulations was carried out under condition of high strain rates ranging from 10^{5}–10^{7} s^{-1}, the effects of strain rate, shock pulse duration and the nonlinear elastic properties are investigated. Relaxed configurations using dislocation dynamics show formation of dislocation micro bands and weak dislocationShehadeh *et al.,* (2005).

There is scanty information about temperature profile in the Lithosphere, the available temperature profile covers the depth from 100Km in the upper mantle to deeper depths.Among notable research carried out on stress include the origin of tectonic stress Bott and Kusznir, (1984), stress in the lithosphere (Zoback and Zoback, 2002)reported that in situ stress measurements and inferences based on topography and flexure all suggested that shear stresses in the upper lithosphere are fairly large and are controlled by the frictional strength of the faulted crust and maintain that this frictional failure is manifest as slow, steady-state creep deformation in the lower crust and upper mantle and brittle deformation in the upper crust.

The existing knowledge have not really involved the aspect of high pressure and high temperature as regards to the impact on volume of ore deposits and the source of gold deposits which is still a proposal. Also, some elements can be used as exploration tools for gold in an area when confirmed in the geochemistry of soil.Richard (1996), reported that soil geochemistry has proved an effective technique in exploration for gold, the author stated further that programme of soil geochemistry was conducted in an area previously explored by many different exploration groups using a variety of geochemical techniques which was based on the sampling of near-surface soil at depths of 10–20 cm, pulverizing and analyzing the < 2 mm fraction for Au and As. Anomalies related to mineralization were usually better developed in near-surface soil than deeper bedrock samples.

Also, there is scanty information about the temperature profile within the lithosphere. The available information of temperature profiles covers the lower mantle and the outer core, these profiles were derived in terms of the parametric earth model (PEM) found from normal modes of the earth according to Dziewonski *et al*., (1975). In this work we have determined the thermodynamic properties of unrefined gold deposits from Itagunmodi, SouthwestNigeria and the temperature profile in the lithosphere and the information was used in the determination of its source. Some values were given by some authors for the temperature profile among them are: Stacey (1977), Jeanloz and Richter (1979), Anderson (1980) and Brown and Shankland (1980). At the base of the lithosphere, different values of temperature were given by Watts, (2007), William, (2007), Chloe and Claude, (2007). The temperature profile in the upper mantle is not related to the seismic profile in the same way, the origin of temperature profiles in the upper mantle region were usuallyobtained from heat flow data extrapolations.

CHAPTER THREE

MATERIALS AND METHODS

3.1 The Study Area

The study area is Itagunmodi is included under materials and methods, the town is very close to towns such as: Ile-Ife and Ilesha in Osun State, Southwest Nigeria, the town is under Atakunmosa local government area in Osun state. The gold deposits from Itagunmodi are located in the clayey soil types which have been derived from variably migmatised gneiss, biotite-and-biotite hornblende-gneiss and weathered amphibolite respectively. Itagunmodi is located on latitude $7^{o}31^{'}60^{''}N$ longitude $4^{o}39^{'}0^{''}E$ and altitude (meters) 347 the time zone is east. The approximate population for 7km radius from this point is 12655. The analyses were carried out on thirty gold samples that were selected from different locations in Itagunmodi Southwest Nigeria. The sites locations were divided into five main zones namely A to E. Six samples was taken from each zone for analyses. Thereafter, the unrefined gold samples were taken to the laboratory for analyses. The zones were labeled in the following order:

Zone A comprises of samples 1- 6, zone B contains samples 7-12, zone C contains samples 13-18, zone D contains samples 19-24 while zone E comprises of samples 25-30 respectively. The latitude and longitude of the site are shown in Table 3.1.

The geology of the study area is Precambrian basement complex gneisses, migmatised and Schist associated with amphibolite. The map of Itagunmodi gold mining town is shown in Figure 3.1a while the map showing the location of the site isshown in Figure 3.1b.

Table 3.1: Latitude and longitude of the Sites

Zone	Latitude (North)	Longitude (East)
A	$7^{\circ}\ 31^{'}$	$4^{\circ}\ 39^{'}$
B	$7^{\circ}\ 32^{'}$	$4^{\circ}\ 39^{'}$

C $7^{\circ}\ 31^{'}\ 4^{\circ}\ 39^{'}$

D $7^{\circ}\ 32^{'}\ 4^{\circ}\ 39^{'}$

E $7^{\circ}\ 31^{'}\ 4^{\circ}\ 38^{'}$

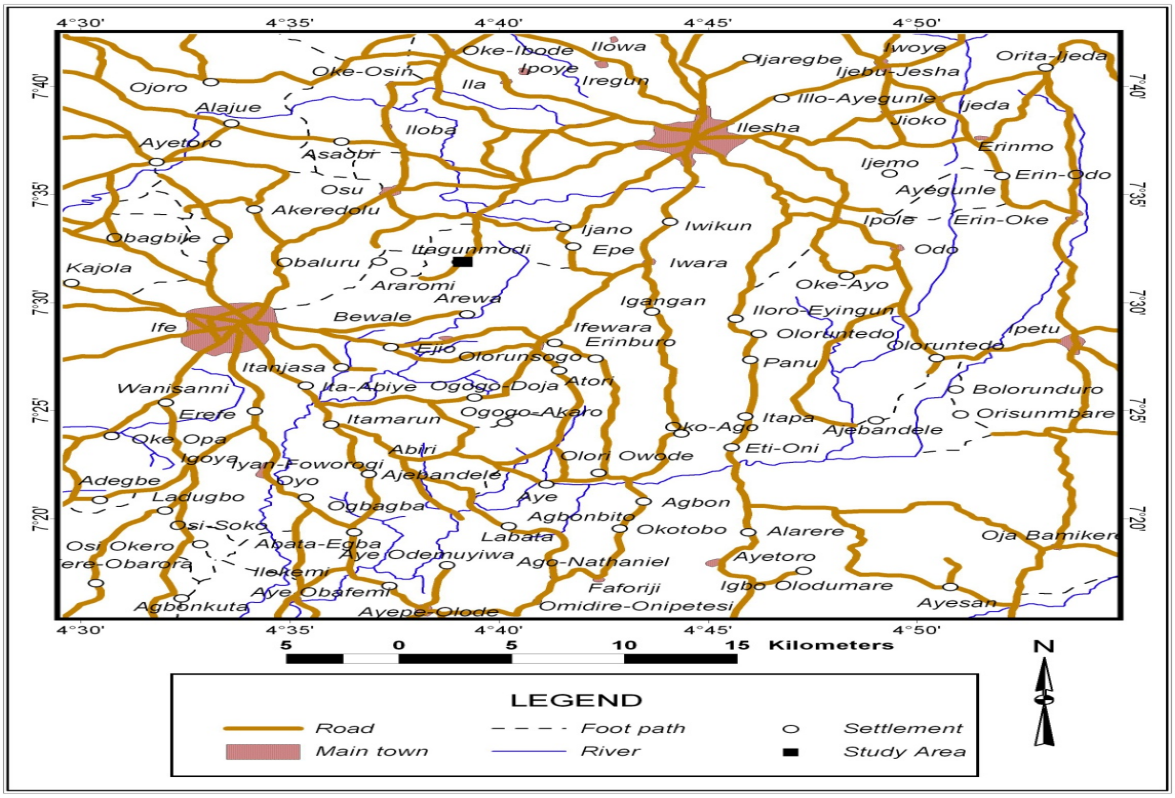

Figure 3.1a: Map of the Study Area

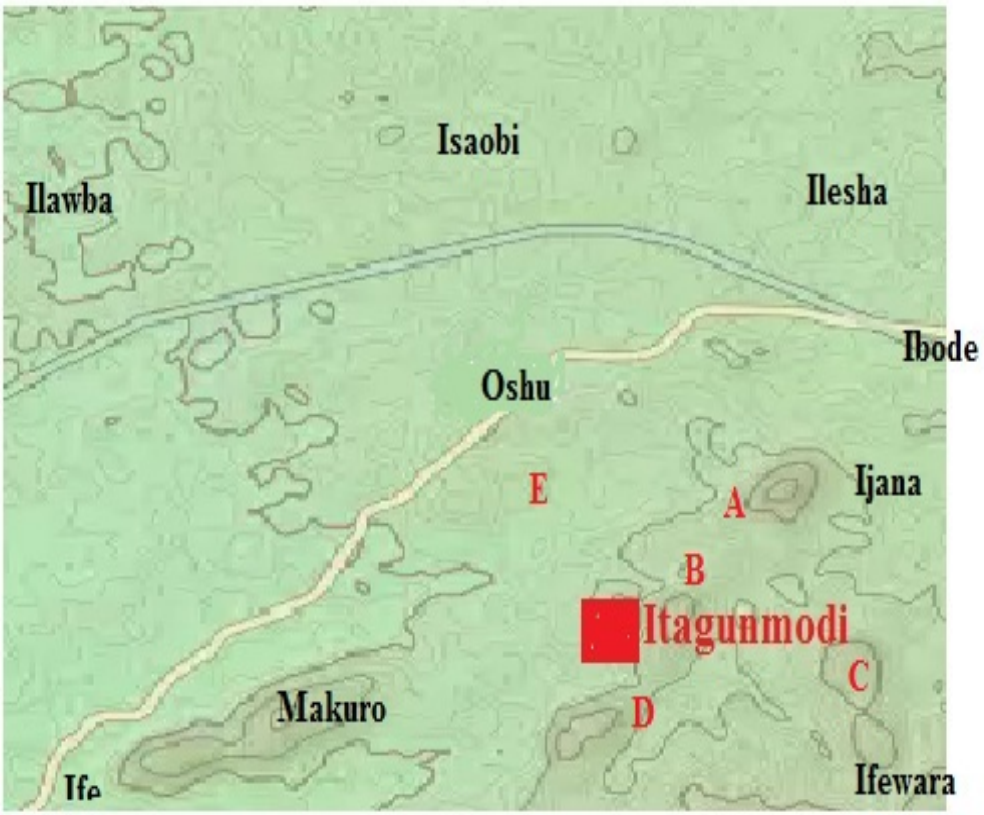

Figure 3.1b: Location Map of the Site

3.2 Mining Site

The following Figures 3.2 (a-d) shows some of the mining sites

Figure 3.2a: Itagunmodi Gold Mining Site

Figure 3.2b: Itagunmodi Gold Mining Site

Figure 3.2c: Itagunmodi Gold Mining Site

Figure 3.2d: Itagunmodi Gold Mining Site

3.3 Procedure for Atomic Absorption Spectrophotometer

The most accurate and sensitive method used in analyzing of wide range of metals is the Atomic Absorption Spectroscopy (AAS). The efficiency of detection is enhanced by overcoming the restrictions associated with flame photometry. In the analyses, a representation of the rock sample was first pulverized and digested using wet method of digestion in nitric acid. About 0.5g of each sample was measured into the dry digestion tube; 3 to 4 drops of distilled water were added to wet the sample. Thereafter, 5ml of hydrochloric acid was added to the sample and the solution was stirred. The digesting tube was left overnight without warming. The samples were leached out with 5ml of 6M hydrochloric acid into a measured test tube and made up to 20ml mark with distilled water. In other to avoid cracking, the content was shaken vigorously and the resulting solution was referred to as solution. The stock was used directly to determine the elements.

3.4 Determination of Pressure and Temperature using Improved High-Pressure Vessel

The gold samples were placed in an improved high- pressure vessel, the pressure vessel is part of a fast capacitor discharged circuit and it has a static pressure above $600\ MPa$that can be reached with distilled water and the pressure transmitting medium. The voltage drops across it and the temperature were recorded as a function of time. The initial volume (V_0), the room temperature (T_0) and the initial pressure (P_0) of the samples were recorded. Thereafter, subsequent values of pressure, temperature and volume of the samples were recorded as the temperature increased with time. The laboratory analyses carried out on the samples was repeated three times for each of the sample and their average values were recorded. During the heating period, the current through the samples, voltage across the samples, were measured as function of time. Since the main emphasis of this work was to investigate the effects of high pressure and high temperature on the volume of the samples as functions of the surrounding pressure which were measured with pressure gauge and the temperature was measured from the thermocouple or thermo well which is within the vessel. The volume of gold was measured with graduated attached cylindrical flask. The data were analyzed using Mie-Grüneisen equation of state. The model was applied to determined thermal pressure (ΔP_{Th}), compressed volume ($\Delta V/V$) and the bulk modulus (K_T) and also to predict the future state of the gold from that location.The picturesbelow

(Figure 3.3) represent high pressure and high temperature vessel and the attached temperature controller unit while Figure 3.4 is 4842 Temperature Controller with Expansion Options.

In this work we looked at stress in the lithosphere from the surface at $0\ Km$ to the depth of $150\ Km$, the rate of Stress in the Crustal part of the lithosphere were compared to that of the mantle part of the lithosphere and examined the kind of disparity in these values.

Figure 3.3: High Temperature/High Pressure Reactor,
500mL, with 4842 Temperature Controller

Figure 3.4: 4842 Temperature Controller with Expansion Options

3.4.1 The Values of Initial Temperature and Pressure of Samples

The following initial values were recorded for temperature, pressure and volume for sample 1:

Initial temperature,$T_0 = 42.0$ ℃

Initial pressure,$P_0 = 0.0\ MPa$

Initial volume of the sample,$V_0 = 0.150 * 10^{-3}\ m^3$

The initial values for temperature, pressure and volume for sample 2 are recorded below:

Initial temperature,$T_0 = 42.0$ ℃

Initial pressure,$P_0 = 0.0\ MPa$

Initial volume of the sample,$V_0 = 0.160 * 10^{-3}\ m^3$

The following initial values were recorded for temperature, pressure and volume for sample 7:

Initial temperature,$T_0 = 42.0$ ℃

Initial pressure,$P_0 = 0.0\ MPa$

Initial volume of the sample,$V_0 = 0.142 * 10^{-3} m^3$

The initial values for temperature, pressure and volume for sample 8 are recorded below:

Initial temperature,$T_0 = 42.0$ ℃

Initial pressure,$P_0 = 0.0\ MPa$

Initial volume of the sample,$V_0 = 0.144 * 10^{-3}\ m^3$

The following initial values for temperature, pressure and volume for sample 13 are recorded:

Initial temperature,$T_0 = 42.0$ ℃

Initial pressure,$P_0 = 0.0\ MPa$

Initial volume of the sample,$V_0 = 0.144 * 10^{-3}\ m^3$

The initial values for temperature, pressure and volume for sample 14 are recorded below:

Initial temperature,$T_0 = 42.0$ ℃

Initial pressure,$P_0 = 0.0\ MPa$

Initial volume of the sample,$V_0 = 0.162 * 10^{-3}\ m^3$

The initial values recorded for temperature, pressure and volume for sample 19 are stated below:

Initial temperature,$T_0 = 42.0$ ℃

Initial pressure,$P_0 = 0.0\ MPa$

Initial volume of the sample,$V_0 = 0.169 * 10^{-3}\ m^3$

The initial values recorded for temperature, pressure and volume for sample 20are stated below:

Initial temperature,$T_0 = 42.0$ ℃

Initial pressure,$P_0 = 0.0\ MPa$

Initial volume of the sample,$V_0 = 0.170 * 10^{-3} m^3$

The initial values recorded for temperature, pressure and volume for sample 25 are stated below:

Initial temperature,$T_0 = 42.0$ ℃

Initial pressure,$P_0 = 0.0\ MPa$

Initial volume of the sample,$V_0 = 0.178 * 10^{-3}\ m^3$

The initial values recorded for temperature, pressure and volume for sample 26 are stated below:

Initial temperature,$T_0 = 42.0$ ℃

Initial pressure,$P_0 = 0.0\ MPa$

Initial volume of the sample,$V_0 = 0.180 * 10^{-3}\ m^3$

3.5 Theoretical Background

3.5.1 Mie-Grüneisen Equation of State

The increase in internal pressure ΔP_{Th} caused by heating a solid at constant temperature (thermal pressure) is given by the equation below;

$$\left(\frac{\partial P}{\partial T}\right)_V = \alpha K_T = \gamma_{th}\frac{C_V}{V} \tag{3.1}$$

Integration of (3.1) at constant volume also yields:

$$\Delta P_{Th} = P_2 - P_1 \equiv \frac{\lambda_{th}}{V}\int_{T_1}^{T_2} C_V\, dT = \frac{\gamma_{th}}{V}(E_2 - E_1) = \gamma_{th}\frac{\Delta E}{V} \tag{3.2}$$

Where E is the internal energy. Hence:

$$\Delta P_{Th} = \gamma_{th}\frac{\Delta E}{V} \tag{3.3}$$

This is the equation of state of Mie-Gruneisen. The Gruneisen parameter is the coefficient relating the thermal pressure to the thermal energy per unit volume:

$$\gamma_{th} = V\frac{\Delta P_{Th}}{\Delta E} \tag{3.4}$$

The integration of (3.1) at constant volume also yields:

$$\Delta P_{Th} = \int_{T_1}^{T_2} \alpha\, K_T dT \tag{3.5}$$

$$\frac{\Delta P_{Th}}{K_T} = \frac{\Delta V}{V} = \alpha \Delta T \tag{3.6}$$

$$\frac{\Delta V}{V} = \alpha(T - T_0) \tag{3.7}$$

$$\frac{\Delta P_{Th}}{K_T} = \frac{\Delta V}{V} \tag{3.8}$$

$$\frac{\Delta P_{Th}}{K_T} = \alpha \Delta T \tag{3.9}$$

$$\alpha = \frac{1}{T}\frac{dV}{V_0} \tag{3.10}$$

The volume strain is given the relation:

$$\Delta\eta = 1 - \frac{V}{V_0} \tag{3.11}$$

The melting temperature T_m and the volume of a solid phase $\Delta V / V_0$ can be related by the equation:

$$T_m = T_m^{\,0}\{1 + C[\Delta V / V_0]\} \tag{3.12a}$$

The melting curve temperatures were obtained from the equation below:

$$t = t_0 + b_1 P + b_2 P^2 + b_3 P^3 \tag{3.12b}$$

where b_1, b_2, b_3 are constants called melting-curve parameters. This show that the melting point of the materials increases with increase in pressure

3.5.2 Determination of temperature profile in the lithosphere from fourier'slaw

In the crustal part of the lithosphere, radioactivity is strongly concentrated and there is upward concentration of it within the crust. The heat flux, Q_0, and radiogenic heating q_0, of surface rocks are both variable, when these variables were correlated, the correlation leads to a simple model

for the depth distribution of heat sources. According to Lachenbruch (1970), it was noted that a linear relationship exists between them and that relation is given by the equation below:

$$\dot{Q}_0 = A + B\dot{q}_0 \tag{3.13}$$

the equation could be explained by assuming an exponential variation of radiogenic heat with depth,

$$\dot{q}_0 = q_0 \exp(-z/z_0) \tag{3.14}$$

The total crustal heat, Q_C is the integral from the surface to the mantle–crust boundary at depth z_{MC},

$$\dot{Q}_C = \dot{q}_0 \int_0^{z_{MC}} \exp(-z/z_0)dz \tag{3.15}$$

$$\dot{Q}_C = \dot{q}_0 z_0[1-\exp(-z_{MC}/z_0)] \approx \dot{q}_0 z_0 \tag{3.16}$$

We require $z_{MC} \geq z_0$. Then $B = z_0$ and A=Q_{MC} is the heat flux from the mantle into the crust. With the above equations of crustal heat, the temperature profile was calculated.

The Fourier's law was used in the calculation of the temperature profile in the Lithosphere. The Fourier's law is the heat flux, Q, through a surface at any depth z, using equation below:

$$\dot{Q} = k_C \frac{dT}{dz} = \dot{Q}_{MC} + \dot{q}_0 z_0 - \int_0^z \dot{q}dz \tag{3.17a}$$

$$k_C \frac{dT}{dz} = \dot{Q}_{MC} + \dot{q}_0 z_0 \exp(-z/z_0) \tag{3.17b}$$

The temperature profile is calculated as stated in the equation below

$$T(z) - T_0 = \frac{\dot{Q}_{MC} z}{k_c} + \frac{\dot{q}_0 z_0}{k_c} \int_0^z \exp(-z/z_0)dz \tag{3.18a}$$

$$T(z) - T_0 = \frac{\dot{Q}_{MC} z}{k_C} + \frac{\dot{q}_0 z^2}{k_C} \exp(-z/z_0) \tag{3.18b}$$

The crustal part is calculated using equation 3.18b while the mantle part was calculated using the equation 3.19:

$$T(z)-T_M=\frac{\dot{Q}_{AM}z}{k_M}+\frac{\dot{q}_M z_0}{k_M}\int_0^z \exp(-z/z_M)dz \qquad (3.19a)$$

$$T(z)-T_M=\frac{\dot{Q}_{AM}z}{k_M}+\frac{\dot{q}_M z^2}{k_M}\exp(-z/z_M) \qquad (3.19b)$$

Equation 3.19b was used to calculate the profile for the mantle part of the lithosphere.

3.5.3 Determination of stress and bulk modulus in the lithosphere

The model proposed from Heim's rule that the assumption of a lithostatic state as we penetrate deeper into the Earth's crust was applied in calculation of stress from the surface to the depth of the lithosphere. The stress is given by the equation stated below:

$$P(z)=\int_0^Z \rho(z)gdz=\rho gz \qquad (3.20)$$

Where g is the gravitational acceleration and z is the depth within the Earth's crust, while ρ is the density of the layers of the Earth and P is the stress.

CHAPTER FOUR

RESULTS AND DISCUSSIONS

4.1 Results of Elemental Analyses

The table below shows the elements present in soil samples collected from Itagunmodi gold deposit's sites.

Table 4.1 consist of the following elements; Iron (Fe), Copper (Cu), Zinc (Zn), Manganese (Mn) and Barium (Ba), respectively, they were confirmed from the elemental analysescollectively called pathfinder elements. Apart from the elements mentioned above, there was also black soil that was found in the mining sites, this soil can be used as exploration tool. The elements together with the black soil can be used as one of the rudimentary tools in search of these types of minerals.When these elements are confirmed in the geochemistry of soil; it gives the sign that gold is present in the area.

4.2 Results of the Laboratory Analyses Carried Out on Gold Samples

The results of experimental analyses carried out on the selected unrefined gold samples were shown in Tables 4.2 - 4.31.

Table 4.1: Trace Element composition (ppm)

Ba	Rb	Ce	Zr	Cr	V	Zn	Cu	Fe	Mn
67.22	8.02	3.40	1.52	11.22	1.76	21.02	2.16	7.65	0.02

Table 4.2: Average Values of Temperature, Volume and Pressure (sample 1)

Time (hr)	T ^{o}C	V*10^{-3}ΔV (m^3)	ΔV/V_0 (m^3)	V/V_0 Strain	P (Mpa) Stress	ΔP (Mpa)	B (Gpa) Strain	ΔηΔP_{TH} Volume	(Gpa)
0.5	2328.	10.143	0.007	0.047	0.953	436.4	406.4	8.65	0.047	0.831

Table 4.3: Average Values of Temperature, Volume and Pressure (sample 2)

Time (hr)	T °C	V*10^{-3} (m^3)	ΔV (m^3)	ΔV/V$_0$ Strain	V/V$_0$ Stress	P (Mpa)	ΔPB (Mpa)	Δη (Gpa)	Strain Volume
0.5	2329.2	0.152	0.008	0.050	0.950	438.5	408.5	8.17	0.050
1.0	2388.4	0.141	0.019	0.119	0.882	450.7	420.7	3.54	0.119

The obtained unrefined gold samples collected from zone A were shown in Tables 4.2 and4.3 respectively. Six samples were analyzed. Tables 4.4 – 4.7 containing the results for other four samples in the zone were shown in Appendix II.

The results of the laboratory analyses recorded for sample 1 are shown in Table 4.2, there is compression in volume and it was also observed that the bulk modulus decreased with increase in both temperature and pressure while the volume strain increased with increase in both

temperature and pressure.The implication of increase in volume strain was the effect that the application of pressure created on the sample by lowering the volume while the increase in temperature will not cause any increase in the volume because of the negative impact of pressureon the sample. The graph of volume strain against time and the graph of bulk modulus against temperature for sample 1 are shown in Figures 4.1a and 4.1b.

Figure 4.1a represents the graph of volume strain against time for sample 1. In the figure, the strain rate was 0.000027 s^{-1},the rate increased with increase in time which conformed to literature laboratory values for materials, examples of the materials with such character are Polycarbonate (PC), Polymethylmethacrylate (PMMA), and Polyamideimide (PAI) was reported by Richeton and Adharapurapu, (2006). The coefficient of sample determination which determine the goodness of the fit was 0.9895.

Figure 4.1b represents the graph of bulk modulus against temperature for sample 1, it was noticed from the graph that the bulk modulus of the sample decreased with increase in temperature. The behavior of the sample showed that the materials of this kind exhibit a kind of volume compression which increased with rise in both temperature and pressure.

From Table 4.3, it was also noticedthat the bulk modulus decreased with increase in both temperature and pressure while the volume strain increased with increase in both temperature and pressure. Also, there was compression in volume as a result of the application of pressure on the sample, the higher the pressure the more volume compressed. There was similar observation in the trend of the results obtained for sample 2. The graph of volume strain against time and the graph of bulk modulus against temperature for sample 2 are shown in Figures 4.2a and 4.2b.

Figure 4.2a represents the graph of volume strain against time for sample 2. In the figure, the strain rate was 0.000026 s^{-1}, this rate increased with increase in time which also conformed to literature laboratory values for materials, Vani *et al.,* (2004) reported some examples such as Chromium, Molybdenum, Niobium and Iron whose strain rate increased with time increase; the coefficient of sample determination for goodness of the fit was 0.9947.

The graph of bulk modulus versus temperature for sample 2 is shown in Figure 4.2b, the effect of rise in temperature result to a decrease in the bulk modulus of the sample as seen from the appearance of the shape the graph. There was a large drop in the bulk modulus at the initial heating period follow by a gradual drop in its values.

The graphs for Tables 4.4 – 4.7 are shown in Appendix II.

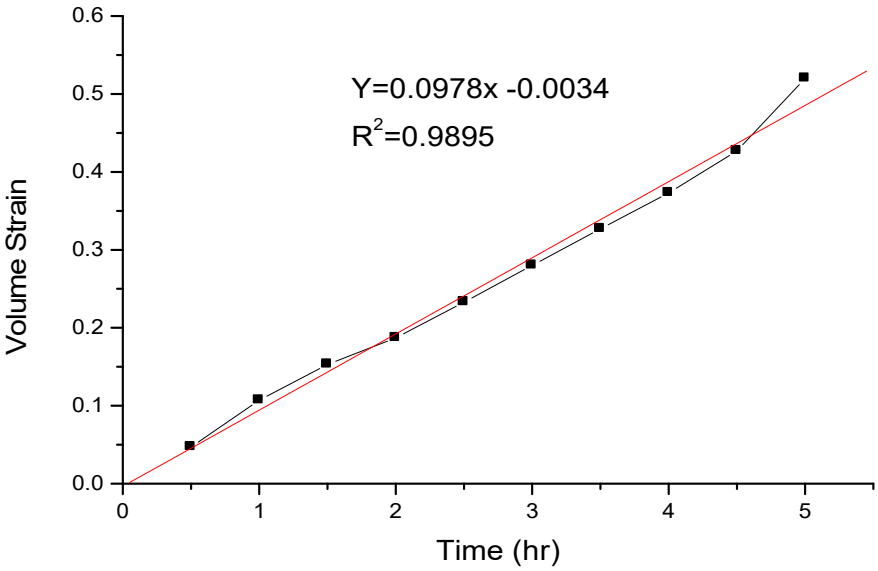

Figure 4.1a: Volume Strain Plotted AgainstTime (sample 1)

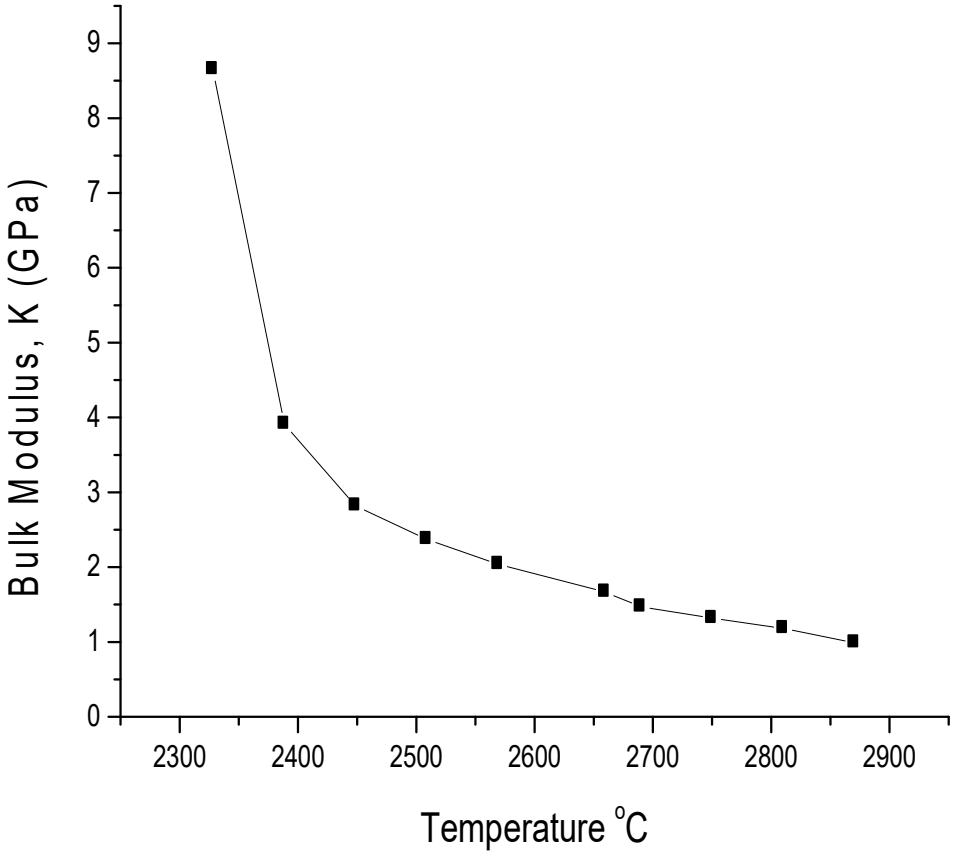

Figure 4.1b: Bulk Modulus AgainstTemperature (sample 1)

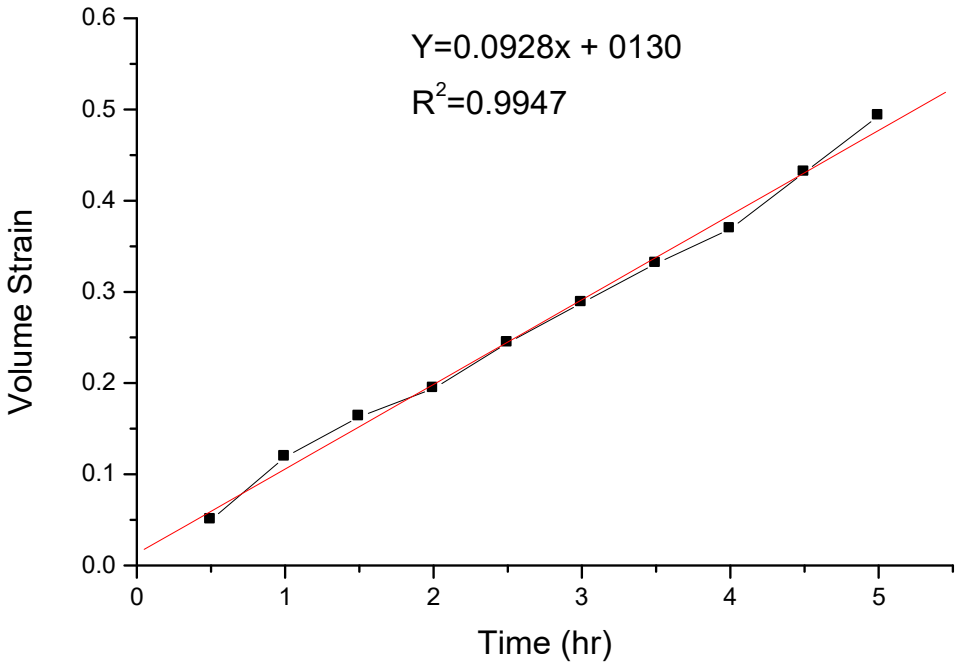

Figure 4.2a: Volume Strain Plotted AgainstTime (sample 2)

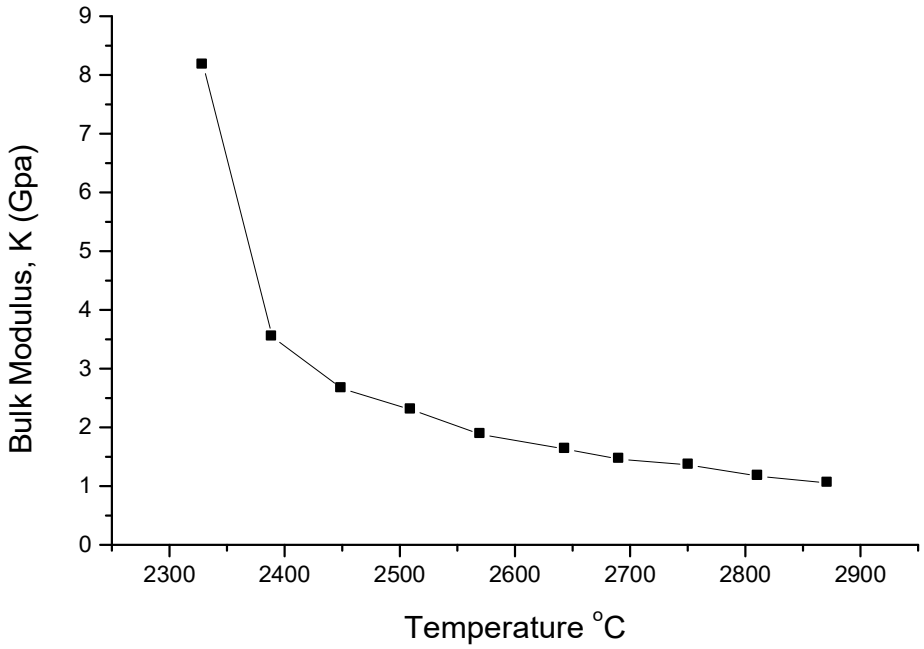

Figure 4.2b: Bulk Modulus AgainstTemperature (sample 2)

Table 4.8: Average Values of Temperature, Volume and Pressure (sample 7)

Time (hr)	T °C	V*10^{-3} (m^3)	ΔV (m^3)	ΔV/V_0 Strain	V/V_0	P (Mpa)	ΔP (Mpa)	B (Gpa)	Δη Volume Strain
0.5	2310.2	0.135	0.007	0.049	0.951	431.0	401.0	8.18	0.049
1.0	2370.1	0.128	0.014	0.099	0.901	443.2	413.2	4.17	0.099
1.5	2429.9	0.121	0.021	0.148	0.852	455.2	425.2	2.87	0.148
2.0	2429.9	0.114	0.028	0.197	0.803	467.3	437.3	2.22	0.197
2.5	2549.5	0.107	0.035	0.246	0.754	479.3	449.3	1.83	0.246
3.0	2607.7	0.099	0.043	0.303	0.697	491.4	461.4	1.52	0.303
3.5	2669.2	0.092	0.050	0.352	0.648	503.4	473.4	1.34	0.352
4.0	2757.0	0.084	0.058	0.408	0.592	515.5	485.5	1.19	0.408
4.5	2788.8	0.076	0.066	0.465	0.535	527.6	497.6	1.07	0.465
5.0	2848.7	0.042	0.100	0.704	0.296	539.7	509.7	1.72	0.704

Table 4.9: Average Values of Temperature, Volume and Pressure (sample 8)

Time (hr)	T °C	V*10^{-3} (m^3)	ΔV (m^3)	ΔV/V$_0$ Strain	V/V$_0$ Stress	P (Mpa)	ΔPB (Mpa)	Δη (Gpa)	Volume Strain
0.5	2314.1	0.137	0.007	0.049	0.951	432.4	402.4	8.21	0.049
1.0	2375.1	0.130	0.014	0.097	0.903	444.5	414.5	4.27	0.097
1.5	2433.9	0.123	0.021	0.146	0.854	456.6	426.6	2.92	0.146
2.0	2493.8	0.117	0.027	0.188	0.813	468.7	438.7	2.33	0.188
2.5	2553.7	0.110	0.034	0.236	0.764	480.8	450.8	1.91	0.236
3.0	2613.7	0.103	0.041	0.285	0.715	492.9	462.9	1.62	0.285
3.5	2684.2	0.097	0.047	0.331	0.674	505.0	475.0	1.44	0.331
4.0	2733.5	0.089	0.055	0.382	0.618	517.1	487.1	1.28	0.382
4.5	2793.4	0.082	0.062	0.431	0.569	529.2	499.2	1.16	0.431
5.0	2853.3	0.044	0.100	0.694	0.306	541.3	511.3	0.74	0.694

Tables 4.8 and 4.9 were representations of tables obtained for the unrefined gold samples collected from zone B, in this zone, six samples were also analyzed. Tables 4.10 – 4.13 containing the results for other four samples in this zone were shown in Appendix II.

Table 4.8 represent the resultsof the laboratory analyses recorded for sample 7, there was an increase in volume strain because of the application of temperature and pressure on the volume

of the sample while there was also compression in volume. It was also observed that the relative volume decreased gradually with decreased bulk modulus for every observed rise in temperature and pressure. The graph of volume strain against time and the graph of bulk modulus against temperature for sample 7 are shown in Figures 4.7a and 4.7b.

From the graphical representation of volume strain against time for sample 7 shown in Figure 4.7a. The value of strain ratewas 0.000035 s^{-1}, the rate increased with increase in time, the following materials; Copper and Polycrystalline Tantalum reported by Sia*et al*., (1998) exhibit similar behavior; the coefficient of sample determination which determine the goodness of the fit for this sample was 0.9287.

From the graph of bulk modulus against temperature for sample 7 shown in Figure 4.7b, the rise in temperature result to decrease in bulk modulus of the sample. The behavior of the sample showed that the materials in this group show a decrease in thermal volumetric strain which increased with rise in temperature.

From Table 4.9, it was also noticed that the bulk modulus decreased with increase in both temperature and pressure while the volume strain increased with increase in both temperature and pressure. The implication is when temperature increase, molecules move faster and the intermolecular forces that kept them together becomeweaker and as a result, the pressure impacted on the substance increase the compressibility and the melting point of the sample.
The graph of volume strain against time and the graph of bulk modulus against temperature for sample 8 are shown in Figures 4.8a and 4.8b. The graphs for Tables 4.10 – 4.13 are shown in Appendix II.

Figure 4.8a represents the graph of volume strain against time for sample 8. The value of strain rate was 0.000033 s^{-1},the rate increased with increase in time which conformed to literature laboratory values for materials. Bing *et al*., (1997) reported Tantalum as an example of material with such behavior. The goodness of the fit was 0.9032.

Figure 4.8b represents the graph of bulk modulus against temperature for sample 8;it was observed that increase in temperatureresults todecrease in bulk modulus values for the sample as shown in the graph. The interpretation is that the sample belongs to group of materials whosevolume compression increased with rise in both temperature and pressure.

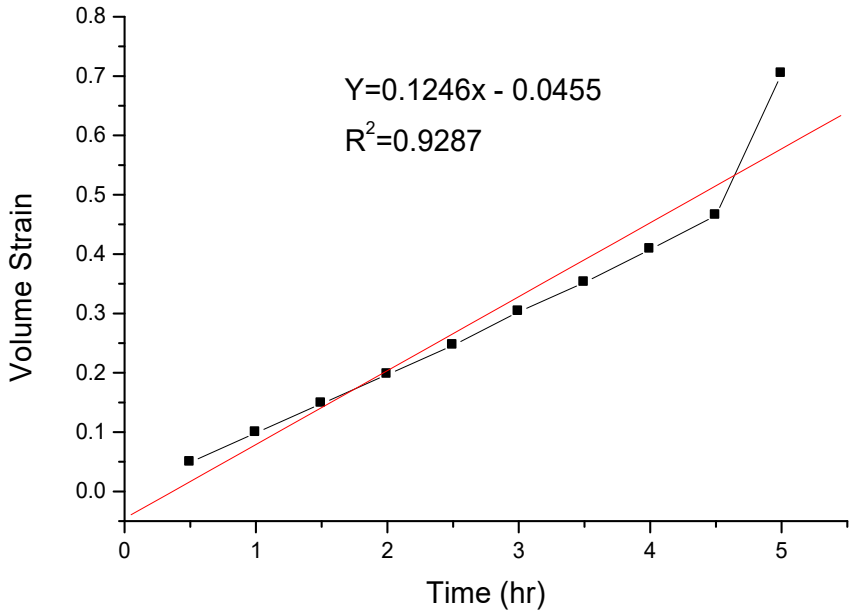

Figure 4.7a: Volume Strain Plotted AgainstTime (sample 7)

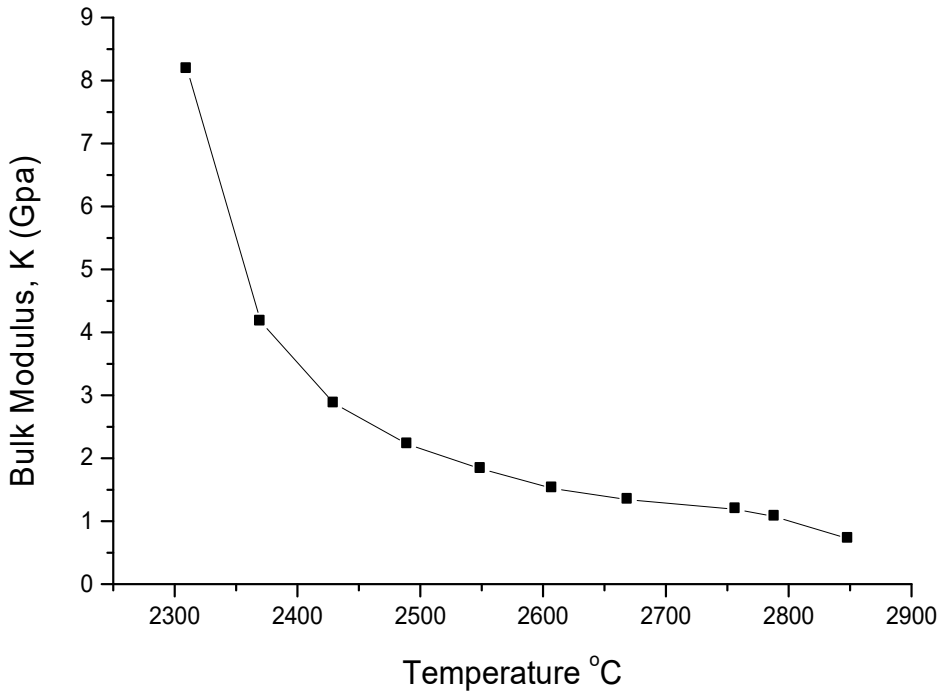

Figure 4.7b: Bulk Modulus AgainstTemperature (sample 7)

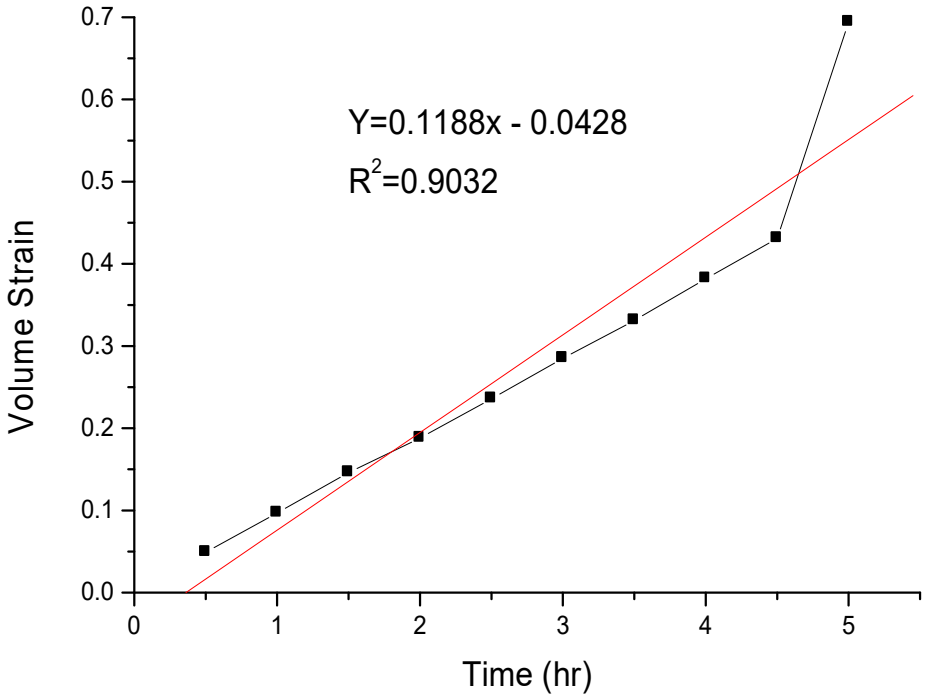

Figure 4.8a: Volume Strain Plotted Against Time (sample 8)

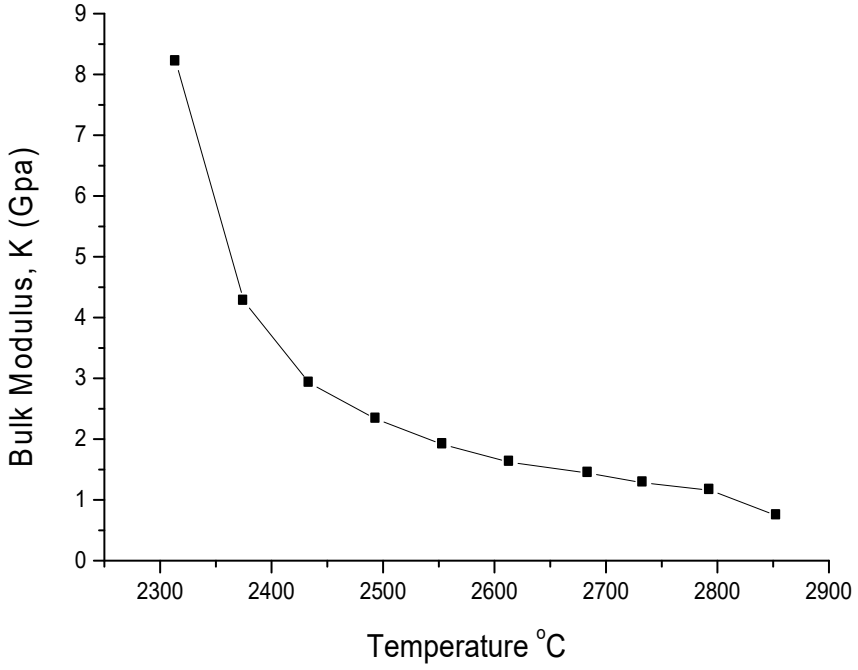

Figure 4.8b: Bulk Modulus Against Temperature (sample 8)

Table 4.14: Average Values of Temperature, Volume and Pressure (sample 13)

Time (hr)	T °C	V*10^{-3} (m^3)	ΔV (m^3)	ΔV/V_0 Strain	V/V_0	P Stress (Mpa)	ΔPB (Mpa)	Δη Strain (Gpa)	Volume
0.5	23	31.3	0.144	0.012	0.077	0.923	438.8	408.8	5.31	0.077
1.0	23	91.6	0.136	0.020	0.128	0.872	451.0	421.0	3.29	0.128
1.5	24	52.0	0.128	0.028	0.179	0.821	463.2	433.2	2.42	0.179
2.0	25	12.3	0.120	0.036	0.231	0.769	475.6	445.6	1.93	0.231
2.5	25	72.6	0.112	0.044	0.282	0.718	487.9	457.9	1.62	0.282
3.0	26	33.0	0.102	0.054	0.346	0.654	500.6	470.6	1.36	0.346
3.5	26	93.3	0.092	0.064	0.410	0.590	512.2	482.2	1.18	0.410
4.0	27	53.7	0.082	0.074	0.474	0.526	524.8	494.8	1.04	0.474
4.5	28	14.0	0.072	0.084	0.538	0.538	537.1	507.1	0.94	0.538
5.0	28	74.0	0.056	0.100	0.641	0.359	549.3	519.3	0.81	0.641

Table 4.15: Average Values of Temperature, Volume and Pressure (sample 14)

Time (hr)	T °C	V*10^{-3} (m^3)	ΔV (m^3)	ΔV/V_0 Strain	V/V_0 Stress	P (Mpa)	ΔP (Mpa)	B (Gpa)	Δη Volume
0.5	2333.4	0.150	0.012	0.074	0.926	439.9	409.9	5.54	0.074
1.0	2394.1	0.142	0.020	0.123	0.877	452.2	422.2	3.43	0.123
1.5	2454.5	0.134	0.028	0.173	0.827	464.5	434.5	2.51	0.173
2.0	2515.0	0.125	0.037	0.228	0.772	476.8	446.8	1.96	0.228
2.5	2575.3	0.116	0.046	0.284	0.716	489.1	459.1	1.62	0.284
3.0	2635.7	0.103	0.059	0.364	0.636	501.4	471.4	1.30	0.364
3.5	2696.1	0.093	0.069	0.426	0.574	513.7	483.7	1.14	0.426
4.0	2756.5	0.083	0.079	0.488	0.512	526.1	496.1	1.02	0.488
4.5	2816.9	0.073	0.089	0.549	0.451	536.7	506.7	0.92	0.549
5.0	2877.3	0.062	0.100	0.617	0.383	550.7	520.7	0.84	0.617

Tables 4.14 and 4.15 were representations of tables obtained for samples collected from zone C; six samples were also analyzed in this zone. Tables 4.16 – 4.19 containing the results for other four samples in the zone were shown in Appendix II.

The application of pressure on volume of sample 13 as seen in Table 4.14 result to lowering of bulk modulus and relativevolume of the sample $\left(\frac{v}{v_0}\right)$decreasedwith increase in both temperature and pressure as observed in the table, the significance of the increase in pressure and temperature

also increased the thermal volumetric strain of the sample. The graph of volume strain against time and the graph of bulk modulus against temperature for sample 13 are represented in Figures 4.13a and 4.13b.

Figure 4.13a represents the graph of volume strain against time for sample 13. In the figure, the value of strain rate was 0.000034 s^{-1},it observed from this graph that the rate increased with increase in time; according to report by Hiroyuki*et al*., (2018), the value conformed to literature laboratory values for materialssuch as Aluminium.The coefficient of sample determination for the goodness of the fit for this sample was 0.9911.

Figure 4.13b represents the graph of bulk modulus against temperature for sample 13, it was noticed from the graph that the bulk modulus of the sample decreased with increase in temperature. Consequently, the process of lowering the temperature applied on a material would increase its bulk modulus. It was also noticed from the graph that volume compression increased with rise in both temperature and pressure.

The results of the analysis for sample 14 was presented in Table 4.15,it was observed that the increase in temperature on the sample did not produce any increase in volume because of the negative impact that application of pressure had on it. Subsequently, bulk modulus decreasedwhile the volume strain increased with increase both temperature and pressure. The graph of volume strain against time and the graph of bulk modulus against temperature for sample 14 are shown in Figures 4.14a and 4.14b.

The graph of volume strain plotted against time forsample 14 is shown in Figure 4.14a.Thestrain rate was 0.000034 s^{-1}as displaced in the figure which also increased with time increment, the coefficient of sample determination which determine the goodness of the fit was 0.9970.

The graph of bulk modulus plotted against temperature for sample 14 is shown in Figure 4.14b. The application of temperature on the sample caused decreased in bulk modulus as seen from the graph. The relation between bulk modulus and temperature shown in the figure implies that volume compression increased with rise in both temperature and pressure.

The graphs for Tables 4.16 – 4.19 are shown in Appendix II.

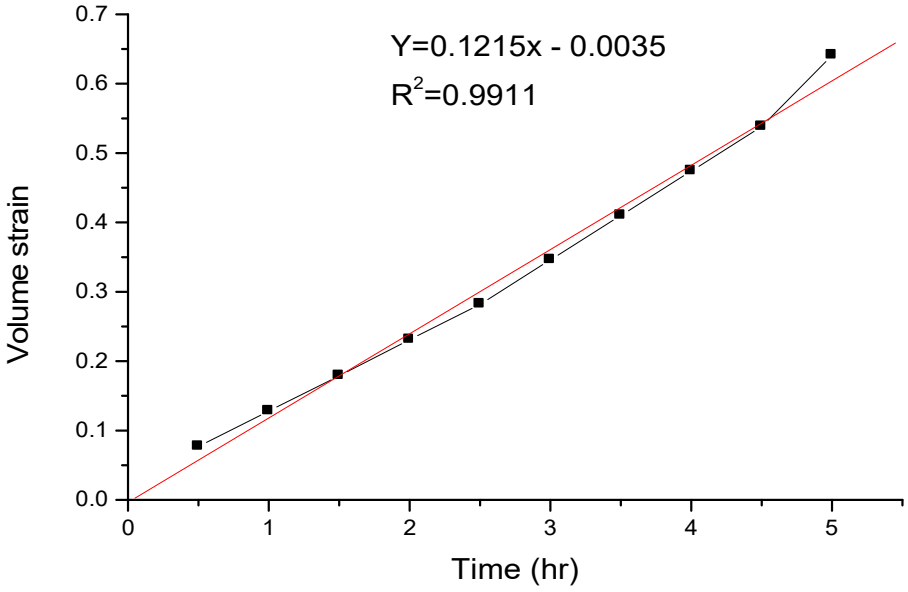

Figure 4.13a: Volume Strain Plotted Against Time (sample 13)

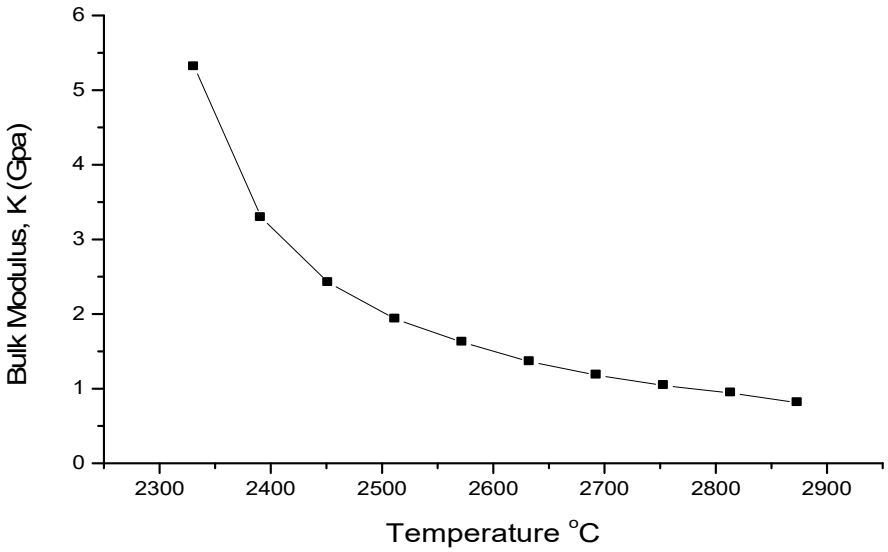

Figure 4.13b: Bulk Modulus Against Temperature (sample 13)

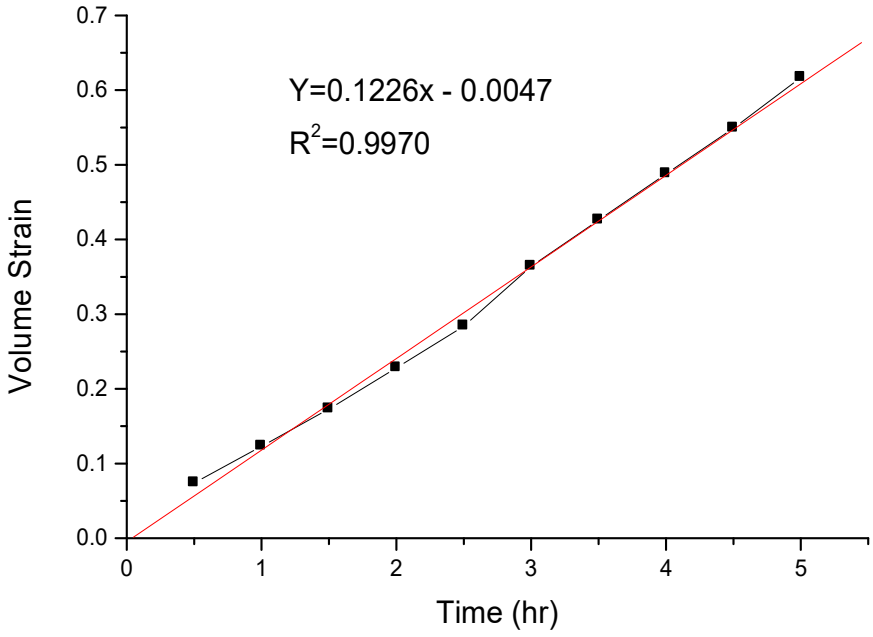

Figure 4.14a: Volume Strain Plotted Against Time (sample 14)

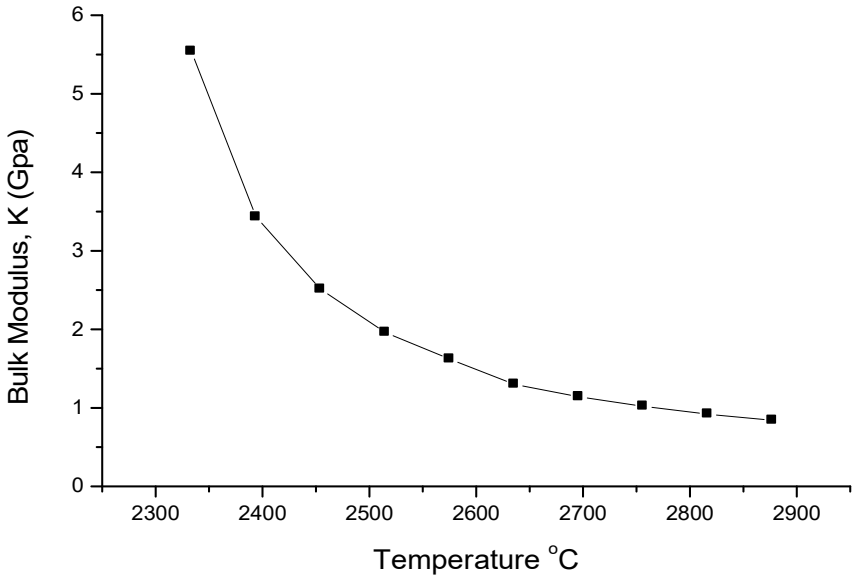

Figure 4.14b: Bulk Modulus Against Temperature (sample 14)

Table 4.20: Average Values of Temperature, Volume and Pressure (sample 19)

Time (hr)	T °C	V*10^{-3} (m^3)	ΔV (m^3)	ΔV/V_0 Strain	V/V_0 Stress	P (Mpa)	ΔP (Mpa)	B Gpa)	Δη Volume
0.5	2341.2	0.158	0.011	0.065	0.935	445.2	415.2	6.39	0.065
1.0	2401.8	0.150	0.019	0.112	0.888	457.6	427.6	3.82	0.112
1.5	2462.4	0.142	0.027	0.160	0.840	470.1	440.1	2.75	0.160
2.0	2523.0	0.134	0.035	0.207	0.793	482.6	452.6	2.19	0.207
2.5	2583.6	0.124	0.045	0.266	0.734	495.0	465.0	1.75	0.266
3.0	2644.3	0.114	0.055	0.325	0.675	507.5	477.5	1.47	0.325
3.5	2704.9	0.104	0.065	0.385	0.615	516.9	486.9	1.26	0.385
4.0	2765.5	0.094	0.075	0.444	0.556	532.4	502.4	1.13	0.444
4.0	2765.5	0.094	0.075	0.444	0.556	532.4	502.4	1.13	0.444
4.5	2826.1	0.084	0.085	0.503	0.525	544.9	514.9	1.02	0.503

Table 4.21: Average Values of Temperature, Volume and Pressure (sample 20)

Time (hr)	T °C	V*10^{-3} (m^3)	ΔV (m^3)	ΔV/V$_0$ Strain	V/V$_0$ Strain	P (Mpa)	ΔP (Mpa)	B (Gpa)	Δη Volume
0.5	2342.3	0.158	0.012	0.071	0.929	460.5	430.5	6.16	0.071
1.0	2402.9	0.150	0.020	0.118	0.882	471.0	441.4	3.74	0.118
1.5	2463.6	0.142	0.028	0.165	0.835	484.4	454.4	2.75	0.165
2.0	2524.1	0.134	0.036	0.212	0.788	479.3	449.3	2.12	0.212
2.5	2584.8	0.124	0.046	0.271	0.729	510.3	480.3	1.77	0.271
3.0	2645.5	0.114	0.056	0.329	0.671	535.2	505.2	1.54	0.329
3.5	2706.1	0.104	0.066	0.388	0.612	536.2	506.2	1.30	0.388
4.0	2766.7	0.094	0.076	0.448	0.553	549.1	519.1	1.16	0.448
4.5	2827.4	0.084	0.086	0.506	0.494	562.1	532.1	1.05	0.506
5.0	2888.0	0.070	0.100	0.588	0.412	575.0	545.0	0.93	0.588

The representatives Tables 4.20 and 4.21 were obtained for the unrefined gold samples collected from zone D. Tables 4.22 – 4.25 containing the results for other four samples in this zone are shown in Appendix II.

From Table 4.20, it was noticed that the bulk modulus decreased with increase in both temperature and pressure. The implication is that increases in pressure result in lowering the bulk modulus of the sample while the volume strain increased with increase in both temperature and pressure. The increase in temperature on the sample will not increase the volume because of the application of pressure on it. The graph of volume strain against time and the graph of bulk modulus against temperature for sample 19 are shown in Figures 4.19a and 4.19b.

Figure 4.19a represents the graph of volume strain against time for sample 19. In the figure, the value of strain rate was 0.000032 s^{-1}, the rate increased with increase in time which conformed to literature laboratory values for materials such as Aluminium, Hiroyuki*et al*., (2018), while the square of the sample correlation which determine the goodness of the fit was 0.9942.

Figure 4.19b represents the graph of bulk modulus against temperature for sample 19;the application of pressure and temperature lowers the bulk modulus of the sample.

Table 4.21 showed the result of the analysis recorded for sample 20. From the table, as the temperature and pressure increase, there was increased in thermal volumetric strain of the sample. These increase result to decreased in bulk modulus such that a wide gap existed between the first and second value after which there was gradual decrease been observed. Figures 4.20a and 4.20b represents the graph of volume strain against time and the graph of bulk modulus against temperature for sample 20.

The graph of volume strain plotted against time for sample 20 is shown in Figure 4.20a. It was noticed that the value of strain rate for this sample was 0.000032s^{-1} as seen from the graph, the rate increased with increase in time which conformed to literature laboratory values for materials; the coefficient of sample correlation which determine the goodness of the fit was 0.9952.

The representative graph of bulk modulus against temperature for sample 20 is shown in Figure 4.20b, the bulk modulus of the sample decrease with the application of temperature. The sample behavior showed that thevolume compression increased with rise in temperature.

The graphs for Tables 4.21 – 4.24 are shown in Appendix II.

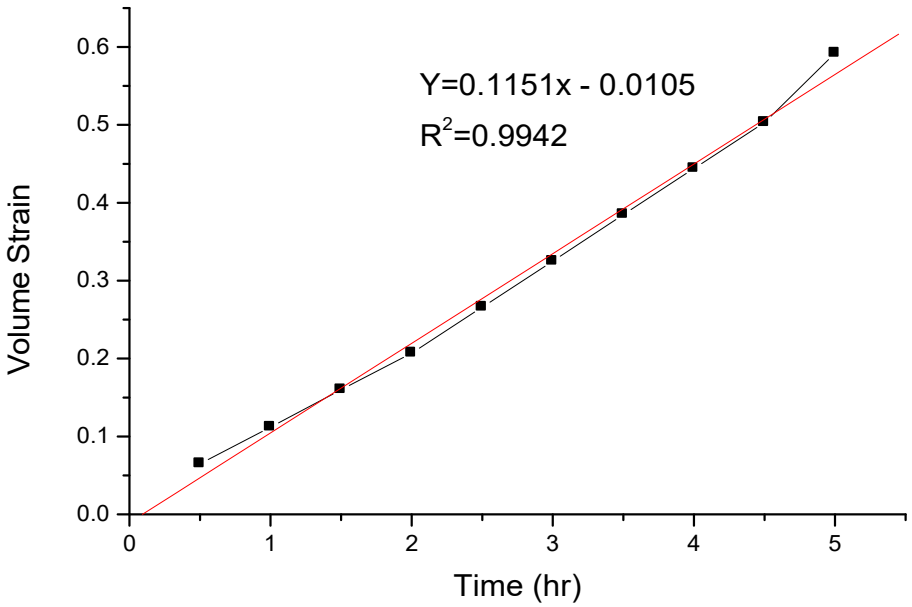

Figure 4.19a: Volume Strain Plotted Against Time (sample 19)

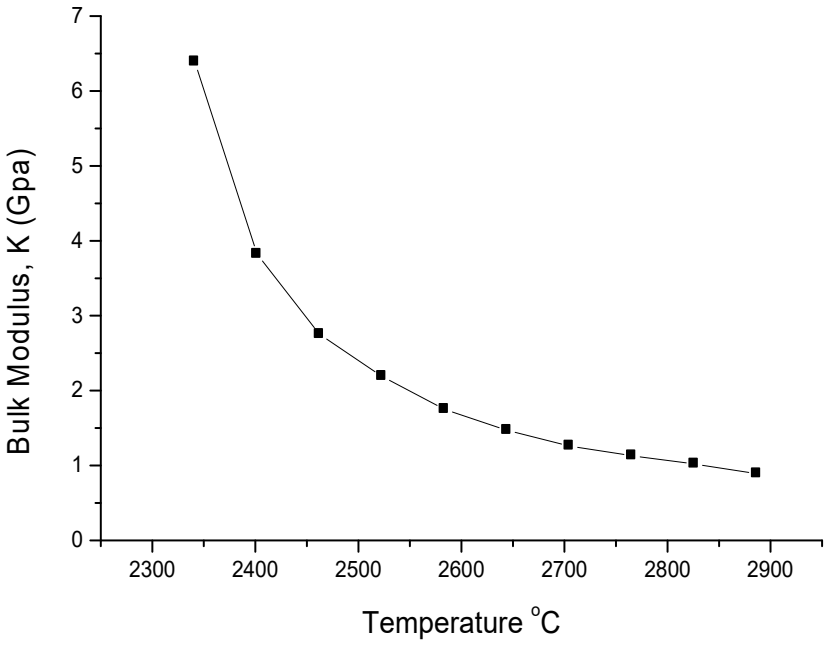

Figure 4.19b: Bulk Modulus Against Temperature (sample 19)

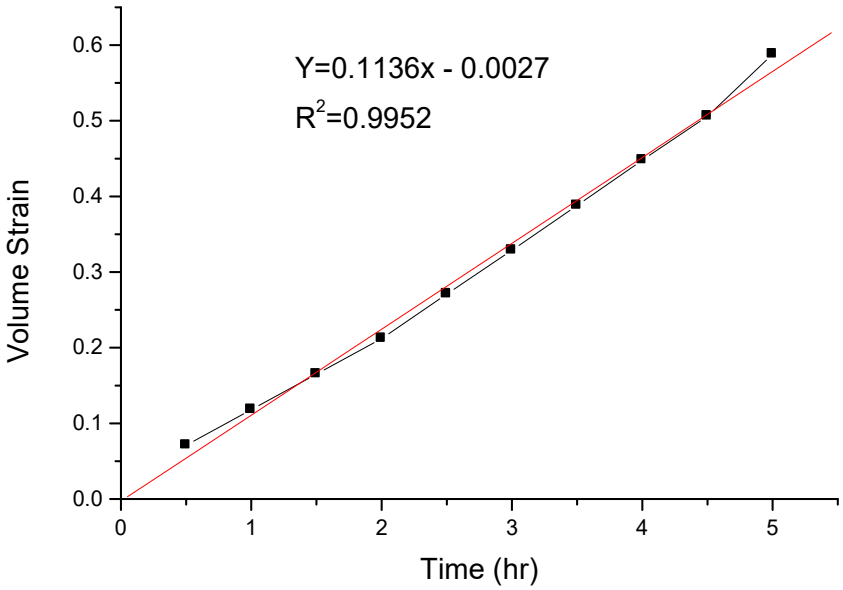

Figure 4.20a: Volume Strain Plotted Against Time (sample 20)

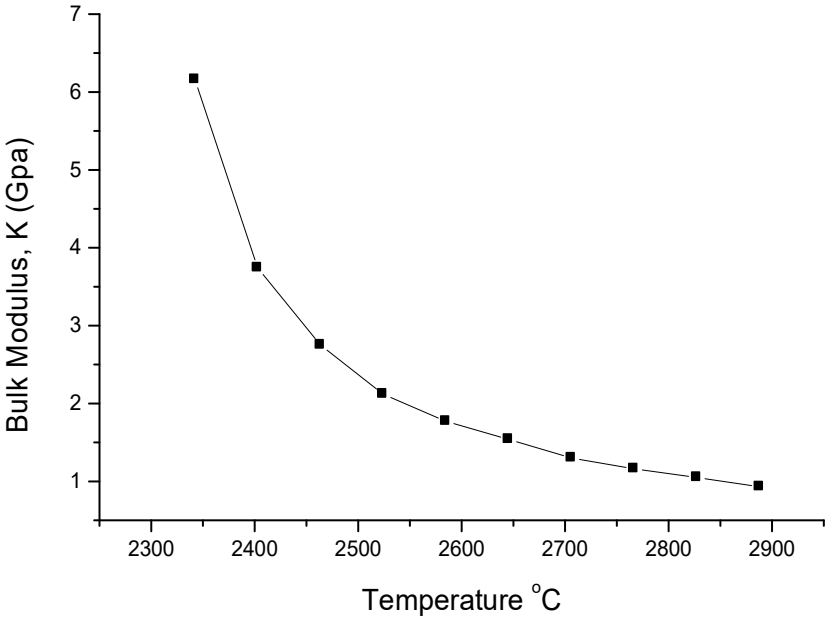

Figure 4.20b: Bulk Modulus Against Temperature (sample 20)

Table 4.26: Average Values of Temperature, Volume and Pressure (sample 25)

Time (hr)	T °C	V*10^{-3} (m^3)	ΔV (m^3)	ΔV/V_0 Strain	V/V_0 Stress	P Strain	ΔP (Mpa)	B (Mpa)	Δη (Gpa)	Volume
0.5	2346.9	0.166	0.012	0.067	0.933	451.3	421.6	6.29	0.067	
1.0	2407.6	0.158	0.020	0.112	0.888	463.9	433.9	3.87	0.112	
1.5	2468.4	0.150	0.028	0.157	0.843	476.6	446.6	2.84	0.157	
2.0	2529.1	0.142	0.036	0.202	0.798	489.2	459.2	2.27	0.202	
2.5	2589.9	0.132	0.046	0.258	0.742	401.8	471.8	1.83	0.258	
3.0	2650.7	0.122	0.056	0.315	0.685	514.5	484.5	1.54	0.315	
3.5	2711.4	0.112	0.066	0.371	0.629	527.1	497.1	1.34	0.371	
4.0	2772.2	0.102	0.076	0.427	0.573	539.7	509.7	1.19	0.427	
4.5	2832.9	0.092	0.086	0.483	0.517	552.4	522.4	1.08	0.483	
5.0	2893.7	0.078	0.100	0.562	0.438	565.0	535.0	0.95	0.562	

Table 4.27: Average Values of Temperature, Volume and Pressure (sample 26)

Time (hr)	T °C	V*10^{-3} (m^3)	ΔV (m^3)	ΔV/V_0 Strain	V/V_0 Stress	P (Mpa)	ΔP (Mpa)	B (Gpa)	Δη Volume
0.5	2350.2	0.168	0.012	0.067	0.933	452.9	422.9	6.31	0.067
1.0	2411.1	0.160	0.020	0.111	0.888	465.6	435.6	3.92	0.111
1.5	2472.0	0.152	0.028	0.156	0.843	478.2	448.2	2.87	0.156
2.0	2532.8	0.144	0.036	0.200	0.798	490.9	460.9	2.30	0.200
2.5	2593.7	0.134	0.046	0.256	0.742	503.6	473.6	1.85	0.256
3.0	2654.5	0.124	0.056	0.311	0.685	516.3	486.3	1.56	0.311
3.5	2715.4	0.111	0.069	0.383	0.629	529.0	499.0	1.30	0.383
4.0	2779.3	0.101	0.079	0.439	0.573	541.6	511.6	1.17	0.439
4.5	2837.1	0.091	0.089	0.494	0.517	554.3	524.3	1.06	0.494
5.0	2898.0	0.068	0.100	0.556	0.438	567.0	537.0	0.97	0.556

The obtainedunrefined gold samples collected from zone E were shown in Tables 4.28 – 4.31 respectively. The results for other four samples in this zone are shown in Appendix II.

From Table 4.26, it was observed that the bulk modulus decreased with increase in both temperature and pressure while the volume strain increased with increase in both temperature and pressure. The graph of volume strain against time and the graph of bulk modulus against temperature for sample 25 are shown in Figures 4.25a and4.25b.

The graph of volume strain plotted against time for sample 25 is shown in Figure 4.25a, it was observed from the figure that the value of strain rate was 0.000030 s^{-1}, which increased with increase in time, the value conformed to literature laboratory values for materials such as aluminium, Polycrystalline Tantalum, Sia*et al*., (1998). The square of the sample correlation which determine the goodness of the fit was 0.9976.

The graph of bulk modulus plotted against temperature for sample 25 is presented in Figure 4.25b, the bulk modulus of the sample decreased with increase in temperature as observed from the graph. There was volume compression which increased with rise in both temperature and pressure.

The results obtained from the analysis carried out on sample 26 is shown in Table 4.27, when there was application of temperature and pressure on the sample, it was observed that the relative volume, $\left(\frac{v}{v_0}\right)$decreased along with the bulk modulus decreasedwhile the volume strain increased with the increase in both temperature and pressure. The graph of volume strain against time and the graph of bulk modulus against temperature for sample 26 are shown in Figures 4.26a and 4.26b.

In Figure 4.26a that represents the graph of volume strain against time for sample 26. The strain rate was 0.000031 s^{-1}, the rate increased with increase in time which conformed to literature laboratory values for materialswhile the square of the sample correlation for the goodness of the fit was 0.9956.

Figure 4.26b represents the graph of bulk modulus against temperature for sample 26, it was noticed from the graph that the bulk modulus of the sample decreased with increase in temperature. The behavior of the sample showed that the material in this category exhibit a type of volume compression which increased with rise in both temperature and pressure.

The graphs for Tables 4.28 – 4.31 are shown in Appendix II.

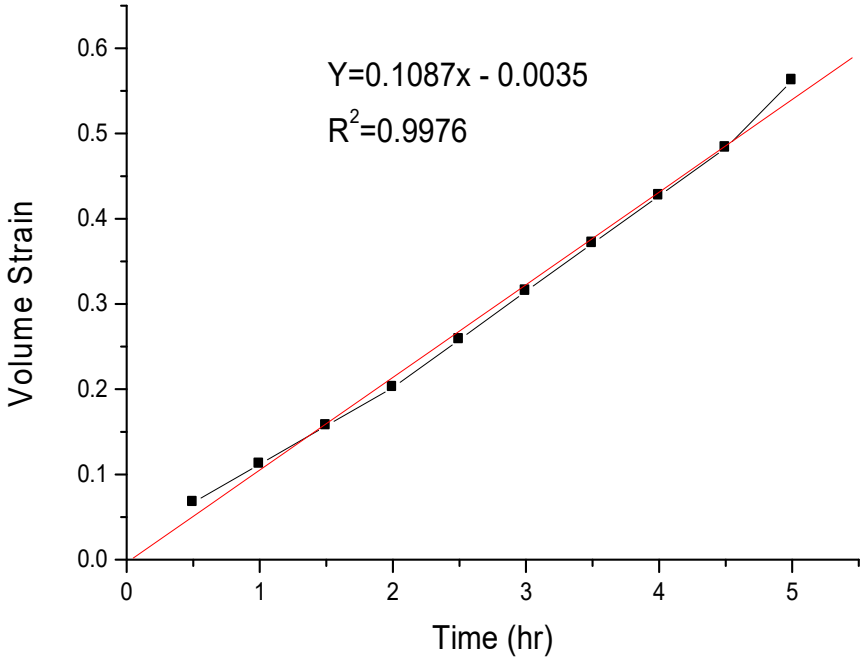

Figure 4.25a: Volume Strain Plotted against Time (sample 25)

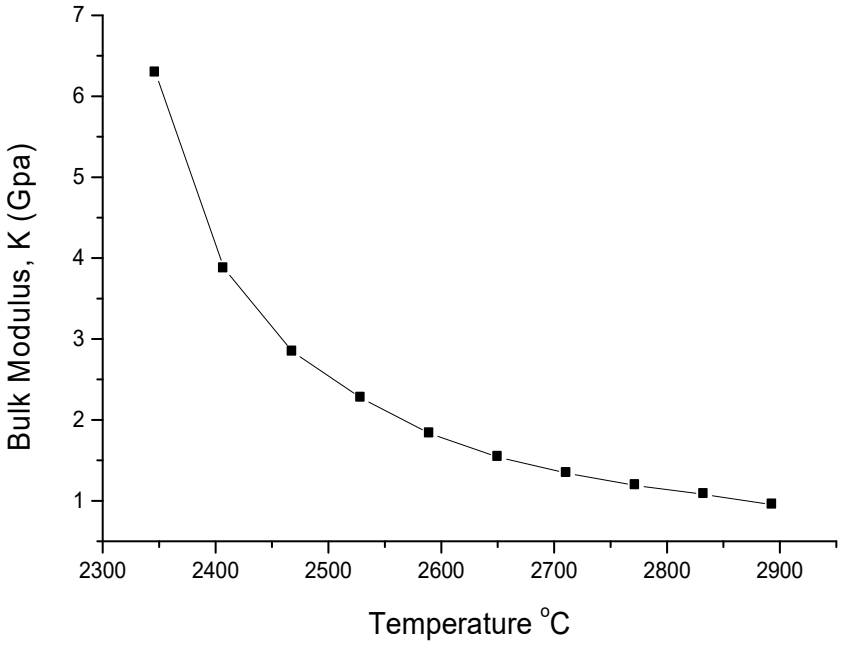

Figure 4.25b: Bulk Modulus against Temperature (sample 25)

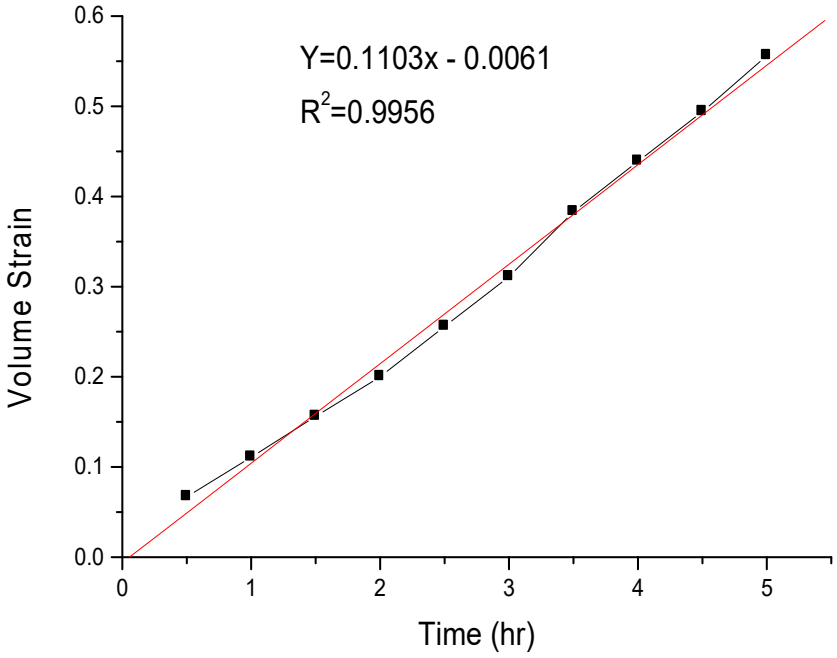

Figure 4.26a: Volume Strain Plotted against Time (sample 26)

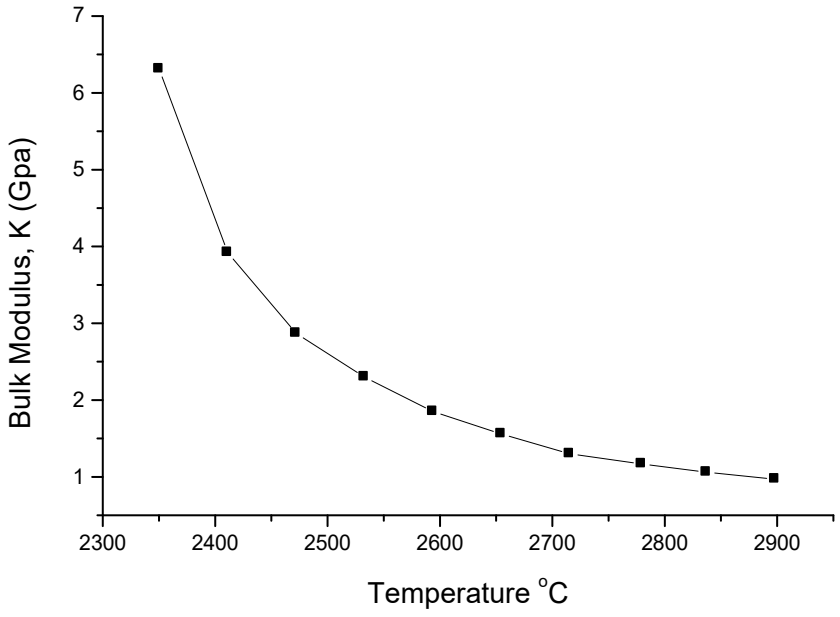

Figure 4.26b: Bulk Modulus against Temperature (sample 26)

4.3 Melting Curve Parameters

The table below represents melting curve parameters that were used to determine the melting temperature of Itagunmodi gold with variation in pressure.

The values obtained for melting temperatures for Itagunmodi was determined using equation (equation 3.12b) with melting-curve parameters when varying the pressures are shown in Table 4.32. From Table 4.33, at zero degree, the melting point of the unrefined gold was1064 ℃. It was observed that as the pressure increases, the melting point also increased which means that when the pressure applied on any material of this kind is raised, the melting point will also increase.

Table 4.33 showed the result of the effects of the variation of pressure on a material. When examining the effect, it was noticed that by increasing the pressure applied on gold, its melting point will no longer be its laboratory value; the value is raised by certain amount of value. This is a direct relationship between pressure and melting temperature.

Figure 4.31 showed the graph of melting temperature against pressure. The graph was linear which showed that the melting point increased with increase in temperature, the implication is that any increase in pressure that is applied on any material will result to increase in its melting temperature. The coefficient of correlation which determined the goodness of the graph was 0.9976.

Table 4.32: Melting-Curve Parameters

b_1	b_2	b_3
5.4356	1.0753 $\times 10^{-2}$	-2.4927×10^{-4}

where b_1, b_2 and b_3 respectively are constants called melting-curve parameters after (Jagannadham and George, 1971).

Table 4.33: Melting Temperatures for Itagunmodi Gold at Varying Pressures

$\boldsymbol{P(Kbar)}$	$T/℃$
0	1064.0
5	1091.4
10	1118.9
15	1147.1
20	1175.0
25	1202.7
30	1230.0
35	1256.7
40	1282.7
45	1307.7
50	1331.5
55	1354.0
60	1375.0
65	1394.3

.

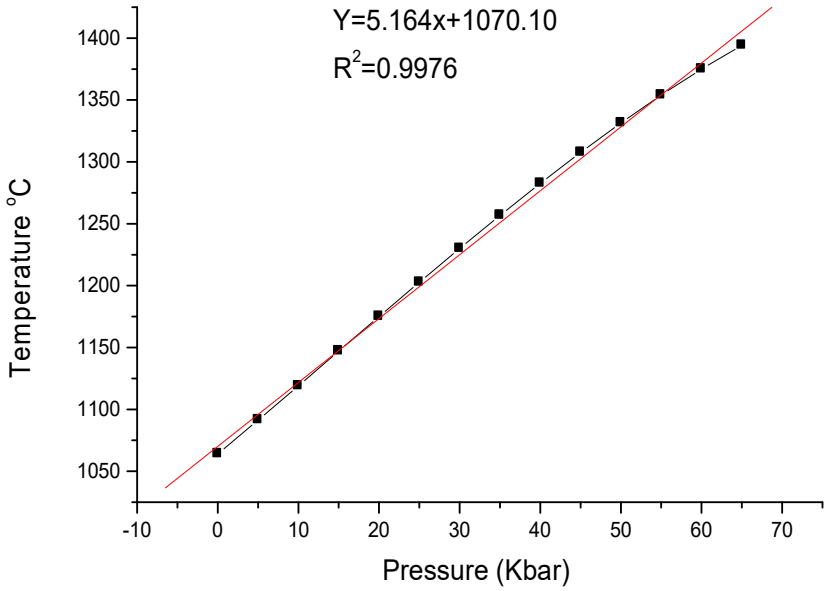

Figure 4.31: Melting Temperature against Pressure for Itagunmodi Gold

4.4 Temperature Profile

The values obtained for the temperature profile were shown in Table 4.34, from the table, the values of temperature increased with increase in depth of the lithosphere. The values were further used for the calculations of bulk modulus in the lithosphere using equation (3.9) and that of stress using equation (3.30);

From the table, the stress and bulk modulus also increased with increase in depth.

The graph of temperature against depth in Figure 4.32 was linear between 0and 30 Kmuntil a wide gap between 30and 40 Km, the linearity of the graph indicate a certain section which represent discontinuity region between the crust and the mantle in the layers of the Earth's interior, after that region, the linearity of the graph reappear up to the depth of 150 Km.

The graph of stress against depth in Figure 4.33 was linear between 0 and 30 Km, after depth from 30 to 40 Km, a little shift occurred which indicate a region of discontinuity between the crust and the mantle, thereafter, the other portion was linear up to the 150 Kmdepth. The stress increased at the rate of 33 MPa/Kmwhile the confidence limit is 0.9994. The graph of bulk modulus against depth in Figure 4.32 show that the bulk modulus increased with increase in depth, there was a decreased in the bulk modulus between 30and 40 Km, thereafter, the bulk modulus increased again gradually from 40to 150 Km.

Table 4.34: Temperature Profile in the lithosphere

Depth, Z (Km)	T (K)	T ^{o}C	P (MPa)	Bulk Modulus (GPa)
0	300.0	27.0	0.00	0.00
10	400.0	127.0	275.25	49.15
20	500.0	227.0	550.48	78.64
30	600.0	327.0	825.72	98.30
40	1068.8	795.8	1302.84	87.07
50	1131.3	858.3	1628.55	103.00
60	1193.8	920.8	1954.26	117.00
70	1256.3	983.3	2279.97	130.00
80	1318.8	1045.8	2605.68	141.00
90	1381.3	1108.3	2931.39	152.00
100	1443.8	1170.8	3257.10	161.00
110	1506.3	1233.3	3582.81	171.00
120	1568.8	1295.8	3908.52	178.00
130	1631.3	1358.3	4234.23	185.00
140	1693.8	1420.8	4559.94	192.00
150	1756.3	1483.3	4885.65	199.00

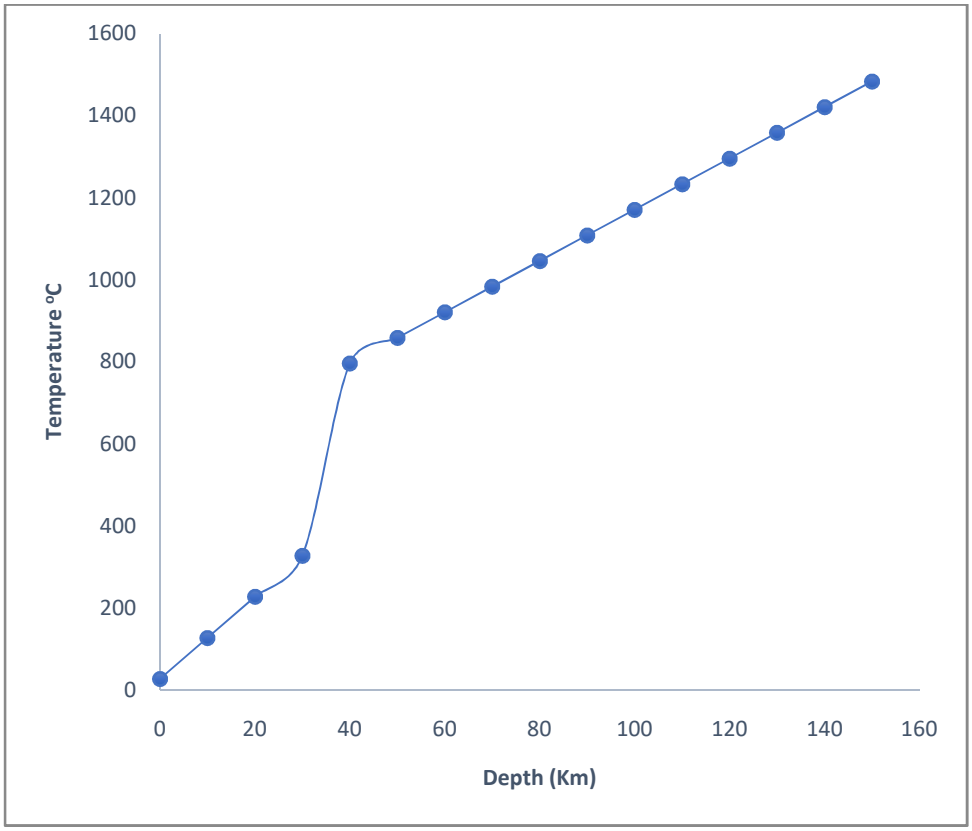

Figure 4.32: Graph of Temperature against Depth (Lithosphere)

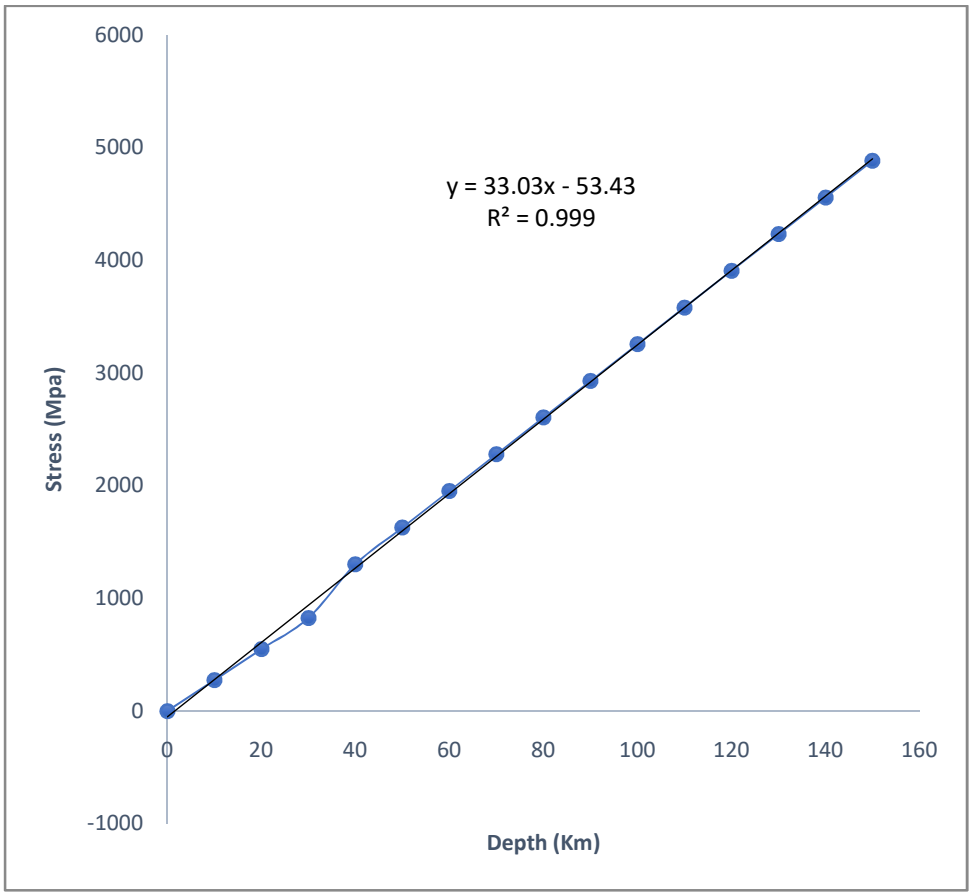

Figure 4.33: Graph of Stress against Depth (Lithosphere)

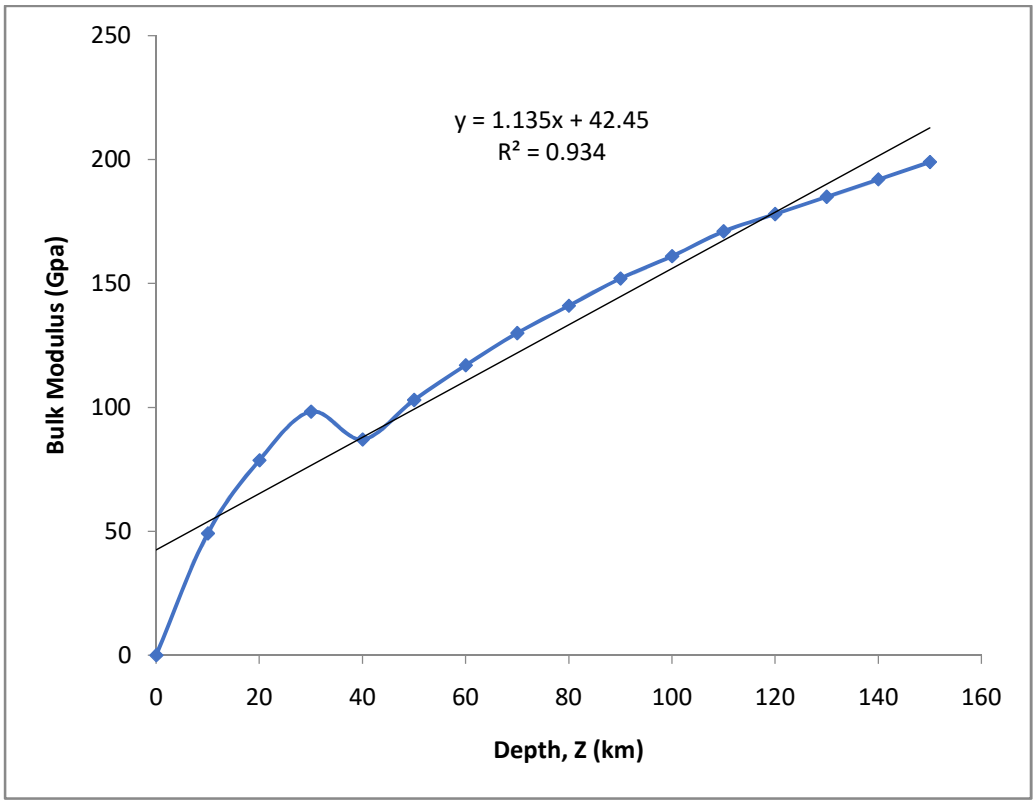

Figure 4.34: Graph of Bulk Modulus against Depth (Lithosphere)

4.5 Discussion

The metal analyses were carried out to confirm the pathfinder elements, the following pathfinder elements Fe, Cu, Zn, Mn, and Ba were confirmed as shown in Table 4.1. In this work black soil was found to be present at the deposits sites which can also be used as exploration tools.

Figures 4.1 – 4.30a represents the volume strain plotted against temperature for all the samples, the graphs show an increase in strain results in a lowering of αK_T at high value of temperature. The strain rate of the unrefined gold from Itagunmodi was$10^{-5}s^{-1}$, it falls between $10^{-3} - 10^{-9}s^{-1}$, this conformed to the laboratory values for creep deformation for materials with slow time-dependent deformation. Since its bulk modulus decreases moderately with time. Also, this material can be used for interior and external decorations that do not required much load and in areas where little or no stress is needed in the area of operation of devices, examples, in door bell, hands of clock, wrist watches etc., gold is a Ferromagnetic metal, such as soft magnetic materials, others include Ag, Cu, Zn, Cd and Hg respectively, whichcan be used to increase the magnetic flux density (B) produced when an electric current is passed through material it can also be applied in core for electromagnets, electric motors, transformers, generators, other electric equipment etc.

Figures 4.1 – 4.30b represents the plots of bulk modulus against temperature for all samples. The values of the bulk modulus tend towards zero with increased in temperature and time. This shows that the bulk modulus decreases at high temperature due to increase in strain $\Delta\eta$, that means the more the applied stress on materials of this kind the lesser the bulk modulus.

The results of the analysis conducted showed that as pressure and temperature increases, the volume of the unrefined gold from Itagunmodi reduces, meaning that the compression in volume of these deposits increases moderately. The model used was of the form: $\Delta P_{Th} = \propto K_T(T - T_0)$ and$\Delta V/V_0 = \propto (T - T_0)$, where αK_T, α, represent the slope respectively. The average values of pressure, temperature and compressed volume ranged from $436.40 - 549.00\ MPa$, $2327.30 - 2871.70$ ℃and the bulk modulus K_T ($V=V_0$) decreases with temperature for the analyzing values of $(\partial K_{T0}/\partial p)_T$ [i.e. $V=V_0$], the bulk modulus ranged from $0.68 - 9.85\ GPa$ for all the samples.

The thermal data for the samples shows that K_T ($V=V_0$) decreases with temperature (T) for experimental values of ($\partial K_T/\partial P$). The slope $\partial K_T/\partial T$ is $-9.172\ GPa/$℃for sample1 as a representation of the samples. It was also observed that the trend of bulk modulus when compared with time shows that the bulk modulus decreases with increase in time (or temperature), it is an indication that a time will come when the gold from Itagunmodi will be

very scarce or may not even be available because at a point in the lithosphere, migration of gold to other places can occur, which means the size of the sample depreciate further at higher values of temperature. The volume strain is about $10^{-5}s^{-1}$. In past work, a modified approach of the Mie-Grüneisen equation of state has been attempted leading to an evaluation of bulk moduli at different temperatures for CdTe, Si and $NaClO_3$ it was assumed that the main change of bulk modulus with temperature arises from the associated small volume changes, (Rajagopalan, 1979).hide

Experimentally, all materials are compressible (i.e., K is finite). Physically, as the temperature is increased through the gold; the distance between the molecules is expected to increase (Turner*et al*., 1994). The resulting decrease in the bulk modulus may be attributed to the consequent decrease in the slope of the inter-atomic potential, as samples of unrefined gold was heated and softens, it becomes more compressible.

The effect is when the pressure exerted on a substance is increased, the volume the substance occupies decreases, which means the intermolecular distance decreases, solids have almost no intermolecular distance, a liquid have very small intermolecular distances and gases a large intermolecular distance. When the intermolecular distance decreases, the state of matter is lowered. (A solid is a lower state of matter than a liquid, and a liquid is a lower state of matter than a gas). Basically, when the pressure on a substance increases, the lower state of matter is stabilizing. Compressibility and melting point also increase with increase in pressure.

The temperature profile of the Lithosphere covers the surface to depth of about $150\ Km$, while the temperature ranged from 27 ℃ to 1483.3 ℃. It increases linearly until the discontinuity region at about $30\ Km$ down the crust before the shift in direction in the mantle part of the lithosphere as shown in Figure 4.32. In the crustal part, the temperature increases at 10 ℃$/Km$ and the rate of increase was 6.3 ℃$/Km$in the mantle part of the lithosphere as shown in Table 4.34. The melting temperatures for the unrefined gold using the equation with melting-curve parameters show that increase in pressure raised the melting point of unrefined gold as shown in Table 4.33, which means the metal will melt at higher temperatures with increase in pressures. The melting curve equation 3.12b show that the melting temperatures ranged between 1064 ℃to 1394.3 ℃in the pressure ranged between $0\ to\ 65\ Kbar(i.e. 0 - 6500\ MPa)$.

After all the observations from the laboratory analyses and by examining the depth in the lithosphere, we can draw the inference that gold originated from the mantle, if we correlate the

melting point of the gold samples $(1064\ ℃)$with the temperature profile, it corresponds to depth ranged from $80-90\ Km$in the upper mantle part of the lithosphere with pressure in the ranged $2605.68-2931.39\ MPa$, $(i.e.26-29)Kbar$, as shown inTable 4.34, after this depth it was observed that the trend continues up to $150\ Km$.The pressure effect will not allow the metal to be in another state of existence, the melting point also increases with increase in pressure and as a result, gold existed as solid at the source.
Since materials arranged themselves based on their density irrespective of where they are found today, those with lighter density will be from lower depths.

In Figure 4.33, the stress increase at the rate of about $33\ MPa/Km$ in the lithosphere, at about $50\ Km$depth and beyond, the stress is above $1600\ MPa$ which is enough to cause transport of Itagunmodi gold and when that occur, gold will migrate and can be seen in fracture or fault zones at any depth in the subsurface as they were discovered in different proportion today. In Figure 4.34, the bulk modulus increases at the rate of$1.136\ GPa/Km$ in the lithosphere. The bulk modulus increases with depth because as we go deeper in the lithosphere, density, temperature and pressure increases due to compositional and phase changes.

In Figures: 4.32 – 4.34; there is discontinuity along the boundary between the crust and mantle, between $30-40\ Km$ depth and temperature is above 825 ℃, this is Mohorovicic discontinuity region, it represents region of compositional changes and changes in mineral structures (phase changes and the P-wave velocity increases at that boundary).

CHAPTER FIVE

CONCLUSION

5.1 Conclusion

It is likely that in some years to come the gold present in this location may likely be in small proportion or in form of ashes compare to the past years and its present state because leaching may take place which can aid the channel of gold to different location. Also, one should not have neglected that the increase in pressure and temperature within the Earth crust increases

downto the core of the Earth. Erosion can wash the precious metal away thereby transport and deposit gold in other location when the soil become loose with increase in thermal pressure and heat, at a point called the melting point (T=1063±2) ºC, as reported by Stimson (1961) this metal can melt and transportation of gold ispossible. The results show that there is decrease in volume of gold at high pressures and high temperatures. This could be one of the reasons why gold found in that area was in grained form and not in big rock form as in some places. Hence, gold has been used as a pressure marker for in situ X-ray experiments under high pressure and high temperature because of its chemical stability and moderate compressibility (Okube *et al*., 2002). Some years back, gold in this area are likely in bigger form but as at present, Itagunmodi gold deposits occurs in grained form.

Since all materials are compressible, the singularity is of no practical import. This interpretation is consistence with experiments cited above. The experimental analysis shown that the rate at which the volume of the gold from Itagunmodi compressed means the high temperature thermodynamic properties mean the decay in bulk modulus for every rise in temperature. Analysis of high temperature and pressure conducted on volume show that the volume of gold will continue to decrease. In future,gold found in this area may become scantybecause of compression in volume and stress that also acted on the every material at every point in time irrespective of their location in the interior part of the Earth, the depth of location is also vital as pressure continue to build up, it may lead to fault because when its accumulation is much, there is tendency that in the process of looking for way to escape, the forces possess by the pressure create openings in the soil and, in the process, leaching takes place thereafter, some of these gold will find their way deeper in the soil while some are transported through the soil by process like weathering and migrate to new locations.

In conclusion, the pressure ranged from $436.40 - 549.00\ MPa$, temperature ranged from $2327.30 - 2871.70$ ℃,while the compressed volume ranged from $0.041 - 0.690 \times 10^{-3} m^3$.The strain rate of the gold samples is about $10^{-5} s^{-1}$ while the bulk modulus of gold from Itagunmodi ranged from $0.68 - 9.85\ GPa$ Gpa. The temperature profile ranged from $27 - 1483.3$ ℃in depth ranged from $0 - 150\ Km$while the stress in the lithosphere increasedat 33 MPa/Km while bulk modulus increased at$1.136\ GPa/Km$.

The strain rate increased from the value to higher strain rates, this property of strain shows that gold samples has elastic plastic deformation behavior. The volume strain increased from lower value at the initial time to higher volume strain with increment of time. The increase in volume strain is also attributed to the increment in value of applied stress, this increase in volume strain and applied stress are steady as shown in Tables 4.2 - 4.31. The bulk modulus has a sharp decrease in its values at the beginning of the heating process and thereafter, there was a steady decrease in the values as shown in Figures 4.1b – 4.2b; and other representatives' graphs for bulk modulus against temperature. The pressure ranged shows that the increase in the applied pressure moderate as shown in Tables 4.2 – 4.31. For small change in volume, large value of applied pressure is required. In the lithosphere, both stress and bulk modulus increased with depth from 0 – 150 Km. From the results obtained from the analysis of h e gold samples, the bulk modulus, relative volume($\Delta V/V_0$) decreases with increment in applied stress.

5.2 Contribution to Knowledge

In conclusion, both volume and bulk modulus of gold in Itagunmodi decreases moderately with time. At the source, the strain rate shows that it exists in bigger form and the depth of formation is the lithosphere. In future, the gold from this location may become scanty; leaching may take place that may lead to transportation of minerals to various locations where new discovery may be found. The bulk modulus increases with depth, density, temperature and pressure increases due to compositional and phase changes and mineral elements originated from different depths. The stress increases down the lithosphere at the rate of33 MPa/Km.

Estimated temperature at crust-mantle boundary using Lindemann's Laws of fusion was $277\,℃\,(550\,K)$; our calculated value was $327\,℃\,(600\,K)$. The temperature, according to a notable source at depth between $100-140\,Km$ the temperature ranged from $1100-1400\,℃$

and also, it ranged from $1200 - 1440$ ℃respectively, our calculated value for the same depth $100 - 140\ Km$, ranged from $1170.8 - 1420.8$ ℃.

At the base of the lithosphere, there are values given which includes:1330 ℃, 1280 ℃and 1600 ℃ respectively. Our calculated value of base value was 1483.3 ℃.We have determined the temperature profile in the lithospherewhich ranged from $27 - 1483.3$ ℃,

The research information can be used to predict another form of mining exploration tool for fine-grained gold deposits for places without known history of the deposit. Other metallic materials that could exhibit the same nature of bulk modulus that is moderate with temperature rise can be used for similar purpose as in case of this sample. The strain rate (i.e. a value of about $10^{-5}s^{-1}$) show that it has creep formation. The temperature profile for the lithosphere ranged from$27 - 1483.3$ ℃. The stress obtained for the lithosphere means there is possibility for transport of the deposit when the stress that exists within where it could originate is greater than that of its melting value.

5.3 Recommendation

We recommend that all mining activities taken place on our environment should be monitored because the lithosphere is brittle. Also, civil Engineers or building Engineers should work with geophysicist and geologist to study the nature of soil before structures were erected on land. Since tectonic motion is universal, all activities taking place everywhere should be check. in order to reduce the damage resulted from all anti Earth activities, the government on their part should regulate mining activities as well as drilling of water boreholes in the country, because illegal mining and haphazard of water boreholes are not friendly to the environment.

References

Abdullah, S.,Yunoh, M.F., Jalar, A. and Kamarudin, H. 2008. Effects of Strain Rates on the Characterization of 99.99% Gold Wire: *A Case Study in Micro Tensile Test Proceedings of the 1st WSEAS International Conference on Materials Science (MATERIALS'08)*

Ajeigbe, O.M., Adeniran, O. J. and Babalola, O. A. 2014. Mineral Prospecting Potentials of Osun State: *European Journal of Business and Management.* Volume 6, No. 2, pp 115 -223

Anderson, L. O., 1980. The temperature profile in the upper mantle. *Journal of Geophysical Research* volume 84, pp 7003 - 7010

Ashley, R.P., 1982. Occurrence model for enargite-gold deposits, in Erickson, R.L., ed., Characteristics of Mineral Deposit Occurrences: *United States Geological Survey, Open File Report* 82-795, p. 144-147. </p>

Bello, A. 2012. The use of Electrical Resistivity Technique to Delineate Gold deposit site. *International Journal of Science and Technology,* Vol 2, No 8, 2012

Bing,J. L., Kenneth, S. V., Said, A. and Scotts, S. 1997. Modeling the mechanical behavior of tantalum. *Article in Metallurgical and Materials Transactions A.*

Boboris, K., Pottlacher, G., and Jager, H., 1999. Determination of the Critical point of gold; *International Journal of Thermophysics,* Vol. 20, 4 p. 1289 – 1297**.**

Bott, M. H. P. and Kusznir, N. J. 1984. The origin of Tectonic Stress in the lithosphere. *Tecronophysits,* 105 (1984) *Elsevier Science Publishers B. V. Amsterdam*- p 1-13.
Boyle, R. W. 1979. The geochemistry of gold and its deposits: *Geological Survey of Canada Bulletin* 280, 584 p.
Brown, J. M., and Shankland, T. J., 1980. Thermodynamic parameters in the earth as determined from seismic profiles. *Geophysics Journal*.

Cogley, J. G. 1984.Continental margins and the extent and number of the continents. *Reviews of Geophysics.* 22(2):101-122

Colin, P. B. 2014. Characterization of strain rate dependence in the mechanical behavior of gold thin films. *Research gate.net publication.*

Chloe, M. and Claude, J. 2007. Secular cooling and thermal structure of continental lithosphere: *Earth and Planetary Science Letters volume* 257 pg 83–96 Science Direct Secular.

Dube, B., Gosselin, P., Mercier, L. P., Hannington, M., and Galley, A., 2007. Gold-rich volcanogenic massive sulphide deposits, in Good fellow, W.D., ed., Mineral Deposits of Canada: A Synthesis of Major Deposit-Types, District Metallogeny, the Evolution of Geological Provinces, and Exploration Methods: *Geological Association of Canada, Mineral Deposits Division, Special Publication* 5, p. 75-94. </p>

Dziewonski, A.M., Hales, A. L. and Lapwood, E. R. 1975; Parametrically simple earth models consistent with geophysical data, *Physics Earth Planet Interiors volume* 10, pp 12 - 48.

Espinosa, H. D. and Prorok, B. C. 2003. Size effects on the mechanical behavior of gold thin films. *Journal of Materials Science* 38, no. 20: 4125-4128.

Gudlavalleti, S., Kumar, K. S. and Anand, L. 2002. Stress-strain response of free standing nano-crystalline gold thin-films. *Materials Research Society Symposium - Proceedings* 695: 425-430.

Guilbert, J. M. and Park, Jr. C. F. 1986. The Geology of Ore Deposits. *W. H. Freeman and Company,* 985 pp.

Harold, K., Williams, L.N., and Roger, P. A. 1997. Gold: *U.S. Geological survey*

Hast, N. 1969. The state of stress in the upper part of the Earth's crust. *Tectonophysics* 8:169–211

He, L. X, Zeng, R. L, and Lin, L. Q. 1993. Gold geology of Guizhou Province. *Beijing, Geology Publishing House,* 156p. (In Chinese)

He, L. X. 1996. A genetic model for gold deposits in southwestern Guizhou: a co-source of heat, water and ore-materials. *Guizhou Geology,* 13(2): 154-160. (In Chinese)

Hedenquist, J.,W., Arribas, A.,R., and Gonzalez, U. E. 2000. Exploration for epithermal gold deposits, Chapter 7 in Hagemann, S.,G., and Brown, P.,E., eds., Gold in 2000: Society of Economic Geologists, *Reviews in Economic Geology,* v. 13, p. 245-277. </p>

Hiroyuki, Y., Tsuyoshi, K., Ryota, M., Tomoyuki, K. and Minemitsu, O. 2018. Strain Rate Dependence of Material Strength in AA5xxx Series Aluminum Alloys and Evaluation of Their Constitutive *Equation Hiroyuki Yamada. Metals*. Volume 8, 579.

Hoge, K. G. and. Mukherjee, A. K (1977). 'The temperature and strain rate dependence of the flow stress of tantalum', *J. Mater. Sci.,*1977, 12, 1666–1672.

Holbrook, W. S, Mooney, W. D, Christensen, N. I. 1992. The seismic velocity structure of the deep continental crust. In: *Fountain D.M, Arculus R and Kay R. W, editors. Continental Lower Crust. Amsterdam: Elsevier;* pp. 1-44

Jagannadham, A., and George, C. K., 1971. Melting of gold, Silver and Copper. *Journal of Geophysical Research,* Volume 76, No. 20, pg. 4969 - 4977

Jeanloz, R., and Richter, F. M., 1979. Convection, composition, and the thermal state of the lower mantle, *Journal of Geophysics Research, volume* 84, pp 5497 – 5504

Kenneth, B.L.N., and Bunge, H.P. 2008. Geophysical continua deformation in the Earth interior: *Cambridge University Press:* P 17 -18

Lachenbruch, A. H. 1970. Crustal temperature and heat production: Implications of the linear heat-flow relation. Journal of Geophysical Research (1896-1977), volume 75, issue 17

Li, X. 2003. Bulge test on free standing gold thin films. *Materials Research Society Symposium - Proceedings Thin Films - Stresses and Mechanical Properties* X 795: 437-442.

Mumuni, A. and Adango, M. 2016. Effect of Temperature and Pressure on the Bulk Modulus of a Poroelastic System.*Journal of Hydrogeology & Hydrologic Engineering*

Ni, S. J., Liu, X. F., Jin, J. F., and Lu, Q. X. 1997. Ore-forming fluid geochemistry of the fine disseminated gold deposits in the Dian-Qian-Gui triangle area. *Publish House of Chengdu University of Science and Technology, Chengdu.* 122p.

Noyes, R. 1993. Pollution prevention technology handbook. William Andrew. P. 342. ISBN 0-8155-13311-9

Okube, O., Yosiasa, A., Ohtaka, O., Fukai, H., Katayama, Y., Utsumi, 2002. W. Anharmonicity of gold under high-pressure and high-temperature. *Solid State Communications,* vol. 121, 200, pp235-239

Pascal, V., John, R. S., John, F. and James, H. R. 1987. Temperature effects on the universal equation of state of solids. *The American Physical Society*

Pletcher, D. and Walsh, F. 1990. Industrial electrochemistry. *Springer. p. 244.* ISBN 0-412-30410-4.

Poulsen, K.H., Robert, F., and Dube, B., 2000. Geological Classification of Canadian Gold Deposits*: Geological Survey of Canada,* Bulletin 540, 106 p.

Rajagopalan, S. 1979. Temperature variation of bulk moduli in solids. Il Nuovo Cimento B (1971-1996) volume 51, Issue 2, pages 222–228Richardson, R. M. 1992. Ridge forces, absolute plate motions, and the intraplate stress field. *Journal of Geophysical Research: Solid Earth,* 97 (B8), pp. 11739-11748.

Richeton, J. and Adharapurapu, R. R. 2006. Influence of temperature and strain rate on the mechanical behavior of three amorphous polymers: Characterization and modeling of the compressive yield stress. *International Journal of solids and structure*. Volume 43, Issue 7 – 8, pp 2318 – 2335.

Robertson, E. C. 1996. The interior of the Earth: An elementary description. *Geological Survey Circular* No. 532

Roland, B. and George, D.2008. Rheology of the lower crust and Upper Mantle, *Annual Review of Earth and Planetary Sciences.* (36): 531-67

Rudnick, R. L and Fountain, D. M. 1995. Nature and composition of the continental crust: A lower crustal perspective. *Reviews of Geophysics.* (33): 267-309

Rummel, F. 2005.*Rock mechanics with emphasis on stress.*

Shehadeh, M. A., Zbib, H. M. and De la Rubia, T. D., (2005). 'Modelling the dynamic deformation and patterning in fcc single crystals athigh strain rates: dislocation dynamics plasticity analysis', *Philos. Mag.,*85, 1667–1685.

Sia, N. N., Tomoo, O. and Luqun, N. 1998. A physically-based constitutive model for bcc crystals with application to polycrystalline tantalum. *Journal of the Mechanics and Physics of Solids*. Volume 46, Issue 6, June 1998, Pages 1009-1038

Sillitoe, R. H. 1979. Some thoughts on gold-rich porphyry copper deposits: *Mineralium Deposita,* v. 14, p. 161-174.

Sillitoe, R. H. 1980. Styles of low-grade gold mineralization in volcano-plutonic arcs, in Krai, V.E., and others, eds., Papers given at the precious-metals symposium, Nov. 17-19, 1980, *Sparks, Nev.: Nevada Bureau of Mines and Geology Report* 36, 172 p.

Sillitoe, R. H. 1981. Ore deposits in Cordilleran and island-arc environments of gold deposition, in Foster, R.P., ed., settings: *Arizona Geological Society Digest,* v. XIV, p. 49-69.

Stacey, F. D., 1977. A thermal model of the Earth. Phys. *Earth Planet Int.* 15: 341 – 348.

Stimson H. F. 1961. International Practical Temperature Scale of 1948.*JOURNAL OF RESEARCH of the National Bureau of Standards-A. Physics and Chemistry* Vol. 65A, No. 3, May-June

Susan L. N. 2009. Gold. *Harvard University Press*. p. 10. ISBN 0-674-03590-9. *Retrieved* 2012-04-10.

Taylor, H. P., Jr., 1979. Oxygen and hydrogen isotope relationships in hydrothermal mineral deposits, in Barnes, H.L., ed., *Geochemistry of hydrothermal ore deposits: New York, Wiley-Interscience*, p. 236-277.

Titley, S. R. 1978. Copper, molybdenum, and gold content of some porphyry copper systems of the southwestern and western Pacific: *Economic Geology,* v. 73, p. 977-981. Viljoen

Torbica, S. and Lapcevic, V. 2016. Model for Estimation of Stress Field in the Earth's Crust: Underground Mining Engineering, *University of Belgrade- faculty of Mining and Geology.* (28): 9 – 17

Turner, S.J., Flindell, P.A., Hendri, D.; Hardjana, I.,Lauricella, P.F., Lindsay, R.P., Marpaung, B.,and White, G.P. 1994. Sediment-hosted goldmineralization in the Ratatotok District, NorthSulawesi, Indonesia; *In Mineral Deposits ofIndonesia*: Discoveries of the past 25 years,

Volgyesi, L and Moser, M. 1982. The inner structure of the Earth. *Periodical Polytechnical, Chemical Engineering.* (26):13-14

Watts, A. B., 2007. Crustal and |Lithosphere Dynamics: *Elsevier.* Volume 6*, Oxford University of Oxford, Oxford U. K.*

Watts, A. B. 2001. Isostasy and Flexure of the Lithosphere. England: *Cambridge University Press*

White, W and Klein, E. 2014. Composition of the Oceanic Crust. *New York: Elsevier Ltd*.

William L. 2007. *Fundamentals of Geophysics second edition. Cambridge University Press.*

Zhiwei, B. 2001: Geochemistry of the Sediment-Hosted Disseminated Gold Deposits in Southwestern Guizhou Province, China. *Ph.D. Thesis*

Zhu, L. M, Liu, X. F, Jin, J. F, and He, M. Y. 1998a. The study of the time-space distribution and source of ore-forming fluid for the fine-disseminated gold deposits in the YunnanGuizhou-Gangxi area. *Scientia Geologica Sinica,* 33(4): 463-473. (In Chinese)

Turcotte, D. L. and Oxburg, E. R. 1976. Stress accumulation in the lithosphere. *Tecnophysics.* 35: pp 183 - 199

Vani, S. M., Valsan, K., Bhanu, S. R., Mannan, S. L. 2004. *Article in Metallurgical and Materials Transactions A.*
Verhoogen, J. 1980. Energetics of the Earth, *Nat. Acad. Sci., Washington, D.C*

Zoback, M. L. 1992. First- and second-order patterns of stress in the lithosphere: *the world stress map project. J Geophys Res* 97:11703–11728

Zoback, M. D and Zoback, M. L. 2002a. State of stress in the Earth's lithosphere. In: *Lee WHK (ed)International handbook of earthquake and engineering seismology,* vol 81A, pp 559–568

Appendix I

$B = z_0$, the referenced depth for crustal part of the lithosphere

A= Q_{MC}, the heat flux from the mantle into the crust.

Q_{MC}=25mW m^{-2}

z_0=8 km.

Q_0= 65 m Wm^{-2},

$q_0 z_0$= 40mW m^{-2}.

$\dot{q}_0 = 5 \times 10^{-6} Wm^{-3}$

$B = z_0$

A= Q_{MC}

$z_M = 35\ Km$

T_M, is the referenced temperature for upper part of the mantle

Q_0, heat flow

q=, radiogenic heat flux

$\dot{Q}_0$, mean value of continental heat flux

$\dot{q}_0$, mean value radiogenic heat flux = $5x10^{-6}Wm^{-3}$

$\dot{Q}_C$, total crustal heat = $65mWm^{-2}$

K_C, crustal thermal conductivity = $2.5Wm^{-1}k^{-1}$

K_M, mantle thermal conductivity = $4.0Wm^{-1}k^{-1}$

$\dot{q}_M$, mantle radiogenic heat $= 1.8 \times 10^{-8}\ Wm^{-3}$

$\dot{Q}_{MC}$, mantle –to- crustal heat flux $=25mWm^{-2}$

$g_C, accelerati\ on\ due\ to\ gravity\ in\ the\ crust = 9.83 ms^{-1}$
$g_M, accelerati\ on\ due\ to\ gravity\ in\ the\ mantle = 9.87 ms^{-1}$

$\rho_C, crustal\ density = 2800 Kg/m^3$
$\rho_M, mantle\ density = 3300 Km/m^3$

$\alpha_{Earth}, coefcoefficient\ of\ volume\ \exp ansion\ of\ the\ Earth = 14 \times 10^{-6} K$
$\rho_{Au}, coefficient\ of\ volume\ \exp ansion\ of\ gold = 14 \times 10^{-6} K^{-1}$

P, *pressure*
B, *bulk* mod *ulus*

$\Delta\eta$, *volume strain*

B, Flux Density

Appendix II

Theother relevant tables ofresults of experimental analyses carried out onselected unrefined gold samples for zones A – Eare shown below while the various figures showed the corresponding graphs remainingfor the groups in zones A- E.

Table 4.4: Average Values of Temperature, Volume and Pressure (sample 3)

Time (hr)	T °C	V*10^{-3} (m^3)	ΔV (m^3)	ΔV/V_0 Strain	V/V_0 Stress	P (Mpa)	ΔP (Mpa)	B (Gpa)	Δη Volume
0.5	2329.2	0.148	0.007	0.045	0.955	441.4	411.4	9.14	0.045
1.0	2389.5	0.139	0.016	0.103	0.890	449.4	419.4	4.07	0.103
1.5	2449.7	0.131	0.024	0.155	0.845	462.0	432.0	2.79	0.155
2.0	2510.0	0.127	0.028	0.181	0.819	474.2	444.2	2.45	0.181
2.5	2570.3	0.119	0.036	0.232	0.768	486.5	456.5	1.97	0.232
3.0	2630.6	0.113	0.042	0.271	0.729	498.7	468.7	1.73	0.271
3.5	2690.8	0.105	0.050	0.323	0.677	510.9	480.9	1.49	0.323
4.0	2751.1	0.099	0.056	0.361	0.639	523.2	493.2	1.37	0.361
4.5	2811.4	0.087	0.068	0.439	0.561	535.4	505.4	1.15	0.439
5.0	2871.7	0.055	0.100	0.645	0.355	547.7	517.7	0.80	0.645

Initial temperature,$T_0 = 42.0$ ℃

Initial pressure,$P_0 = 0.0\ MPa$

Initial volume of the sample,$V_0 = 0.155 * 10^{-3} m^3$

From Table 4.4, it was noticed that the bulk modulus decreased with increase in both temperature and pressure while the volume strain increased with increase in both temperature and pressure.

The compression in volume also increased as a result of application of pressure on the sample, the higher the pressure the more volume compressed. The graph of volume strain against time and the graph of bulk modulus against temperature for sample 3 are shown in Figures 4.3a and 4.3b.

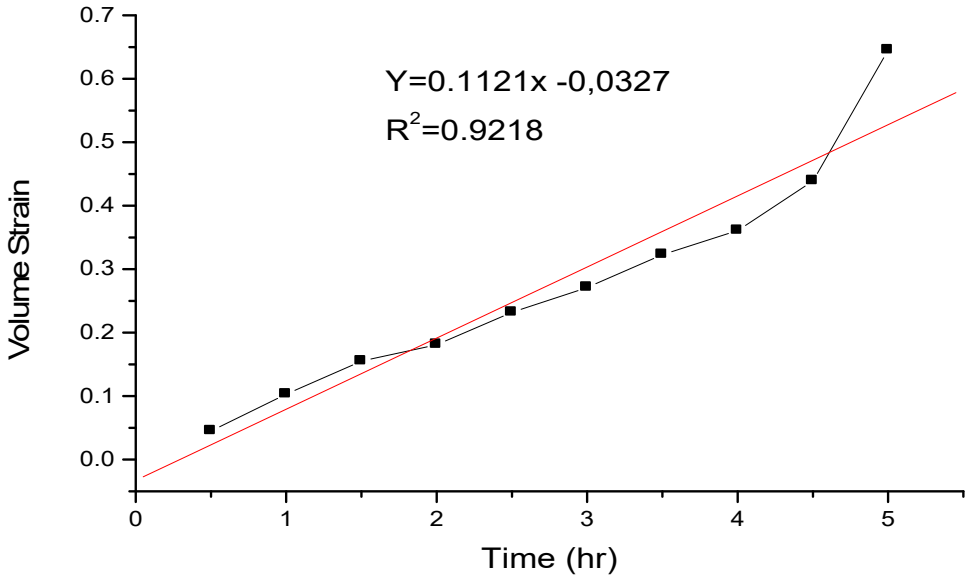

Figure 4.3a: Volume Strain Plotted Against Time (sample 3)

Figure 4.3a represents the graph of volume strain against time for sample 3. In the figure, the strain rate was 0.000031 s^{-1}, the rate increased with increase in time which conformed to literature laboratory values for materials while the coefficient of sample determination which determine the goodness of the fit was 0.9218.

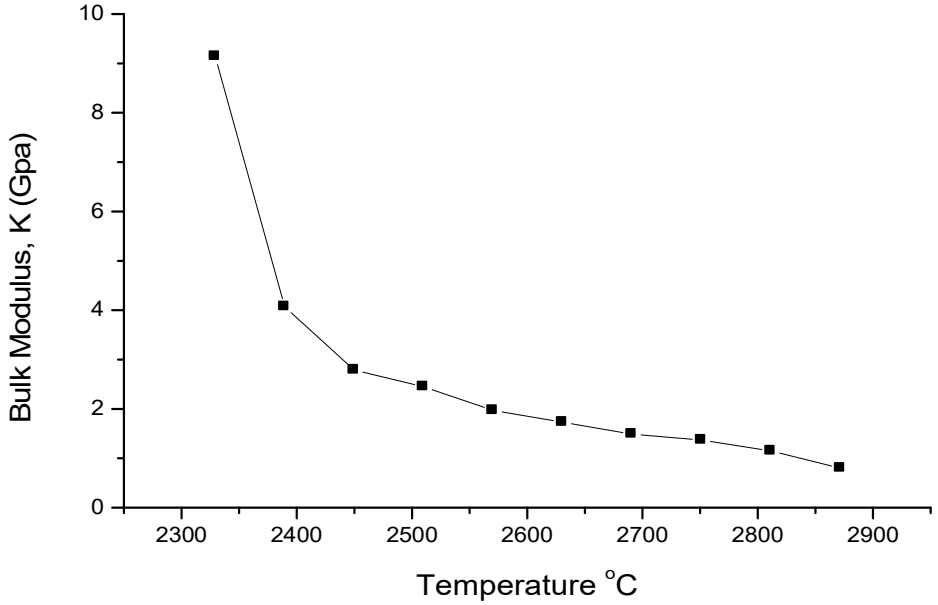

Figure 4.3b: Bulk Modulus Against Temperature (sample 3)

Figure 4.3b represents the graph of bulk modulus against temperature for sample 3, it was noticed from the graph that the bulk modulus of the sample decreased with increase in temperature. The behavior of the sample showed that the materials of this kind exhibit a type of volume compression which increased with rise in both temperature and pressure.

Table 4.5: Average Values of Temperature, Volume and Pressure (sample 4)

Time (hr)	T °C	V*10^{-3} (m^3)	ΔV (m^3)	ΔV/V_0 Strain	V/V_0	P (Mpa)	ΔP (Mpa) Stress	B (Gpa)	Δη Volume Strain
0.5	2327.3	0.139	0.006	0.041	0.959	434.0	404.0	9.85	0.041
1.0	2384.7	0.129	0.016	0.110	0.890	446.2	416.2	3.78	0.110
1.5	2470.6	0.123	0.022	0.152	0.848	458.1	428.1	2.82	0.152
2.0	2505.5	0.117	0.028	0.193	0.807	470.5	440.5	2.28	0.193
2.5	2568.2	0.112	0.033	0.228	0.772	482.6	452.6	1.99	0.228
3.0	2625.3	0.103	0.042	0.290	0.710	494.7	464.7	1.60	0.290
3.5	2688.7	0.100	0.045	0.310	0.690	506.9	476.9	1.54	0.310
4.0	2712.4	0.089	0.056	0.386	0.613	519.0	489.0	1.27	0.386
4.5	2809.1	0.075	0.070	0.483	0.517	531.2	501.2	1.04	0.483
5.0	2869.3	0.045	0.100	0.690	0.310	543.3	513.3	0.74	0.690

Initial temperature,$T_0 = 42.0$ ℃

Initial pressure,$P_0 = 0.0\ MPa$

Initial volume of the sample,$V_0 = 0.145 * 10^{-3} m^3$

From Table 4.5, it was observed that the bulk modulus decreased with increase in both temperature and pressure while the volume strain increased with increase in both temperature and pressure. The graph of volume strain against time and the graph of bulk modulus against temperature for sample 4 are shown in Figures 4.4a and 4.4b.

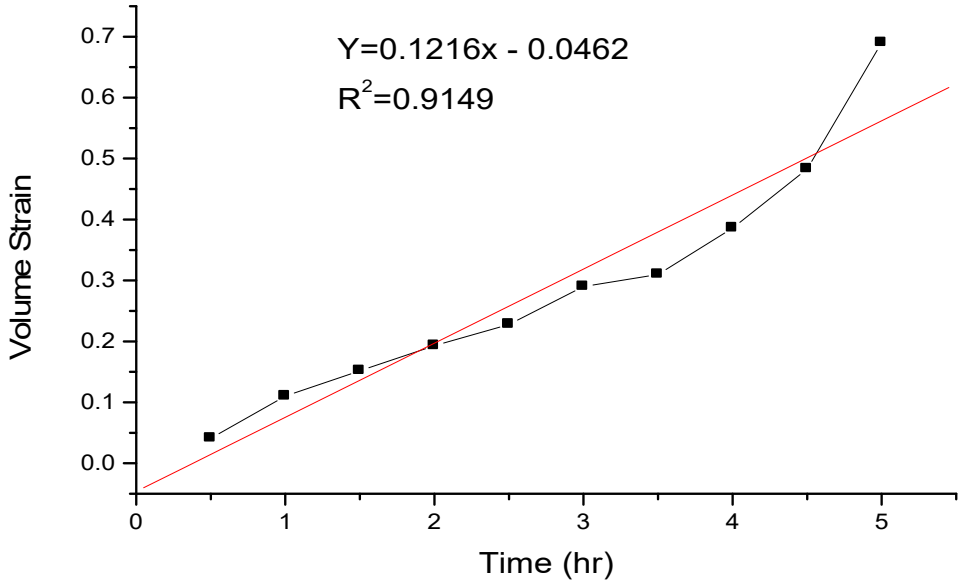

Figure 4.4a: Volume Strain Plotted Against Time (sample 4)

Figure 4.4a represents the graph of volume strain against time for sample 4. In the figure, the value of strain rate was 0.000034 s^{-1}, the rate increased with increase in time which conformed to literature laboratory values for materials while the coefficient of sample determination which determine the goodness of the fit was 0.9149.

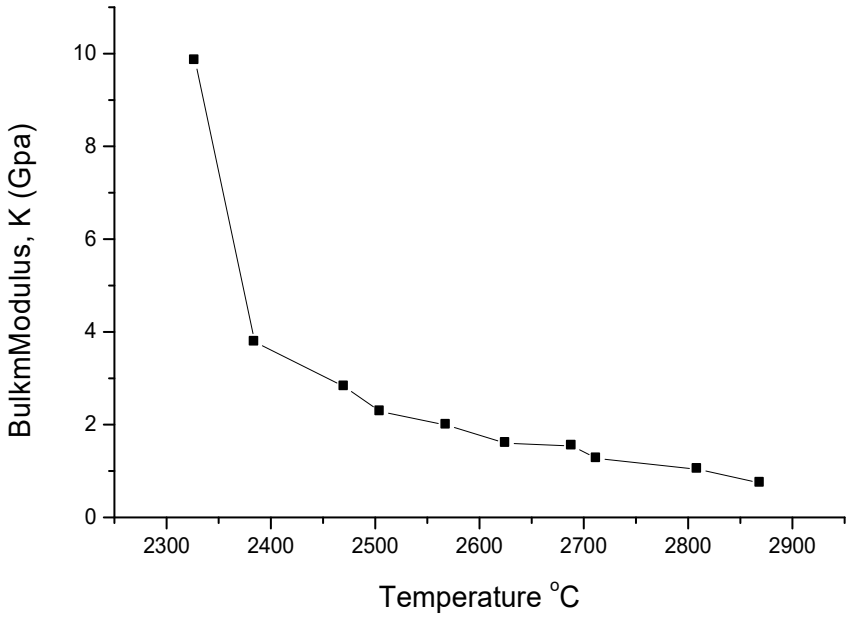

Figure 4.4b: Bulk Modulus Against Temperature (sample 4)

Figure 4.4b represents the graph of bulk modulus against temperature for sample 4, it was noticed from the graph that the bulk modulus of the sample decreased with increase in temperature. The behavior of the sample showed that the materials of this kind exhibit a type of volume compression which increased with rise in both temperature and pressure.

Table 4.6: Average Values of Temperature, Volume and Pressure (sample 5)

Time (hr)	T °C	V*10^{-3} (m^3)	ΔV (m^3)	ΔV/V_0 Strain	V/V_0 Stress	P (Mpa)	ΔP (Mpa)	B (Gpa)	Δη Volume Strain
0.5		2299.0	0.130	0.008	0.058	0.942	418.9	388.9	6.71 0.058
1.0		2358.5	0.122	0.016	0.116	0.884	430.7	400.7	3.45 0.116
1.5		2418.1	0.114	0.024	0.174	0.826	442.5	412.5	2.37 0.174

2.0	2477.7	0.106	0.032	0.232	0.768	453.3	423.3	1.82	0.232
2.5	2537.2	0.098	0.040	0.290	0.710	466.1	436.1	1.50	0.290
3.0	2596.8	0.092	0.046	0.333	0.667	477.9	447.9	1.35	0.333
3.5	2656.3	0.083	0.055	0.399	0.601	489.6	459.6	1.15	0.399
4.0	2715.9	0.076	0.062	0.449	0.551	501.4	471.4	1.05	0.449
4.5	2775.4	0.065	0.073	0.529	0.471	513.2	483.2	0.91	0.529
5.0	2835.0	0.038	0.100	0.725	0.275	525.0	495.0	0.68	0.725

Initial temperature,$T_0 = 42.0$ ℃

Initial pressure,$P_0 = 0.0\ MPa$

Initial volume of the sample,$V_0 = 0.138 * 10^{-3} m^3$

From Table 4.6, it was observed that the bulk modulus decreased with increase in both temperature and pressure while the volume strain increased with increase in both temperature and pressure. The graph of volume strain against time and the graph of bulk modulus against temperature for sample 5 are shown in Figures 4.5a and 4.5b.

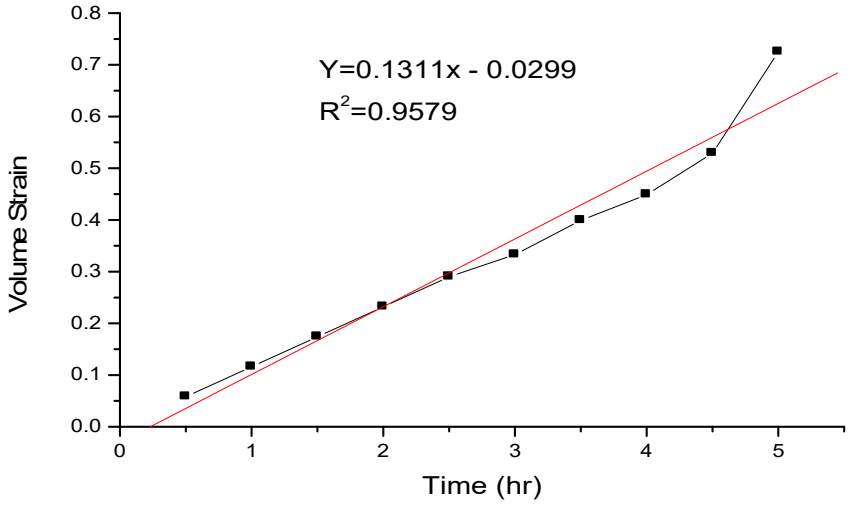

Figure 4.5a: Volume Strain Plotted Against Time (sample 5)

Figure 4.5a represents the graph of volume strain against time for sample 5. In the figure, the value of strain rate was 0.000036 s^{-1}, the rate increased with increase in time which conformed to literature laboratory values for materials while the coefficient of sample determination which determine the goodness of the fit was 0.9579.

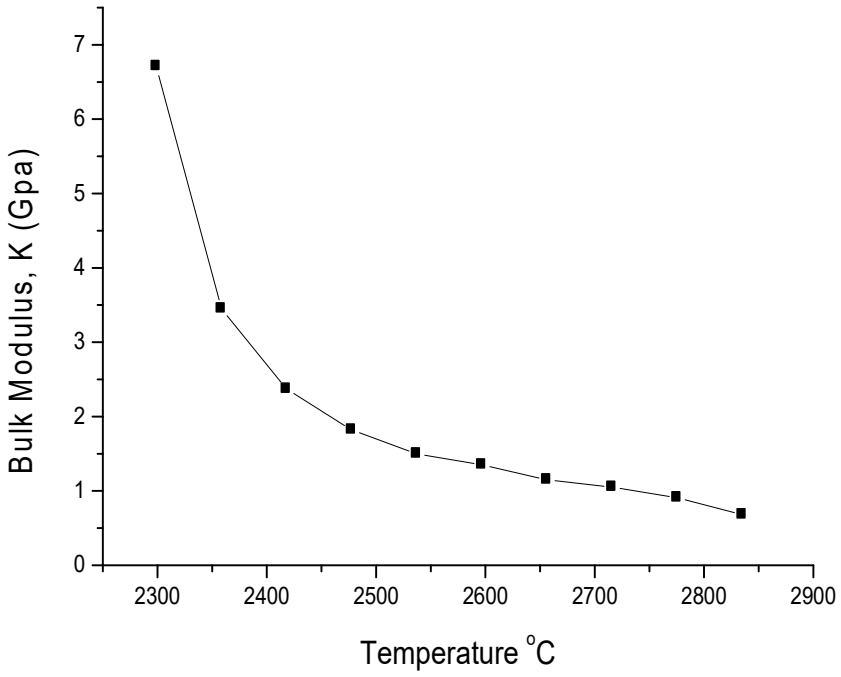

Figure 4.5b: Bulk Modulus Against Temperature (sample 5)

Figure 4.5b represents the graph of bulk modulus against temperature for sample 5, it was noticed from the graph that the bulk modulus of the sample decreased with increase in temperature. The behavior of the sample showed that the materials of this kind exhibit a type of volume compression which increased with rise in both temperature and pressure.

Table 4.7: Average Values of Temperature, Volume and Pressure (sample 6)

Time (hr)	T °C	V*10^{-3} (m^3)	ΔV (m^3)	ΔV/V_0 Strain	V/V_0	P (Mpa)	ΔP (Mpa) Stress	B (Gpa)	Δη Volume Strain
0.5		2303.6	0.134	0.006	0.043	0.957	429.5399.5	9.29	0.043

1.0	2363.3	0.128	0.012	0.086	0.914	441.5	411.5	4.78	0.086
1.5	2423.0	0.122	0.018	0.129	0.871	453.5	423.5	3.28	0.129
2.0	2482.6	0.116	0.024	0.171	0.829	465.5	435.5	2.55	0.171
2.5	2542.3	0.110	0.030	0.214	0.786	477.4	447.4	2.09	0.214
3.0	2602.0	0.104	0.036	0.257	0.743	489.6	459.6	1.79	0.257
3.5	2661.7	0.097	0.043	0.307	0.693	501.6	471.6	1.54	0.307
4.0	2721.3	0.088	0.052	0.371	0.623	513.6	483.6	1.30	0.371
4.5	2781.0	0.081	0.059	0.421	0.579	525.6	595.6	1.18	0.421
5.0	2840.7	0.040	0.100	0.714	0.286	537.7	507.7	0.71	0.714

Initial temperature,$T_0 = 42.0$ ℃

Initial pressure,$P_0 = 0.0\ MPa$

Initial volume of the sample,$V_0 = 0.140 * 10^{-3} m^3$

From Table 4.7, it was observed that the bulk modulus decreased with increase in both temperature and pressure while the volume strain increased with increase in both temperature and pressure. The is compression in volume which also increased as a result of the application of pressure on the sample, the higher the pressure the more volume compressed. The graph of volume strain against time and the graph of bulk modulus against temperature for sample 6 are shown in Figures 4.6a and 4.6b.

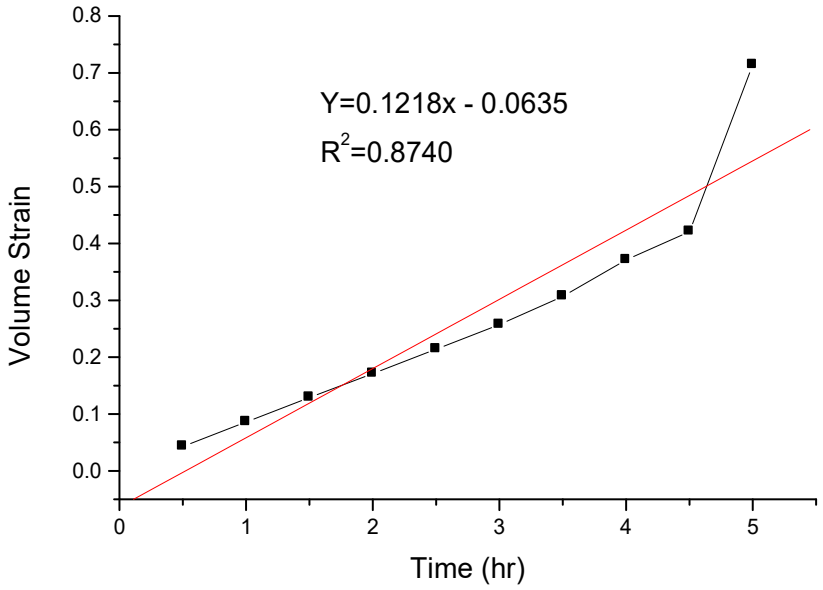

Figure 4.6a: Volume Strain Plotted Against Time (sample 6)

Figure 4.6a represents the graph of volume strain against time for sample 6. In the figure, the value of strain rate was 0.000038 s^{-1}, the rate increased with increase in time which conformed to literature laboratory values for materials while the coefficient of sample determination which determine the goodness of the fit was 0.8740.

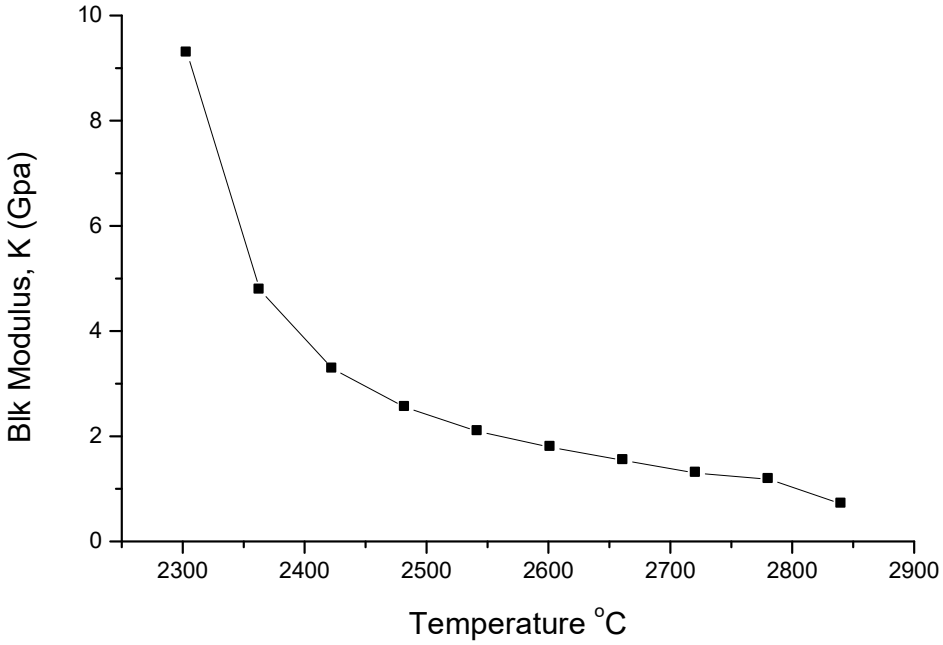

Figure 4.6b: Bulk Modulus Against Temperature (sample 6)

Figure 4.6b represents the graph of bulk modulus against temperature for sample 6, it was noticed from the graph that the bulk modulus of the sample decreased with increase in temperature. The behavior of the sample showed that the materials of this kind exhibit a form of volume compression which increased with rise in both temperature and pressure.

Table 4.10: Average Values of Temperature, Volume and Pressure (sample 9)

Time (hr)	T °C	$V*10^{-3}$ (m^3)	ΔV (m^3)	$\Delta V/V_0$ Strain	V/V_0	P (Mpa)	ΔP (Mpa)	B (Gpa)	$\Delta\eta$ Volume

						Stress			Strain
0.5	2317.8	0.138	0.008	0.058	0.945	443.8	413.87.13		0.058
1.0	2378.4	0.131	0.015	0.103	0.897	445.9	415.94.04		0.103
1.5	2439.8	0.124	0.022	0.151	0.849	458.0	428.0	2.83	0.151
2.0	2498.5	0.117	0.029	0.199	0.801	470.2	440.2	2.21	0.199
2.5	2558.5	0.110	0.036	0.247	0.753	482.3	452.3	1.83	0.247
3.0	2618.6	0.102	0.044	0.301	0.699	494.4	464.4	1.54	0.301
3.5	2678.6	0.094	0.052	0.356	0.644	506.6	476.6	1.34	0.356
4.0	2738.6	0.086	0.060	0.429	0.589	518.7	488.7	1.14	0.429
4.5	2898.6	0.079	0.067	0.459	0.541	530.3	500.3	1.09	0.459
5.0	2858.7	0.046	0.100	0.685	0.315	540.0	510.0	0.74	0.685

Initial temperature,$T_0 = 42.0$ ℃

Initial pressure,$P_0 = 0.0\ MPa$

Initial volume of the sample,$V_0 = 0.146 * 10^{-3} m^3$

From Table 4.10, it was observed that the bulk modulus decreased with increase in both temperature and pressure while the volume strain increased with increase in both temperature and pressure. The graph of volume strain against time and the graph of bulk modulus against temperature for sample 9 are shown in Figures 4.9a and 4.9b.

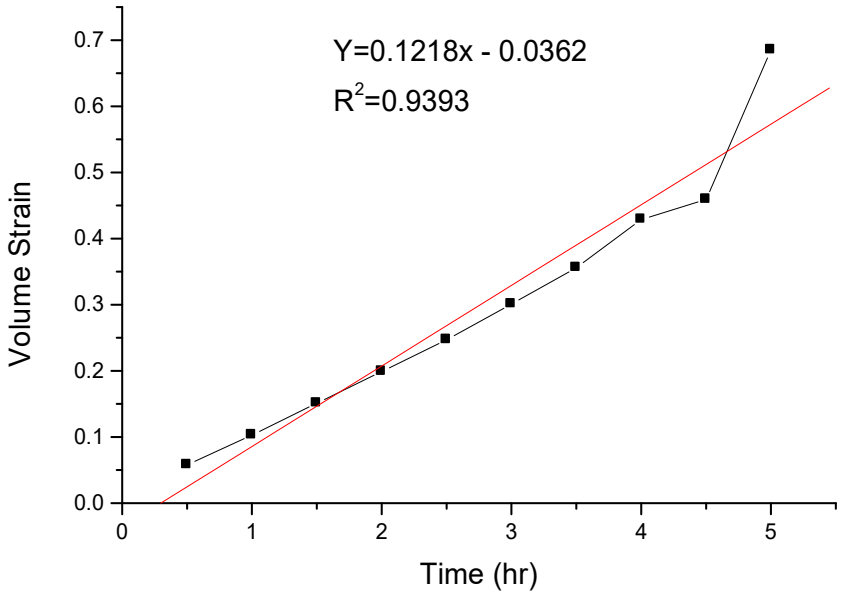

Figure 4.9a: Volume Strain Plotted Against Time (sample 9)

Figure 4.9a represents the graph of volume strain against time for sample 9. In the figure, the value of strain rate was 0.000034 s^{-1}, the rate increased with increase in time which conformed to literature laboratory values for materials while the coefficient of sample determination which determine the goodness of the fit was 0.9393.

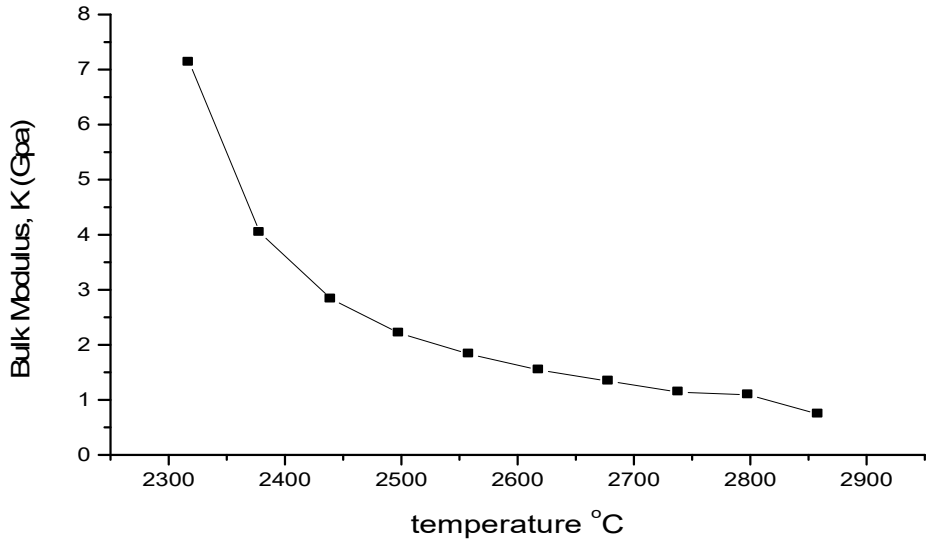

Figure 4.9b: Bulk modulus against temperature (sample 9)

Figure 4.9b represents the graph of bulk modulus against temperature for sample 9, it was noticed from the graph that the bulk modulus of the sample decreased with increase in temperature. The behavior of the sample showed that the material in this category exhibit a type of volume compression which increased with rise in both temperature and pressure.

Table 4.11: Average Values of Temperature, Volume and Pressure (sample 10)

Time (hr)	T °C	$V*10^{-3}$ (m^3)	ΔV (m^3)	$\Delta V/V_0$ Strain	V/V_0	P (Mpa)	ΔP (Mpa) Stress	B (Gpa)	$\Delta\eta$ Volume Strain

0.5	2321.5	0.140	0.008	0.054	0.946	434.8	404.87.50		0.054
1.0	2381.6	0.132	0.016	0.108	0.892	447.0	417.0	3.86	0.108
1.5	2441.7	0.124	0.024	0.162	0.838	459.2	429.2	2.65	0.162
2.0	2516.4	0.116	0.032	0.216	0.784	471.3	441.3	2.04	0.216
2.5	2561.9	0.108	0.040	0.270	0.730	483.5	453.5	1.68	0.270
3.0	2616.0	0.095	0.053	0.358	0.642	495.7	465.7	1.30	0.358
3.5	2682.0	0.087	0.061	0.412	0.588	507.8	477.8	1.16	0.412
4.0	2742.1	0.079	0.069	0.466	0.534	520.0	490.0	1.05	0.466
4.5	2802.2	0.071	0.077	0.520	0.480	532.2	502.2	1.97	0.520
5.0	2862.3	0.048	0.100	0.676	0.324	544.3	514.3	0.76	0.676

Initial temperature,$T_0 = 42.0$ ℃

Initial pressure,$P_0 = 0.0\ MPa$

Initial volume of the sample,$V_0 = 0.148 * 10^{-3} m^3$

From Table 4.11, it was observed that the bulk modulus decreased with increase in both temperature and pressure while the volume strain increased with increase in both temperature and pressure. The graph of volume strain against time and the graph of bulk modulus against temperature for sample 10 are shown in Figures 4.10a and 4.10b.

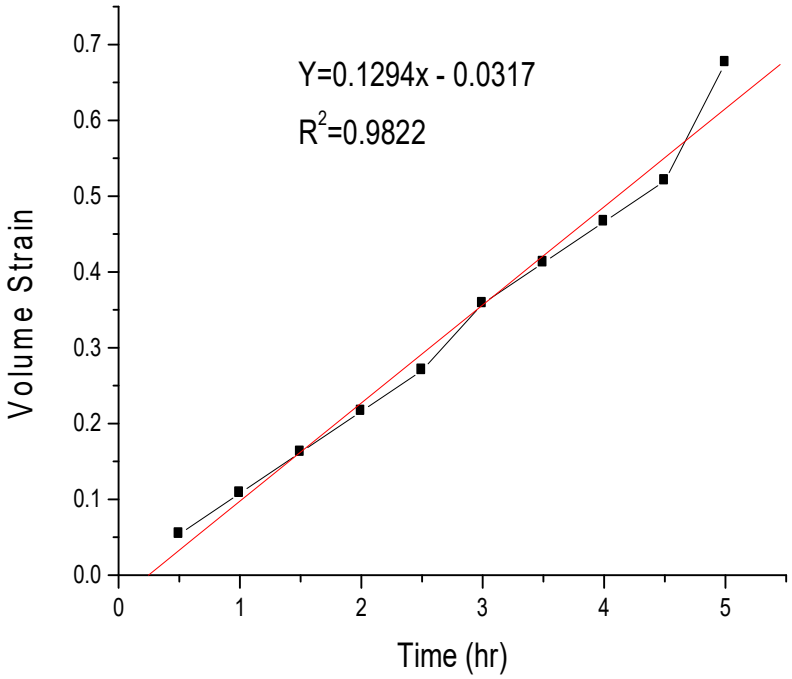

Figure 4.10a: Volume Strain Plotted Against Time (sample 10)

Figure 4.10a represents the graph of volume strain against time for sample 10. In the figure, the value of strain rate was 0.000036 s^{-1}, the rate increased with increase in time which conformed to literature laboratory values for materials while the coefficient of sample determination which determine the goodness of the fit was 0.9822.

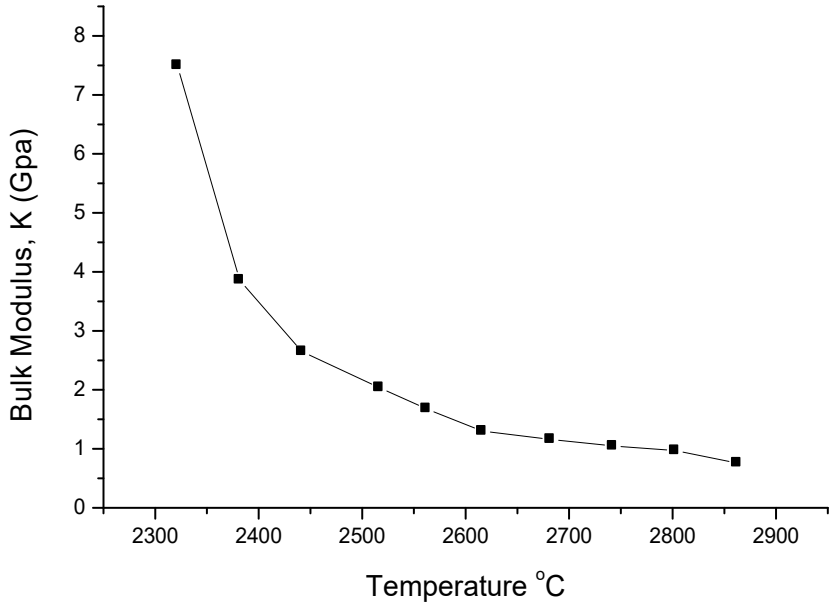

Figure 4.10b: Bulk Modulus Against Temperature (sample 10)

Figure 4.10b represents the graph of bulk modulus against temperature for sample 10, it was noticed from the graph that the bulk modulus of the sample decreased with increase in the temperature. The behavior of the sample showed that the material in this category exhibit a type of volume compression which increased with rise in both temperature and pressure.

Table 4.12: Average Values of Temperature, Volume and Pressure (sample 11)

Time (hr)	T °C	V*10^{-3} (m^3)	ΔV (m^3)	$\Delta V/V_0$ Strain	V/V_0	P (Mpa)	ΔP (Mpa) Stress	B (Gpa)	Δη Volume Strain

0.5	2328.1	0.142	0.010	0.066	0.934	435.1	405.1	6.14	0.066
1.0	2388.4	0.134	0.018	0.118	0.882	448.3	418.3	3.54	0.118
1.5	2427.6	0.126	0.026	0.171	0.829	460.5	430.5	2.52	0.171
2.0	2508.8	0.118	0.034	0.223	0.776	472.8	442.8	1.99	0.223
2.5	2569.2	0.110	0.042	0.276	0.724	484.0	454.0	1.64	0.276
3.0	2629.3	0.102	0.050	0.329	0.671	497.2	467.2	1.42	0.329
3.5	2689.6	0.094	0.058	0.382	0.618	509.4	479.4	1.25	0.382
4.0	2749.2	0.084	0.068	0.447	0.553	521.6	491.6	1.10	0.447
4.5	2856.1	0.076	0.076	0.500	0.500	533.8	503.8	1.01	0.500
5.0	2921.5	0.053	0.100	0.658	0.349	546.0	516.0	0.78	0.658

Initial temperature,$T_0 = 42.0$ ℃

Initial pressure,$P_0 = 0.0\ MPa$

Initial volume of the sample,$V_0 = 0.152 * 10^{-3} m^3$

From Table 4.12, it was observed that the bulk modulus decreased with increase in both temperature and pressure while the volume strain increased with increase in both temperature and pressure. The graph of volume strain against time and the graph of bulk modulus against temperature for sample 11 are shown in Figures 4.11a and 11b.

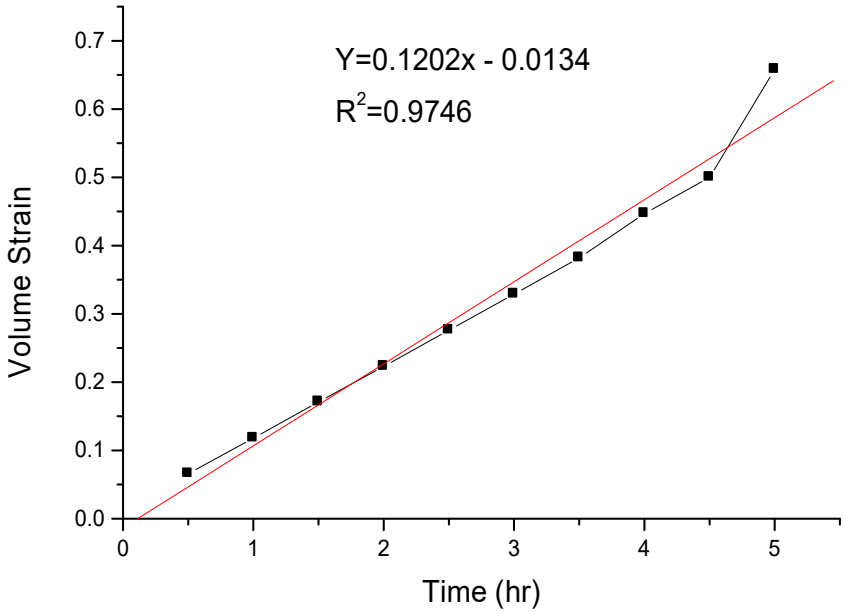

Figure 4.11a: Volume Strain Plotted Against Time (sample 11)

Figure 4.11a represents the graph of volume strain against time for sample 11. In the figure, the value of strain rate was 0.000033 s^{-1}, the rate increased with increase in time which conformed to literature laboratory values for materials while the coefficient of sample determination which determine the goodness of the fit for this sample was 0.9746.

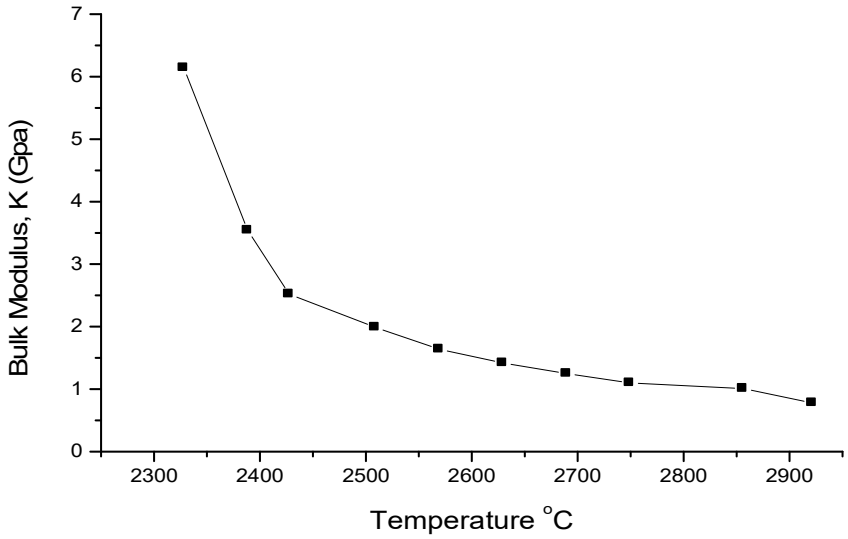

Figure 4.11b: Bulk Modulus Against Temperature (sample 11)

Figure 4.11b represents the graph of bulk modulus against temperature for sample 11, it was noticed from the graph that the bulk modulus of the sample decreased with increase in temperature. The behavior of the sample showed that the materials in this category exhibit a type of volume compression which increased with rise in both temperature and pressure.

Table 4.13: Average Values of Temperature, Volume and Pressure (sample 12)

Time (hr)	T °C	V*10^{-3} (m^3)	ΔV (m^3)	ΔV/V_0 Strain	V/V_0	P (Mpa)	ΔP (Mpa) Stress	B (Gpa)	Δη Volume Strain
	0.5	2330.2	0.142	0.012	0.078	0.922	437.5	407.55.22	0.078

1.0	2390.5	0.133	0.021	0.136	0.864	449.7	419.7	3.09	0.136
1.5	2450.9	0.123	0.031	0.201	0.799	461.9	431.9	2.15	0.201
2.0	2511.1	0.114	0.040	0.260	0.740	474.2	444.2	1.71	0.260
2.5	2571.5	0.105	0.049	0.318	0.682	486.4	456.4	1.44	0.318
3.0	2631.8	0.097	0.057	0.370	0.630	498.7	468.7	1.27	0.370
3.5	2692.1	0.088	0.066	0.429	0.571	510.9	480.9	1.12	0.429
4.0	2752.4	0.079	0.075	0.487	0.513	523.2	493.2	1.01	0.487
4.5	2812.7	0.071	0.083	0.539	0.461	535.4	505.4	0.94	0.539
5.0	2873.0	0.054	0.100	0.649	0.351	547.7	517.7	0.80	0.649

Initial temperature,$T_0 = 42.0$ ℃

Initial pressure,$P_0 = 0.0\ MPa$

Initial volume of the sample,$V_0 = 0.154 * 10^{-3} m^3$

From Table 4.13, it was observed that the bulk modulus decreased with increase in both temperature and pressure while the volume strain increased with increase in both temperature and pressure. The graph of volume strain against time and the graph of bulk modulus against temperature for sample 12 are shown in Figures 4.12a and 4.12b.

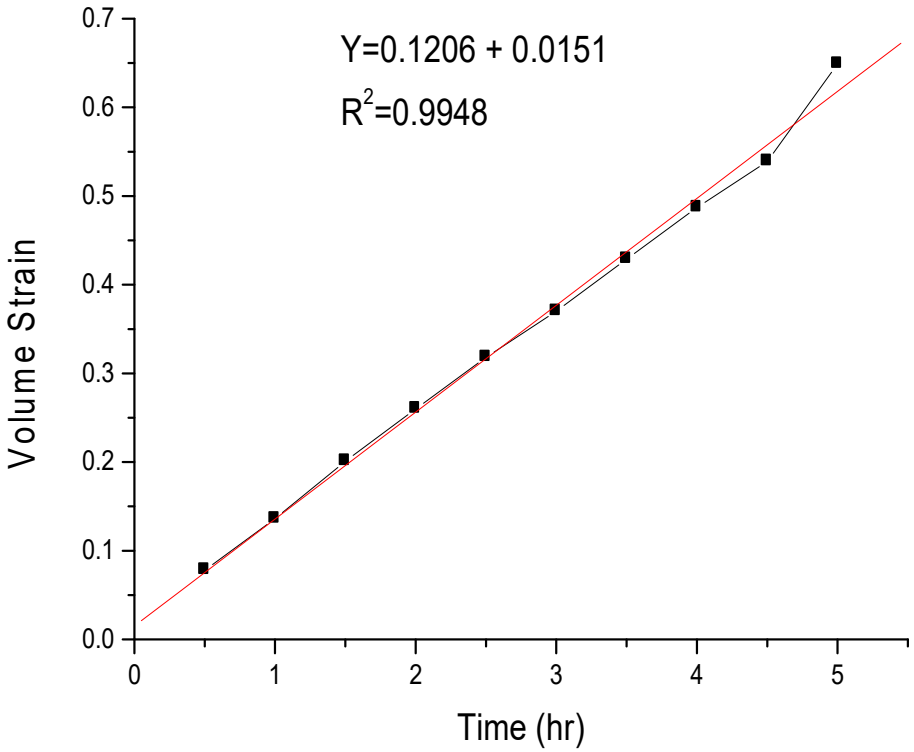

Figure 4.12a: Volume Strain Plotted Against Time (sample 12)

Figure 4.12a represents the graph of volume strain against time for sample 12. In the figure, the value of strain rate was 0.000034 s^{-1}, the rate increased with increase in time which conformed to literature laboratory values for materials while the coefficient of sample determination which determine the goodness of the fit was 0.9948.

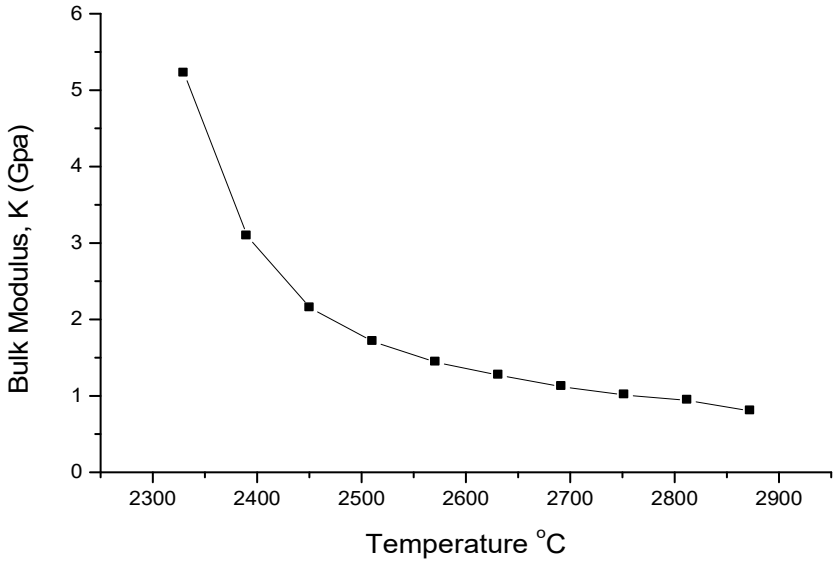

Figure 4.12b: Bulk Modulus Against Temperature (sample 12)

Figure 4.12b represents the graph of bulk modulus against temperature for sample 12, it was seen from the graph that the bulk modulus of the sample decreased with increase in temperature. The behavior of the sample showed that the material in this category show a type of volume compression which increased with rise in both temperature and pressure.

Table 4.16: Average Values of Temperature, Volume and Pressure (sample 15)

Time (hr)	T °C	V*10^{-3} (m^3)	ΔV (m^3)	ΔV/V$_0$ Strain	V/V$_0$	P (Mpa)	ΔP (Mpa)	B (Gpa) Stress	Δη Volume	Strain
0.5	2335.3	0.150	0.013	0.080	0.920	440.6	410.6	5.13	0.080	

1.0	2395.6	0.143	0.020	0.123	0.877	453.0	423.0	3.44	0.123
1.5	2456.2	0.135	0.028	0.271	0.828	465.3	435.3	2.53	0.172
2.0	2516.7	0.127	0.036	0.221	0.799	477.6	447.6	2.03	0.221
2.5	2577.1	0.119	0.044	0.270	0.730	490.0	460.0	1.70	0.270
3.0	2637.6	0.110	0.053	0.325	0.675	502.3	472.3	1.45	0.325
3.5	2698.0	0.100	0.063	0.387	0.613	514.7	484.7	1.25	0.387
4.0	2754.4	0.090	0.073	0.448	0.552	527.0	497.0	1.11	0.448
4.5	2818.9	0.080	0.083	0.509	0.491	539.3	509.3	1.00	0.509
5.0	2897.3	0.063	0.100	0.613	0.387	551.7	521.7	0.85	0.613

Initial temperature,$T_0 = 42.0$ ℃

Initial pressure,$P_0 = 0.0\ MPa$

Initial volume of the sample,$V_0 = 0.163 * 10^{-3} m^3$

From Table 4.16, it was observed that the bulk modulus decreased with increase in both temperature and pressure while the volume strain increased with increase in both temperature and pressure. The graph of volume strain against time and the graph of bulk modulus against temperature for sample 15 are shown in Figures 4.15a and 4.15b.

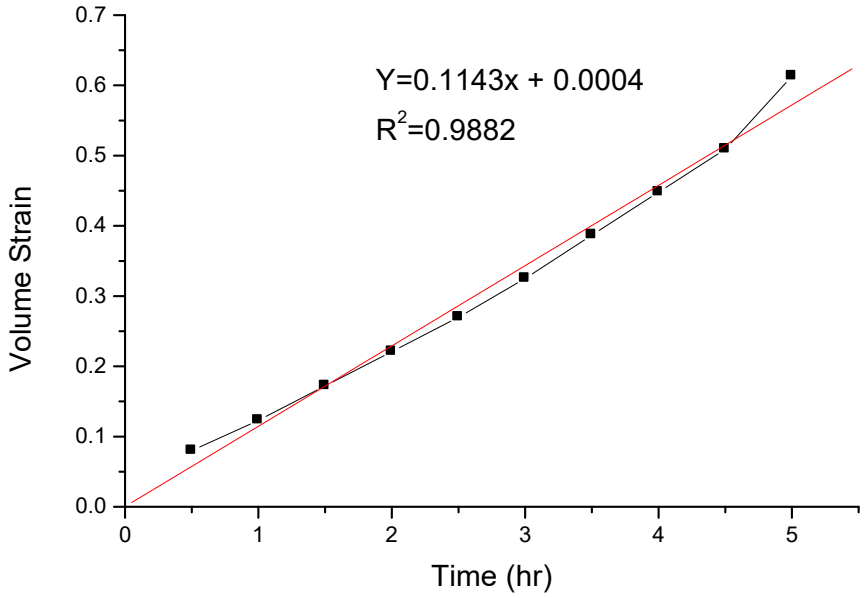

Figure 4.15a: Volume Strain Plotted Against Time (sample 15)

Figure 4.15a represents the graph of volume strain against time for sample 15. In the figure, the value of strain rate was 0.000032 s^{-1}, the rate increased with increase in time which conformed to literature laboratory values for materials while the coefficient of sample determination which determine the goodness of the fit was 0.9882.

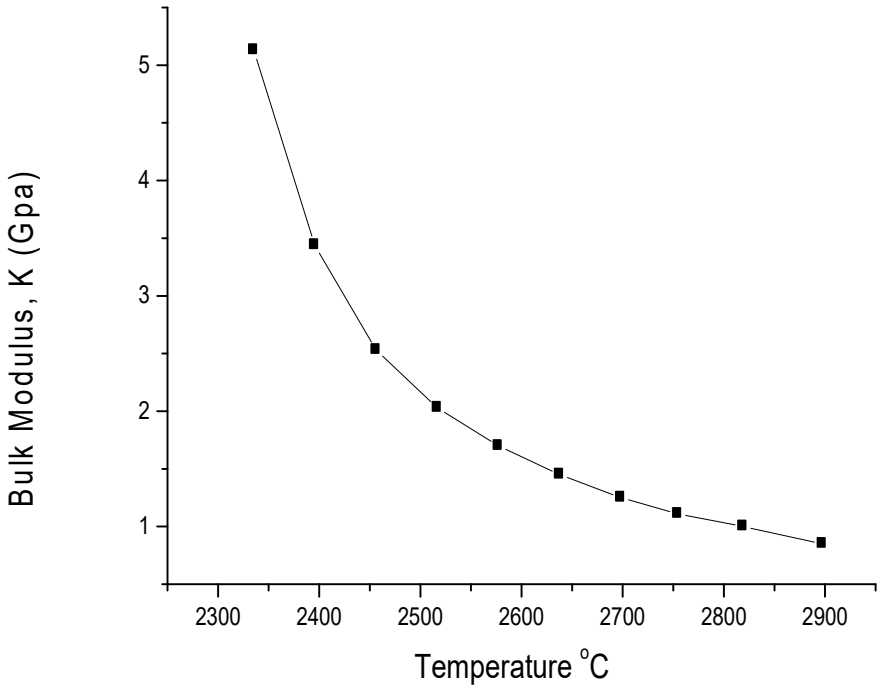

Figure 4.15b: Bulk Modulus Against Temperature (sample 15)

Figure 4.15b represents the graph of bulk modulus against temperature for sample 15, it was noticed from the graph that the bulk modulus of the sample decreased with increase in temperature. The behavior of the sample showed that the material in this category show a type of volume compression which increased with rise in both temperature and pressure.

Table 4.17: Average Values of Temperature, Volume and Pressure (sample 16)

Time (hr)	T °C	V*10^{-3} (m^3)	ΔV (m^3)	$\Delta V/V_0$ Strain	V/V_0	P (Mpa)	ΔP (Mpa)	B (Gpa)	Δη Volume

							Stress		Strain
0.5	2321.9	0.152	0.012	0.073	0.927	441.5	411.6	5.64	0.073
1.0	2397.4	0.144	0.020	0.122	0.878	453.8	423.8	3.47	0.122
1.5	2457.9	0.135	0.029	0.277	0.823	466.2	436.2	2.46	0.177
2.0	2518.4	0.128	0.036	0.220	0.780	478.5	448.5	2.04	0.220
2.5	2578.9	0.119	0.045	0.274	0.726	490.9	460.9	1.68	0.274
3.0	2639.4	0.109	0.055	0.335	0.665	503.2	473.2	1.41	0.335
3.5	2699.9	0.099	0.065	0.396	0.604	515.6	485.6	1.23	0.396
4.0	2760.3	0.089	0.075	0.457	0.543	528.0	498.0	1.09	0.457
4.5	2820.9	0.079	0.085	0.518	0.482	540.3	510.3	0.99	0.518
5.0	2881.3	0.064	0.100	0.610	0.390	552.7	522.7	0.86	0.610

Initial temperature,$T_0 = 42.0$ ℃

Initial pressure,$P_0 = 0.0\ MPa$

Initial volume of the sample,$V_0 = 0.164 * 10^{-3} m^3$

From Table 4.17, it was observed that the bulk modulus decreased with increase in both temperature and pressure while the volume strain increased with increase in both temperature and pressure. The graph of volume strain against time and the graph of bulk modulus against temperature for sample 16 are shown in Figures 4.16a and 4.16b.

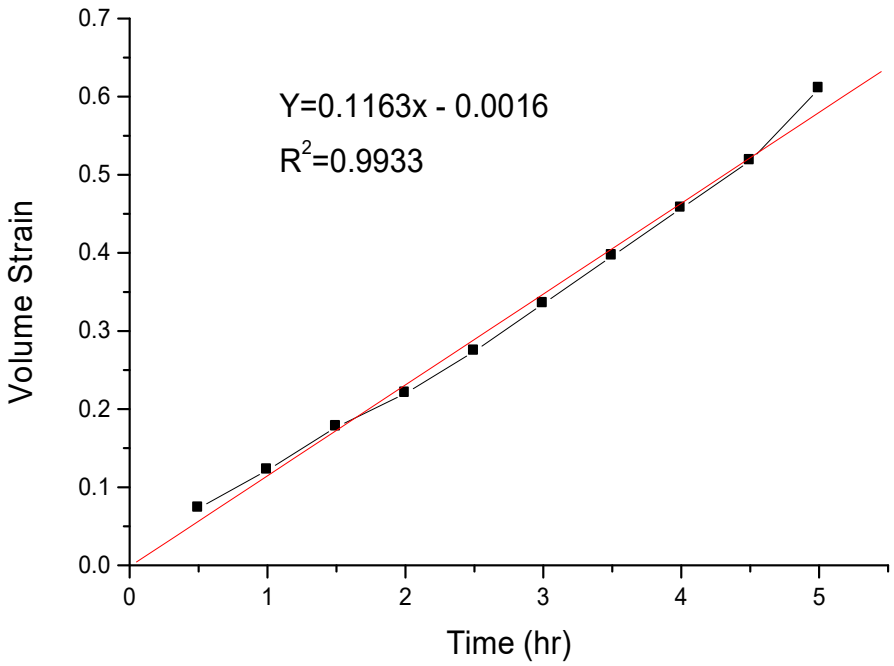

Figure 4.16a: Volume Strain Plotted Against Time (sample 16)

Figure 4.16a represents the graph of volume strain against time for sample 16. In the figure, the value of strain rate was 0.000032 s^{-1}, the rate increased with increase in time which conformed to literature laboratory values for materials while the coefficient of sample determination which determine the goodness of the fit for this sample was 0.9933.

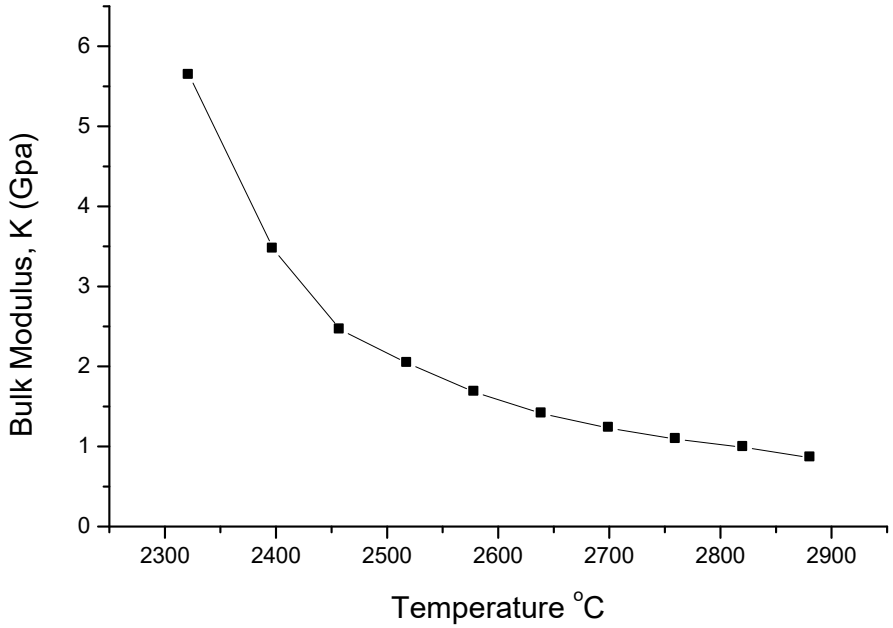

Figure 4.16b: Bulk Modulus Against Temperature (sample 16)

Figure 4.16b represents the graph of bulk modulus against temperature for sample 16, it was noticed from the graph that the bulk modulus of the sample decreased with increase in temperature. The behavior of the sample showed that the material in this category show a type of volume compression which increased with rise in both temperature and pressure.

Table 4.18: Average Values of Temperature, Volume and Pressure (sample 17)

Time (hr)	T °C	V*10^{-3} (m^3)	ΔV (m^3)	ΔV/V_0 Strain	V/V_0	P (Mpa)	ΔP (Mpa)	B (Gpa)	Δη Volume

							Stress		Strain
0.5	2338.5	0.154	0.012	0.072	0.928	442.2	412.2	5.73	0.072
1.0	2459.6	0.146	0.020	0.120	0.880	454.6	424.6	3.54	0.120
1.5	2459.6	0.138	0.028	0.169	0.831	467.0	437.0	2.59	0.169
2.0	2520.1	0.130	0.036	0.217	0.783	479.4	449.0	2.07	0.217
2.5	2580.7	0.120	0.046	0.277	0.723	491.7	461.7	1.67	0.277
3.0	2641.2	0.110	0.056	0.337	0.663	504.1	474.1	1.41	0.337
3.5	2701.7	0.100	0.066	0.398	0.602	516.5	486.5	1.22	0.398
4.0	2762.3	0.090	0.076	0.458	0.542	528.9	498.9	1.09	0.458
4.5	2822.8	0.080	0.086	0.518	0.482	541.3	511.3	0.99	0.518
5.0	2883.3	0.066	0.100	0.602	0.398	553.7	523.7	0.87	0.602

Initial temperature,$T_0 = 42.0$ ℃

Initial pressure,$P_0 = 0.0\ MPa$

Initial volume of the sample,$V_0 = 0.166 * 10^{-3} m^3$

From Table 4.18, it was observed that the bulk modulus decreased with increase in both temperature and pressure while the volume strain increased with increase in both temperature and pressure. The graph of volume strain against time and the graph of bulk modulus against temperature for sample 17 are shown in Figures 4.17a and 4.17b.

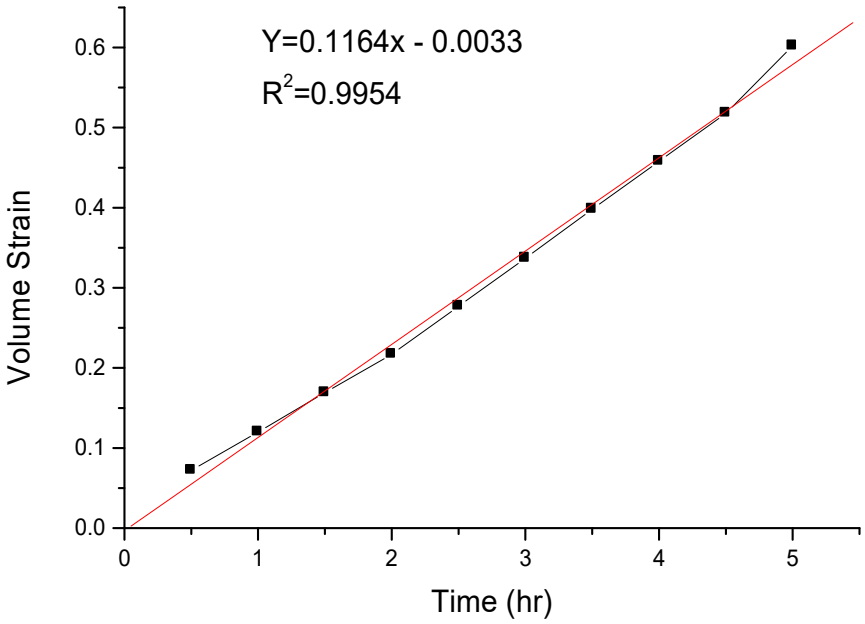

Figure 4.17a: Volume Strain Plotted Against Time (sample 17)

Figure 4.17a represents the graph of volume strain against time for sample 17. In the figure, the value of strain rate was 0.000032 s^{-1}, the rate increased with increase in time which conformed to literature laboratory values for materials while the coefficient of sample determination which determine the goodness of the fit was 0.9954.

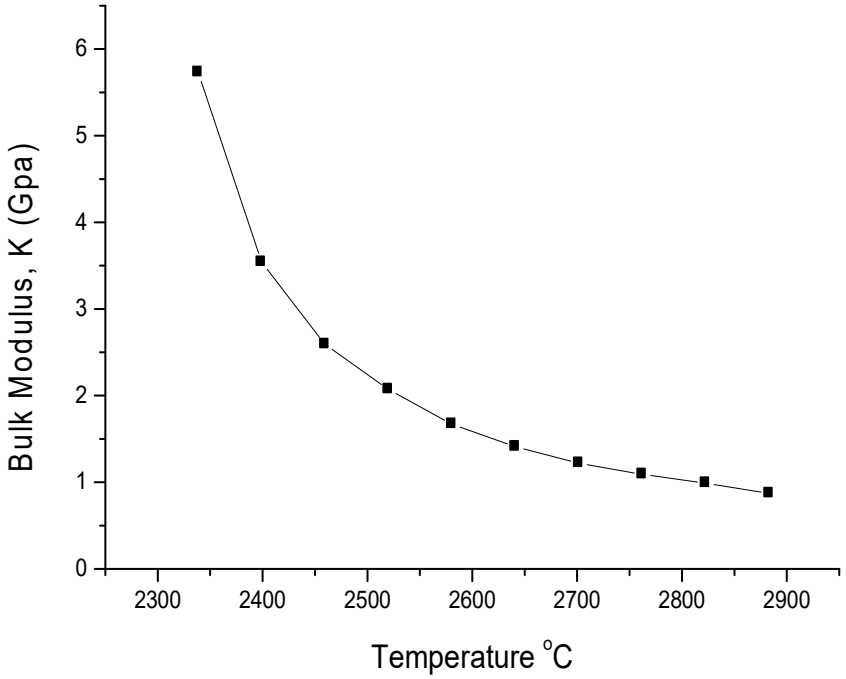

Figure 4.17b: Bulk Modulus Against Temperature (sample 17)

Figure 4.17b represents the graph of bulk modulus against temperature for sample 17, it was noticed from the graph that the bulk modulus of the sample decreased with increase in temperature. The behavior of the sample showed that the material in this category exhibit a type of volume compression which increased with rise in both temperature and pressure.

Table 4.19: Average Values of Temperature, Volume and Pressure (sample 18)

Time (hr)	T °C	V*10^{-3} (m^3)	ΔV (m^3)	$\Delta V/V_0$ Strain	V/V_0	P (Mpa)	ΔP (Mpa) Stress	B (Gpa)	Δη Volume Strain
0.5	2339.9	0.156	0.012	0.071	0.929	443.8	413.8	5.82	0.071
1.0	2400.4	0.148	0.020	0.119	0.881	456.3	426.3	3.58	0.119
1.5	2461.0	0.140	0.029	0.167	0.833	468.7	438.7	2.63	0.167
2.0	2521.6	0.132	0.036	0.214	0.786	481.1	451.1	2.11	0.214
2.5	2582.1	0.123	0.045	0.268	0.732	493.5	463.51.73	0.268	
3.0	2642.7	0.113	0.055	0.327	0.673	505.9	475.9	1.46	0.327
3.5	2703.3	0.103	0.065	0.387	0.613	518.4	488.4	1.26	0.387
4.0	2763.8	0.093	0.075	0.446	0.554	530.8500.8	1.12	0.446	
4.5	2824.4	0.083	0.085	0.506	0.494	543.2	513.31.01	0.506	
5.0	2885.0	0.068	0.100	0.595	0.405	555.7	525.7	0.88	0.595

Initial temperature,$T_0 = 42.0$ ℃

Initial pressure,$P_0 = 0.0\ MPa$

Initial volume of the sample,$V_0 = 0.168 * 10^{-3} m^3$

From Table 4.19, it was observed that the bulk modulus reduced with rise in both temperature and pressure while the volume strain increased with increase in both temperature and pressure. The graph of volume strain against time and the graph of bulk modulus against temperature for sample 18 are shown in Figures 4.18a and 4.18b.

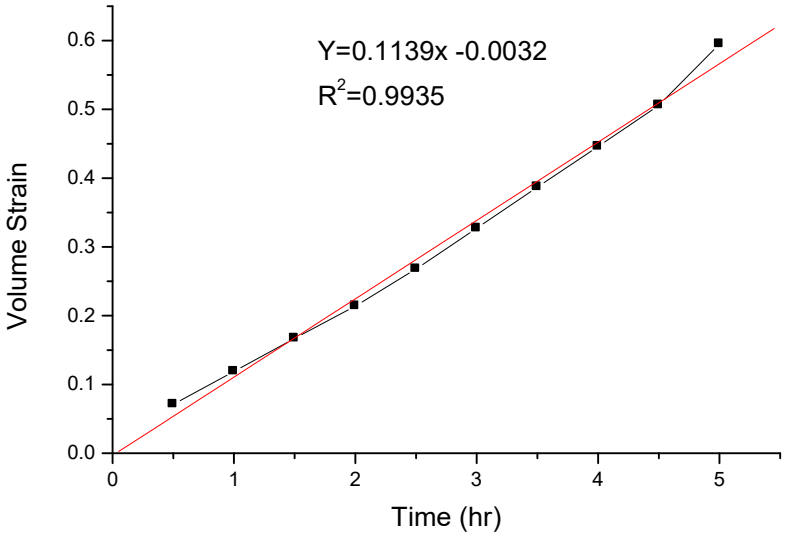

Figure 4.18a: Volume Strain Plotted Against Time (sample 18)

Figure 4.18a represents the graph of volume strain against time for sample 18. In the figure, the value of strain rate was 0.000032 s^{-1}, the rate increased with increase in time which conformed to literature laboratory values for materials while the coefficient of sample determination which determine the goodness of the fit was 0.9935.

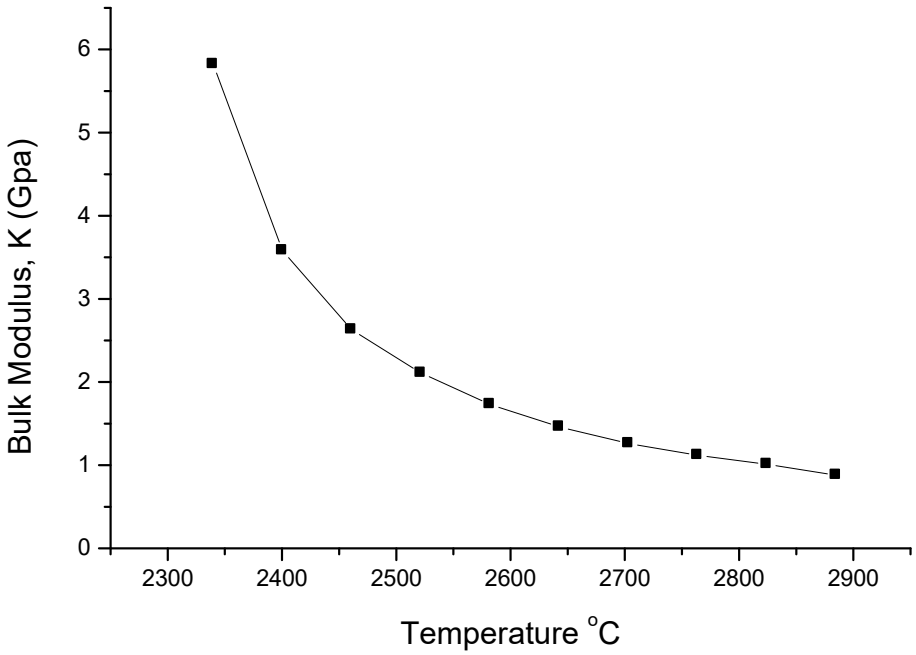

Figure 4.18b: Bulk Modulus Against Temperature (sample 18)

Figure 4.18b represents the graph of bulk modulus against temperature for sample 18, it was noticed from the graph that the bulk modulus of the sample decreased with increase in temperature. The behavior of the sample showed that the material in this category exhibit a type of volume compression which increased with rise in both temperature and pressure.

Table 4.22: Average Values of Temperature, Volume and Pressure (sample 21)

Time (hr)	T °C	V*10^{-3} (m^3)	ΔV (m^3)	$\Delta V/V_0$ Strain	V/V_0	P (Mpa)	ΔP (Mpa) Stress	B (Gpa)	Δη Volume Strain
0.5	2344.1	0.160	0.012	0.070	0.930	447.3	417.3	5.96	0.070
1.0	2404.8	0.152	0.020	0.116	0.884	459.8	429.8	3.71	0.116
1.5	2465.2	0.144	0.028	0.163	0.837	472.3	442.3	2.71	0.163
2.0	2526.2	0.136	0.036	0.204	0.791	484.9	454.9	2.18	0.209
2.5	2586.9	0.126	0.046	0.267	0.733	497.4	467.4	1.75	0.267
3.0	2647.6	0.113	0.059	0.343	0.657	509.9	479.9	1.40	0.343
3.5	2708.2	0.106	0.066	0.384	0.616	520.8	490.8	1.28	0.384
4.0	2769.0	0.096	0.076	0.442	0.558	535.0	505.0	1.14	0.442
4.5	2829.7	0.086	0.086	0.500	0.500	547.5	517.5	1.04	0.500
5.0	2890.5	0.072	0.100	0.581	0.419	560.0	530.0	0.91	0.581

Initial temperature,$T_0 = 42.0$ ℃

Initial pressure,$P_0 = 0.0\ MPa$

Initial volume of the sample,$V_0 = 0.172 * 10^{-3} m^3$

From Table 4.22, it was observed that the bulk modulus decreased with increase in both temperature and pressure while the volume strain increased with increase in both temperature and pressure. The graph of volume strain against time and the graph of bulk modulus against temperature for sample 21 are shown in Figures 4.21a and 4.21b.

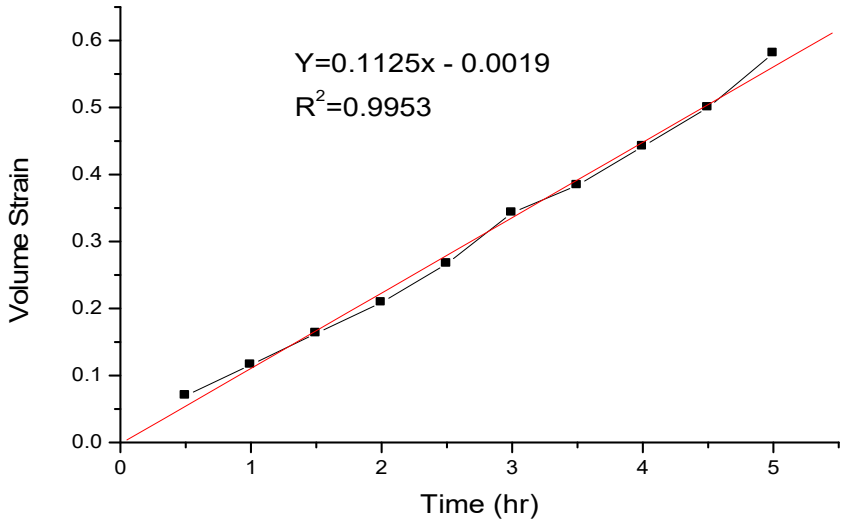

Figure 4.21a: Volume Strain Plotted Against Time (sample 21)

Figure 4.21a represents the graph of volume strain against time for sample 21. In the figure, the value of strain rate was $0.000031s^{-1}$, the strain rate increased with increase in time which conformed to literature laboratory values for materials while the square of the sample correlation which determine the goodness of the fit was 0.9953.

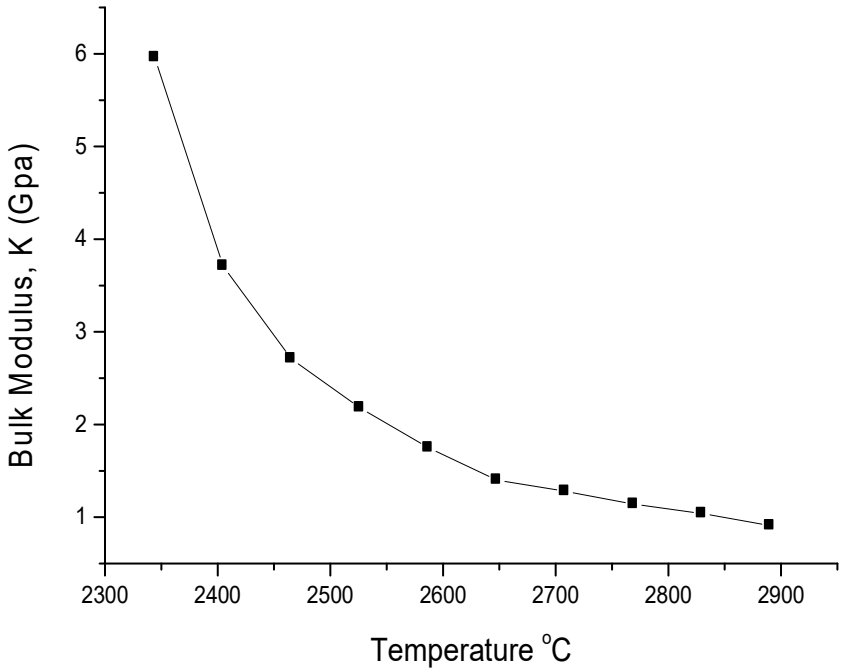

Figure 4.21b: Bulk Modulus Against Temperature (sample 21)

Figure 4.21b represents the graph of bulk modulus against temperature for sample 21, it was noticed from the graph that the bulk modulus of the sample decreased with increase in temperature. The behavior of the sample showed that the material in this category exhibit a type of volume compression which increased with rise in both temperature and pressure.

Table 4.23: Average Values of Temperature, Volume and Pressure (sample 22)

Time	T °C	$V*10^{-3}$	ΔV	$\Delta V/V_0$	V/V_0	P	ΔP	B	$\Delta\eta$

(hr)		(m^3)	(m^3)	Strain		(Mpa)	(Mpa) Stress	(Gpa)	Volume Strain
0.5	1982.7	0.162	0.012	0.069	0.931	448.1	418.16.06		0.069
1.0	2033.6	0.154	0.020	0.115	0.885	460.6	430.6	3.74	0.115
1.5	2084.4	0.146	0.028	0.161	0.839	503.2	473.2	2.94	0.161
2.0	2135.5	0.138	0.036	0.207	0.793	473.2	443.2	2.14	0.207
2.5	2186.4	0.128	0.046	0.264	0.736	498.3	468.3	1.77	0.264
3.0	2237.4	0.118	0.056	0.321	0.678	510.8	480.8	1.50	0.321
3.5	2273.2	0.108	0.066	0.379	0.621	524.1	494.1	1.30	0.379
4.0	2339.1	0.098	0.076	0.437	0.563	535.9	505.9	1.16	0.437
4.5	2390.1	0.088	0.086	0.494	0.506	548.5	518.5	1.05	0.494
5.0	2441.0	0.074	0.100	0.575	0.425	561.0	531.0	0.92	0.575

Initial temperature,$T_0 = 42.0$ ℃

Initial pressure,$P_0 = 0.0\ MPa$

Initial volume of the sample,$V_0 = 0.174 * 10^{-3} m^3$

From Table 4.23, it was observed that the bulk modulus decreased with increase in both temperature and pressure while the volume strain increased with increase in both temperature and pressure. The graph of volume strain against time and the graph of bulk modulus against temperature for sample 22 are shown in Figures 4.22a and4.22b.

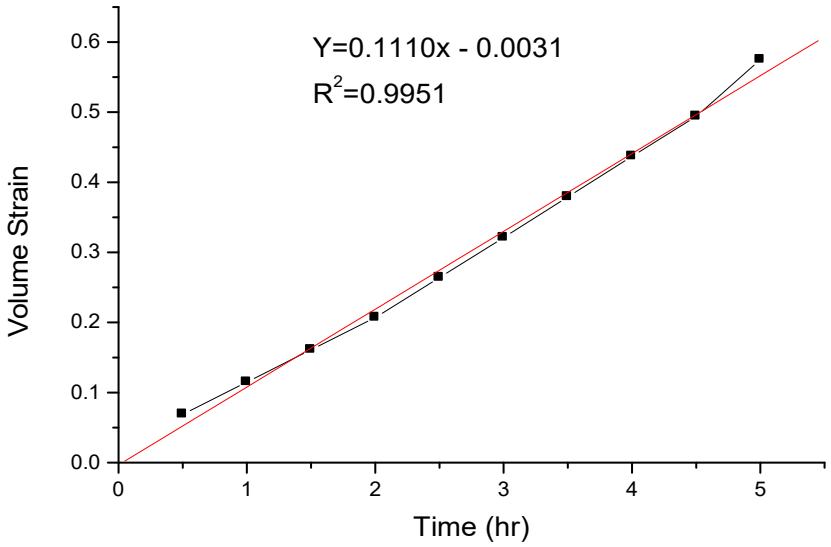

Figure 4.22a: Volume Strain Plotted Against Time (sample 22)

Figure 4.22a represents the graph of volume strain against time for sample 22. In the figure, the value of strain rate was 0.000031 s^{-1}, the rate increased with increase in time which conformed to literature laboratory values for materials while the square of the sample correlation which determine the goodness of the fit was 0.9951.

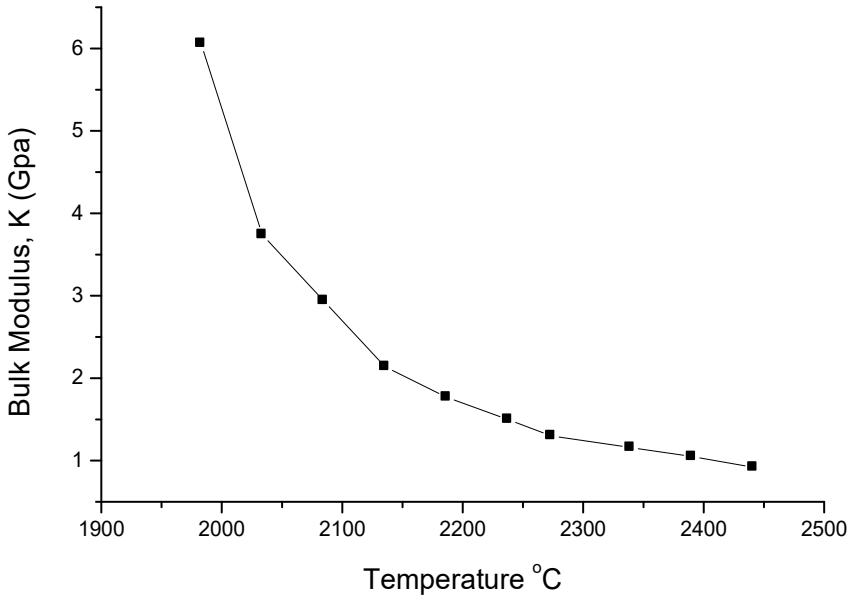

Figure 4.22b: Bulk Modulus Against Temperature (sample 22)

Figure 4.22b represents the graph of bulk modulus against temperature for sample 22, it was noticed from the graph that the bulk modulus of the sample decreased with increase in temperature. The behavior of the sample showed that the material in this category exhibit a type of volume compression which increased with rise in both temperature and pressure.

Table 4.24: Average Values of Temperature, Volume and Pressure (sample 23)

Time (hr)	T °C	V*10^{-3} (m^3)	ΔV (m^3)	ΔV/V$_0$ Strain	V/V$_0$	P (Mpa)	ΔP (Mpa) Stress	B (Gpa)	Δη Volume Strain
0.5	2345.5	0.162	0.013	0.074	0.926	448.9	418.9	5.66	0.074
1.0	2406.2	0.154	0.021	0.120	0.888	461.5	431.5	3.60	0.120
1.5	2466.9	0.146	0.029	0.166	0.834	474.0	444.0	2.67	0.166
2.0	2527.6	0.138	0.037	0.211	0.789	486.6	456.6	2.16	0.211
2.5	2588.4	0.128	0.047	0.269	0.731	499.2	469.2	1.74	0.269
3.0	2649.1	0.118	0.057	0.326	0.674	511.7	481.7	1.48	0.326
3.5	2709.8	0.108	0.067	0.383	0.617	524.3	494.3	1.29	0.383
4.0	2770.5	0.098	0.077	0.440	0.560	536.9	506.9	1.15	0.440
4.5	2831.3	0.088	0.087	0.506	0.503	549.4	519.4	1.03	0.506
5.0	2892.0	0.075	0.100	0.571	0.429	562.0	532.0	0.93	0.571

Initial temperature,$T_0 = 42.0$ ℃

Initial pressure,$P_0 = 0.0\ MPa$

Initial volume of the sample,$V_0 = 0.175 * 10^{-3} m^3$

From Table 4.24, it was observed that the bulk modulus decreased with increased in both temperature and pressure while the volume strain increased with increase in both temperature and pressure. The graph of volume strain against time and the graph of bulk modulus against temperature for sample 23 are shown in Figures 4.23a and 4.23b.

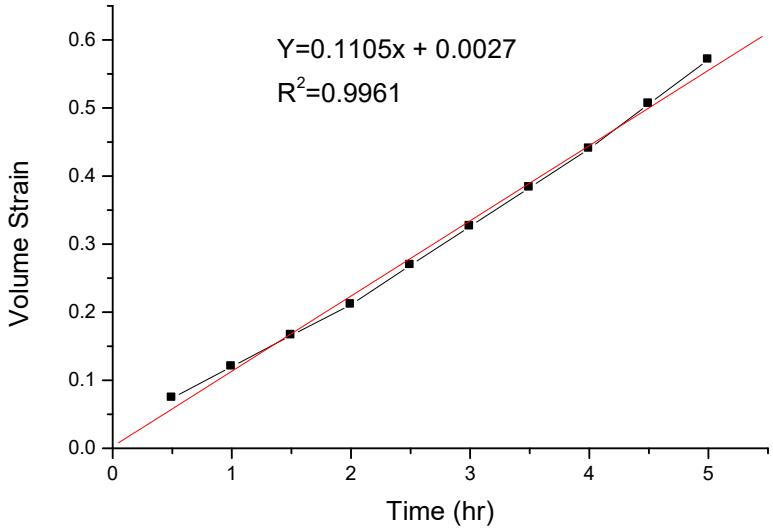

Figure 4.23a: Volume Strain Plotted Against Temperature (sample 23)

Figure 4.23a represents the graph of volume strain against time for sample 23. In the figure, the value of strain rate was 0.000031 s^{-1}, the rate increased with increase in time which conformed to literature laboratory values for materials while the square of the sample correlation which determine the goodness of the fit was 0.9961.

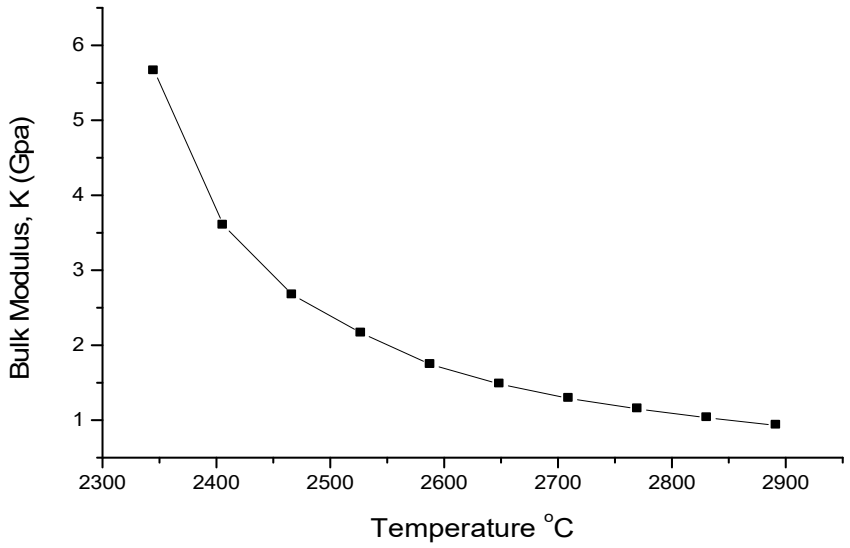

Figure 4.23b: Bulk Modulus Against Temperature (sample 23)

Figure 4.23b represents the graph of bulk modulus against temperature for sample 23, it was noticed from the graph that the bulk modulus of the sample decreased with increase in temperature. The behavior of the sample showed that the material in this category exhibit a type of volume compression which increased with rise in both temperature and pressure.

Table 4.25: Average Values of Temperature, Volume and Pressure (sample 24)

Time (hr)	T °C	V*10^{-3} (m^3)	ΔV (m^3)	ΔV/V$_0$ Strain	V/V$_0$	P (Mpa)	ΔP (Mpa) Stress	B (Gpa)	Δη Volume Strain
0.5	2351.9	0.164	0.012	0.068	0.931	449.7	419.76.17	0.068	
1.0	2412.7	0.156	0.020	0.114	0.886	462.3	432.3	3.79	0.114
1.5	2473.6	0.148	0.028	0.159	0.841	474.8	444.8	2.80	0.159
2.0	2534.5	0.140	0.036	0.205	0.795	487.5	457.5	2.23	0.205
2.5	2595.3	0.130	0.046	0.261	0.739	499.7	469.7	1.80	0.261
3.0	2656.2	0.120	0.056	0.318	0.682	512.6	482.6	1.52	0.318
3.5	2717.1	0.110	0.066	0.375	0.625	525.2	495.2	1.32	0.375
4.0	2778.3	0.100	0.076	0.432	0.568	537.8	507.8	1.18	0.432
4.5	2841.6	0.090	0.086	0.489	0.511	550.4	520.4	1.06	0.489
5.0	2899.7	0.076	0.100	0.568	0.432	563.0	533.0	0.94	0.568

Initial temperature,$T_0 = 42.0$ ℃

Initial pressure,$P_0 = 0.0\ MPa$

Initial volume of the sample,$V_0 = 0.176 * 10^{-3} m^3$

From Table 4.25, it was observed that the bulk modulus decreased with increase in both temperature and pressure while the volume strain increased with increase in both temperature and pressure. The graph of volume strain against time and the graph of bulk modulus against temperature for sample 24 are shown in Figures 4.24a and 4.24b.

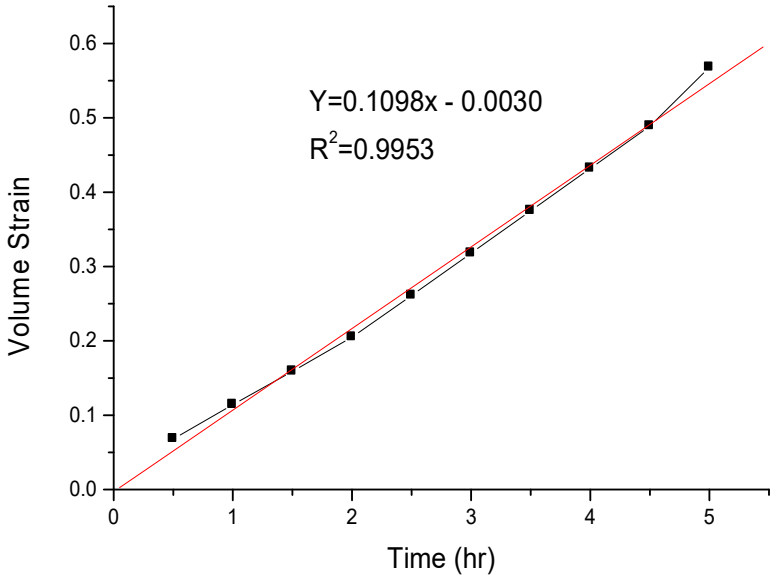

Figure 4.24a: Volume Strain Plotted Against Time (sample 24)

Figure 4.24a represents the graph of volume strain against time for sample 24. In the figure, the value of strain rate was 0.000031 s^{-1}, the rate increased with increase in time which conformed to literature laboratory values for materials while the square of the sample correlation which determine the goodness of the fit was 0.9953.

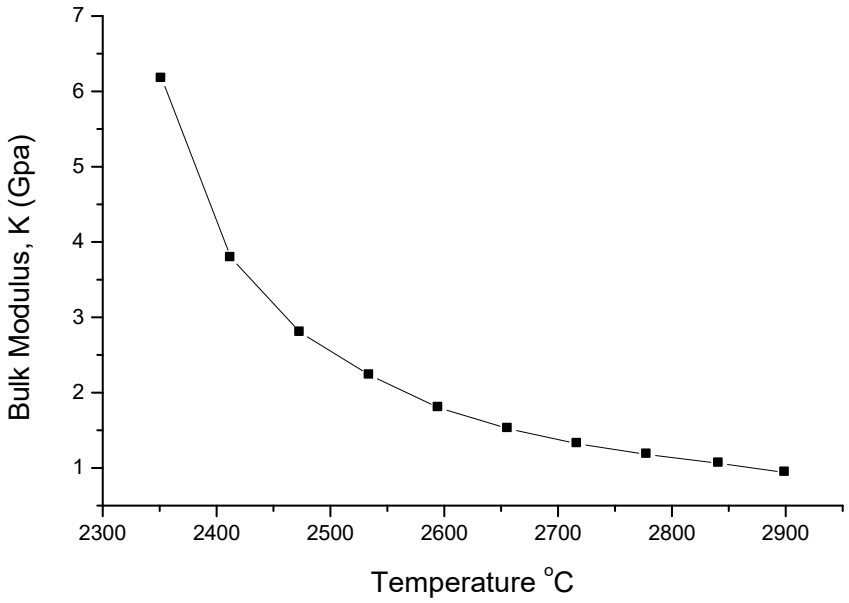

Figure 4.24b: Bulk Modulus Against Temperature (sample 24)

Figure 4.24b represents the graph of bulk modulus against temperature for sample 24, it was noticed from the graph that the bulk modulus of the sample decreased with increase in temperature. The behavior of the sample showed that the material in this category exhibit a type of volume compression which increased with rise in both temperature and pressure.

Table 4.28: Average Values of Temperature, Volume and Pressure (sample 27)

Time (hr)	T °C	V*10^{-3} (m^3)	ΔV (m^3)	$\Delta V/V_0$ Strain	V/V_0	P (Mpa)	ΔP (Mpa) Stress	B (Gpa)	Δη Volume Strain
0.5	2351.8	0.170	0.015	0.082	0.934	454.5	424.5	5.18	0.082
1.0	2412.8	0.162	0.020	0.110	0.890	467.5	437.2	3.97	0.110
1.5	2473.7	0.154	0.028	0.154	0.846	479.9	449.9	2.92	0.154
2.0	2534.6	0.146	0.036	0.198	0.802	492.6	462.6	2.34	0.198
2.5	2595.5	0.136	0.046	0.253	0.747	505.4	475.4	1.88	0.253
3.0	2656.4	0.126	0.056	0.308	0.692	518.1	488.1	1.59	0.308
3.5	2717.3	0.116	0.066	0.363	0.637	530.8	500.8	1.38	0.363
4.0	2778.2	0.106	0.076	0.418	0.582	543.6	513.6	1.23	0.418
4.5	2839.1	0.096	0.086	0.473	0.527	556.3	526.3	1.11	0.473
5.0	2900.0	0.082	0.100	0.549	0.451	569.0	539.0	0.98	0.549

Initial temperature,$T_0 = 42.0$ ℃

Initial pressure,$P_0 = 0.0\ MPa$

Initial volume of the sample,$V_0 = 0.182 * 10^{-3} m^3$

From Table 4.28, it was observed that the bulk modulus decreased with increase in both temperature and pressure while the volume strain increased with increase in both temperature and pressure. The graph of volume strain against time and the graph of bulk modulus against temperature for sample 27 are shown in Figures 4.27a and 4.27b.

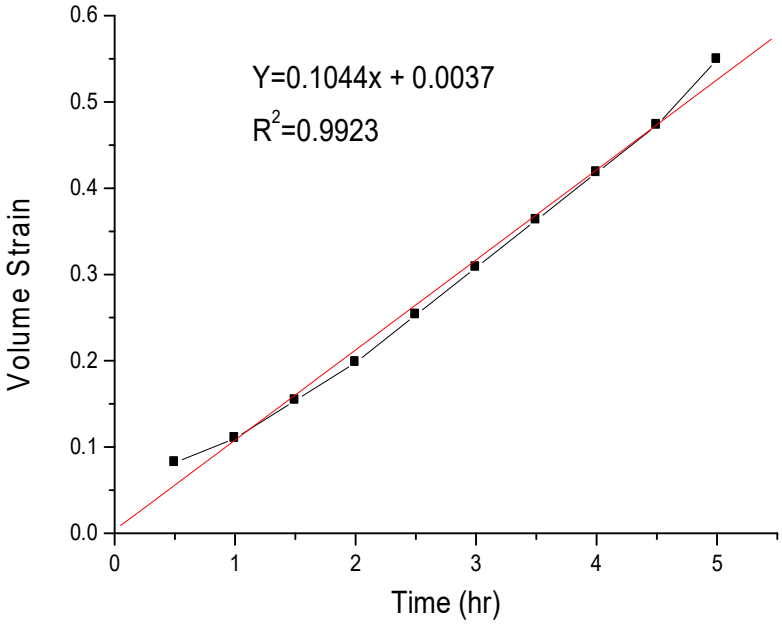

Figure 4.27a: Volume Strain Plotted Against Time (sample 27)

Figure 4.27a represents the graph of volume strain against time for sample 27. In the figure, the value of strain rate was 0.000029 s^{-1}, the rate increased with increase in time which conformed to literature laboratory values for materials while the square of the sample correlation which determine the goodness of the fit was 0.9923.

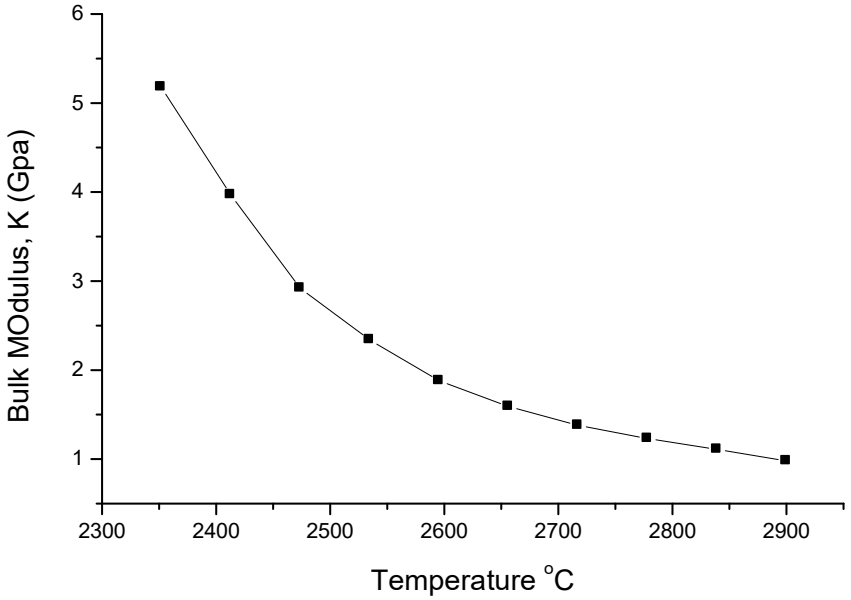

Figure 4.27b: Bulk Modulus Against Temperature (sample 27)

Figure 4.27b represents the graph of bulk modulus against temperature for sample 27, it was noticed from the graph that the bulk modulus of the sample decreased with increase in temperature. The behavior of the sample showed that the material in this category exhibit a type of volume compression which increased with rise in both temperature and pressure.

Table 4.29: Average Values of Temperature, Volume and Pressure (sample 28)

Time	T °C	$V*10^{-3}$	ΔV	$\Delta V/V_0$	V/V_0	P	ΔP	B	$\Delta\eta$

(hr)		(m^3)	(m^3)	Strain		(Mpa)	(Mpa) Stress	(Gpa)	Volume Strain
0.5	2353.5	0.172	0.012	0.065	0.935	456.6	426.6	6.56	0.065
1.0	2414.4	0.164	0.020	0.109	0.891	469.4	439.4	4.03	0.109
1.5	2475.4	0.156	0.028	0.152	0.848	482.2	452.2	2.98	0.152
2.0	2536.3	0.148	0.036	0.196	0.804	495.0	465.0	2.37	0.196
2.5	2597.2	0.138	0.046	0.250	0.750	507.7	477.0	1.91	0.250
3.0	2658.2	0.128	0.056	0.304	0.696	520.5	490.5	1.61	0.304
3.5	2719.1	0.118	0.066	0.359	0.641	533.3	503.3	1.40	0.359
4.0	2780.1	0.108	0.076	0.413	0.587	546.1	516.1	1.25	0.413
4.5	2841.0	0.098	0.086	0.467	0.533	558.9	528.9	1.13	0.467
5.0	2902.0	0.084	0.100	0.543	0.457	571.7	541.71.00		0.543

Initial temperature,$T_0 = 42.0$ ℃

Initial pressure,$P_0 = 0.0\ MPa$

Initial volume of the sample,$V_0 = 0.184 * 10^{-3} m^3$

From Table 4.29, it was observed that the bulk modulus decreased with increase in both temperature and pressure while the volume strain increased with increase in both temperature and pressure. The graph of volume strain against time and the graph of bulk modulus against temperature for sample 28 are shown in Figures 4.28a and 4.28b.

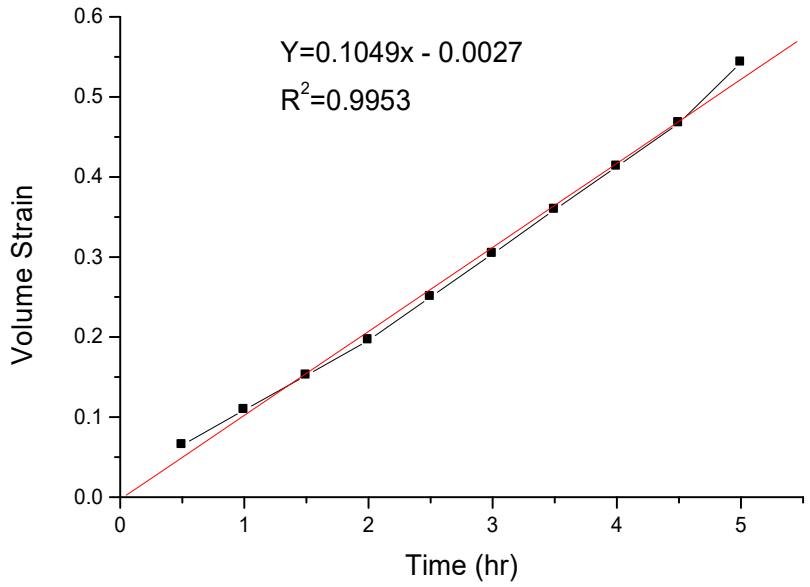

Figure 4.28a: Volume Strain Plotted Against Time (sample 28)

Figure 4.28a represents the graph of volume strain against time for sample 28. In the figure, the value of strain rate was 0.000029 s^{-1}, the rate increased with increase in time which conformed to literature laboratory values for materials while the square of the sample correlation which determine the goodness of the fit was 0.9953.

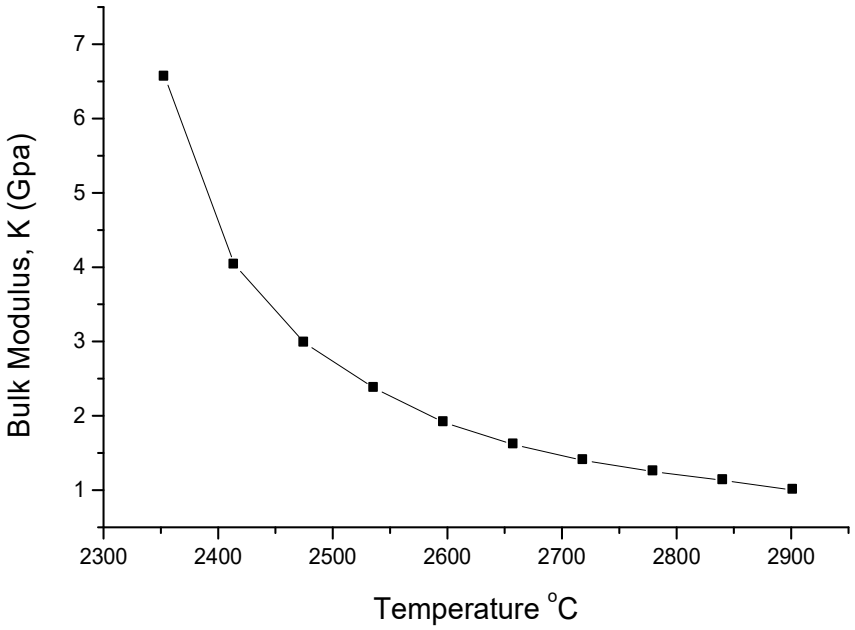

Figure 4.28b: Bulk Modulus Against Temperature (sample 28)

Figure 4.28b represents the graph of bulk modulus against temperature for sample 28, it was noticed from the graph that the bulk modulus of the sample decreased with increase in temperature. The behavior of the sample showed that the material in this category exhibit a type of volume compression which increased with rise in both temperature and pressure.

Table 4.30 Average Values of Temperature, Volume and Pressure (sample 29)

Time (hr)	T °C	V*10^{-3} (m^3)	ΔV (m^3)	ΔV/V_0 Strain	V/V_0	P (Mpa)	ΔP (Mpa)	B (Gpa)	Δη Volume

							Stress		Strain
0.5	2354.5	0.174	0.012	0.065	0.935	458.2	428.2	6.59	0.065
1.0	2415.5	0.166	0.020	0.108	0.892	471.6	441.6	4.09	0.108
1.5	2476.5	0.158	0.028	0.151	0.849	483.9	453.93.01	0.151	
2.0	2537.2	0.150	0.036	0.194	0.806	496.7	466.7	2.41	0.194
2.5	2598.2	0.140	0.046	0.247	0.753	509.5	479.5	1.94	0.247
3.0	2659.4	0.130	0.056	0.301	0.699	528.4	498.4	1.66	0.301
3.5	2720.4	0.120	0.066	0.355	0.645	535.2	505.2	1.42	0.355
4.0	2781.4	0.110	0.076	0.409	0.591	548.0	518.0	1.27	0.409
4.5	2842.3	0.100	0.086	0.462	0.538	560.8	530.8	1.15	0.462
5.0	2903.3	0.086	0.100	0.538	0.462	573.7	543.7	1.01	0.548

Initial temperature,$T_0 = 42.0$ ℃

Initial pressure,$P_0 = 0.0\ MPa$

Initial volume of the sample,$V_0 = 0.186 * 10^{-3} m^3$

From Table 4.30, it was observed that the bulk modulus decreased with increase in both temperature and pressure while the volume strain increased with increase in both temperature and pressure. The graph of volume strain against time and the graph of bulk modulus against temperature for sample 29 are shown in Figures 4.29a and 4.29b.

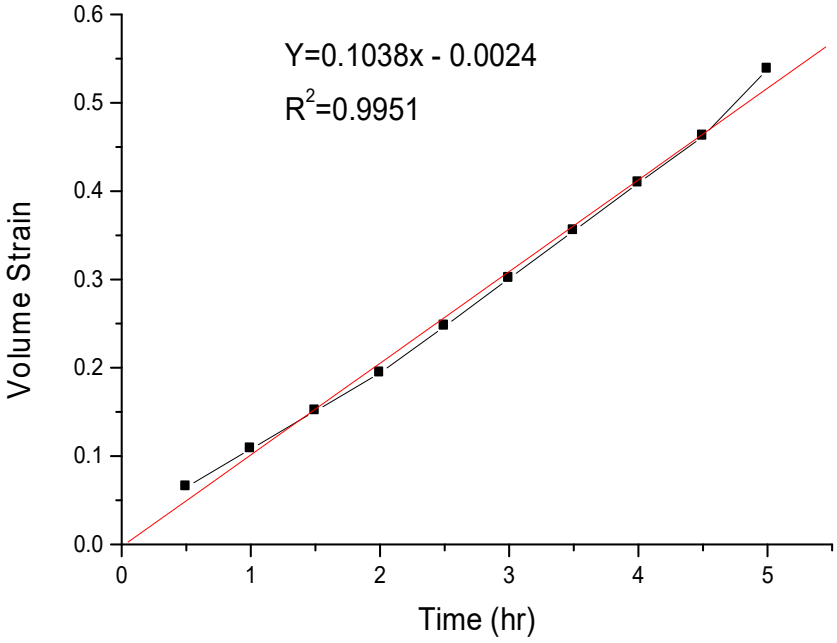

Figure 4.29a: Volume Strain Plotted Against Time (sample 29)

Figure 4.29a represents the graph of volume strain against time for sample 29. In the figure, the value of strain rate was 0.000029 s^{-1}, the rate increased with increase in time which conformed to literature laboratory values for materials while the square of the sample correlation which determine the goodness of the fit for this sample was 0.9951.

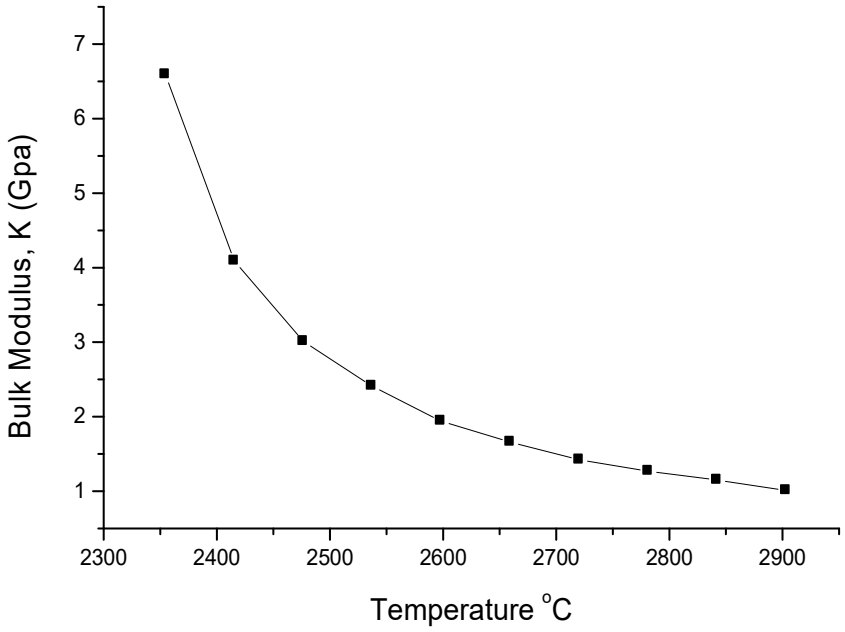

Figure 4.29b: Bulk Modulus Against Temperature (sample 29)

Figure 4.29b represents the graph of bulk modulus against temperature for sample 29, it was noticed from the graph that the bulk modulus of the sample decreased with increase in temperature. The behavior of the sample showed that the material in this category exhibit a kind of volume compression which increased with rise in both temperature and pressure.

Table 4.31: Average Values of Temperature, Volume and Pressure (sample 30)

Time (hr)	T °C	V*10^{-3} (m^3)	ΔV (m^3)	ΔV/V_0 Strain	V/V_0	P (Mpa)	ΔP (Mpa) Stress	B (Gpa)	Δη Volume Strain

0.5	2089.5	0.176	0.012	0.064	0.936	459.8	429.8	6.72	0.064
1.0	2143.4	0.168	0.020	0.106	0.894	472.7	442.7	4.18	0.106
1.5	2197.2	0.160	0.028	0.149	0.851	485.5	455.5	3.06	0.149
2.0	2251.0	0.152	0.036	0.191	0.809	498.4	468.4	2.45	0.191
2.5	2304.8	0.142	0.046	0.245	0.755	511.3	481.3	1.96	0.245
3.0	2358.7	0.132	0.056	0.298	0.702	524.2	494.2	1.66	0.298
3.5	2412.5	0.122	0.066	0.351	0.649	537.0	507.0	1.44	0.351
4.0	2466.4	0.112	0.076	0.404	0.596	549.9	519.9	1.29	0.404
4.5	2520.2	0.102	0.086	0.457	0.543	562.8	532.8	1.17	0.457
5.0	2574.0	0.088	0.100	0.532	0.468	575.7	545.7	1.03	0.532

Initial temperature,$T_0 = 42.0$ ℃

Initial pressure,$P_0 = 0.0\ MPa$

Initial volume of the sample,$V_0 = 0.188 * 10^{-3} m^3$

From Table 4.31, it was observed that the bulk modulus decreased with increase in both temperature and pressure while the volume strain increased with increase in both temperature and pressure. The graph of volume strain against time and the graph of bulk modulus against temperature for sample 30 are shown in Figures 4.30a and 4.30b.

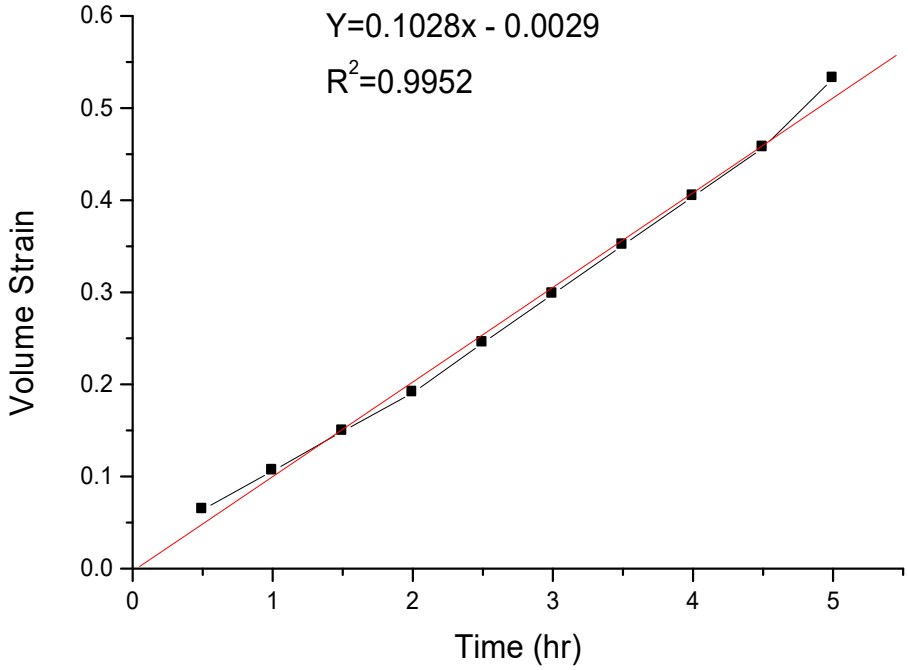

Figure 4.30a: Volume Strain Plotted Against Time (sample 30)

Figure 4.30a represents the graph of volume strain against time for sample 30. In the figure, the value of strain rate was 0.000029 s^{-1}, the rate increased with increase in time which conformed to literature laboratory values for materials while the square of the sample correlation which determine the goodness of the fit for this sample was 0.9952.

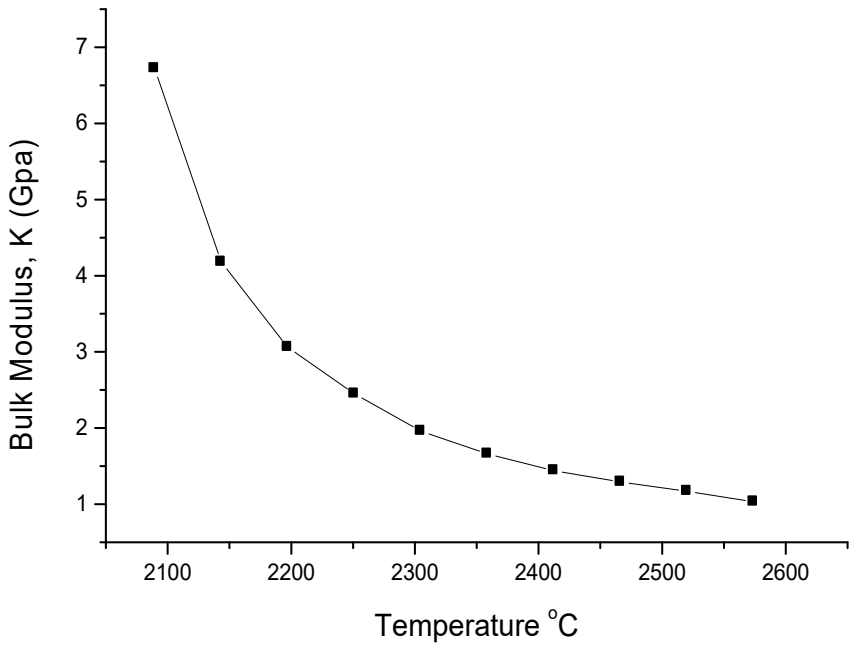

Figure 4.30b: Bulk Modulus Against Temperature (sample 30)

Figure 4.30b represents the graph of bulk modulus against temperature for sample 30, it was observed from the graph that the bulk modulus of the sample decreased with increase in temperature. The behavior of the sample showed that the material in this group exhibit a type of volume compression which increased with rise in both temperature and pressure.